THE STABILITY AND MIXING OF A DENSITY-STRATIFIED HORIZONTAL FLOW IN A SATURATED POROUS MEDIUM

By

E. John List
Research Fellow in Engineering

Project Supervisor:

Norman H. Brooks
Professor of Civil Engineering

Supported by Research Grant No. WP-00680
National Institute of Health
U. S. Public Health Service
Department of Health Education and Welfare

W. M. Keck Laboratory of Hydraulics and Water Resources
Division of Engineering and Applied Science
California Institute of Technology
Pasadena, California

Report No. KH-R-11 December 1965

ACKNOWLEDGEMENTS

To Professor Norman H. Brooks the writer expresses his gratitude and appreciation for the guidance and advice so kindly offered throughout the investigation.

The writer is also indebted to Dr. Robert C-Y Koh for numerous discussions on many aspects of the study and to Dr. P. G. Saffman for a discussion during the development of the instability theory.

Financial assistance received by the writer in the form of Graduate Teaching Assistantships during 1963 and 1964, and a Graduate Research Assistantship during 1965, from the California Institute of Technology is gratefully acknowledged.

The investigation was supported from May, 1964 by Research Grant WP-00680 from the National Institute of Health, United States Public Health Service. The experiments were carried out in the W. M. Keck Laboratory of Hydraulics and Water Resources at the California Institute of Technology.

The writer wishes to thank Mr. Elton F. Daly and Mr. Robert L. Greenway for their invaluable assistance in the design and construction of the laboratory equipment, Mr. Paul Kochendorfer for his willing aid in the laboratory and Mr. Carl Eastvedt for the photography.

This report is a minor revision of a thesis of the same title submitted by the writer in May 1965, to the California Institute of Technology in partial fulfillment of the requirements for the degree of Doctor of Philosophy in Applied Mechanics.

ABSTRACT

The mixing of two miscible fluids in motion in a saturated isotropic porous medium and the stability of the density interface between them has been studied. The density interface was formed by a line source introducing a denser fluid into a uniform confined horizontal flow. It was shown that the half-body thus formed may be approximated to within the density difference by the shape when the densities are equal. The mixing of the two fluids by lateral dispersion along such an interface was investigated experimentally and it was found that up to density differences of at least 1 per cent there was no observable effect on the lateral dispersion coefficient.

A theoretical investigation has been made of the stability of the uniform two-dimensional horizontal motion of two miscible fluids of different density in a saturated, isotropic, homogeneous porous medium. The fluid of higher density overlay the lower density fluid and both were moving with the same seepage velocity in the same direction. The analytical solution for the stability was obtained from the continuity equation, Darcy's law and the dispersion equation by investigating the stability of arbitrary sinusoidal perturbations to the velocity vector and the density profile prescribed by the lateral dispersion of one fluid into the other. A stability equation similar to the Orr-Sommerfeld equation was obtained and a neutral stability curve in a wave number - Rayleigh number plane was found by two approximate methods. The growth rates of instabilities were investigated for a

linear density profile and it has been found that although the flow was always unstable the growth rates of unstable waves could be so low as to form a quasi-stable flow; examples of such flows have been demonstrated experimentally.

TABLE OF CONTENTS

CHAPTER ONE

INTRODUCTION

1.0 Introductory Note

It has long been recognized that water reservoirs such as lakes and oceans have natural density stratifications arising from differences in temperature or in dissolved or suspended material. The same phenomenon also occurs in porous media containing water or other fluid as for example occurs in oil fields, in the Ghyben-Herzberg lens below some oceanic islands (Wentworth (1), Carrier (2), Wooding (3)) and in geothermal fields (Wooding (4)).

However, it is only relatively recently that men have begun to exploit this density stratification and even more recently to study the consequencies of perturbing a natural stratification. The petroleum industry is again one obvious example of the exploitation of this phenomenon. Another, somewhat less welcome, example is the intrusion of sea water into coastal ground water aquifers when the natural ground water outflow is intercepted by wells or catchments, (Harleman and Rumer (5); Bear and Dagan (6)).

Similar density stratifications can occur when hot water or water containing dissolved salts is artificially injected by recharge wells or infiltration ponds. Often when a fluid of density different to the ambient fluid is introduced into a porous medium knowledge is required of the process by which mixing of the alien and ambient fluids occurs. In particular such information should include the role of the density difference in the mixing process. An application of this

knowledge is in the mixing of high salinity reclaimed waste water with relatively high quality, low salinity ground water in order that available water supplies may be extended.

1.1 Previous Work

The mixing of two or more fluids in motion in a porous medium involves a microscale molecular diffusion process within the interstices or pores and a macroscale convective mixing from the arbitrary flow-dividing by the porous medium. The process can be thought of as analogous to turbulent mixing in fluid flow. Since the process involves more than just molecular diffusion and depends on the flow characteristics it is more generally called hydrodynamic dispersion or simply dispersion.

Dispersion is characterized by being a much "faster" process than molecular diffusion, and so regardless of the fact that it is carried on only on the scale of several pore sizes the cumulative effect can be seen on a relatively large scale in a similar way to pure molecular diffusion. Research has therefore been directed at finding a dispersion equation as well as trying to understand the basic mechanism.

Theoretical research has centered about finding a mathematical model which will characterize the phenomenon and its behavior and numerous models have been proposed. A random walk theory was presented by Scheidegger (7); and Saffman (8) assumed that a porous medium was analogous to a network of capillaries in order to apply Taylor's (9) theory of diffusion in laminar flow in tubes. For an appraisal of most of the models that have been proposed the reader is referred to articles by

H. O. Pfannkuch (10) and Bischoff and Levenspiel (11,12).

Scheidegger (13) and de Josselin de Jong (14) give the equation

$$\frac{\partial C}{\partial t} = \frac{\partial}{\partial x_i}\left(D_{ik}\frac{\partial C}{\partial x_k} - u_i C\right)$$

to describe the dispersion of a tracer in steady, saturated flow in a homogeneous isotropic porous medium, where D_{ik} are the components of the factor of dispersion and D is a symmetric second-order tensor, u_i are the components of the seepage velocity (defined later) and C is the relative concentration of the tracer $(0 < C < 1)$. Bear (15) concludes from experiments that the factor of dispersion is an inner product of two tensors: a geometrical dispersivity tensor, $a_{ik\ell m}$, of the porous medium which measures the tendency of the porous medium to disperse the tracer, and the tensor $u_\ell u_m/|u|$ which expresses the influence of the velocity on the dispersion.

When the direction of one axis coincides with a uniform flow then D_{ik} may be written

$$D_{ik} = \begin{bmatrix} a_I u & 0 & 0 \\ 0 & a_{II} u & 0 \\ 0 & 0 & a_{II}\, u \end{bmatrix}$$

where $a_I u = D_L$ is the so-called longitudinal dispersion coefficient and $a_{II} u = D_T$, the lateral dispersion coefficient.

This result is apparently reasonable, Pfannkuch (10), Harleman and Rumer (16), for some ranges of the particle Reynolds number

($R = ud/\nu$) where d is the average particle size; it is obviously untrue when the velocity is very small or zero as this result could give dispersion factors smaller than the molecular diffusion rates. Furthermore, it assumes outright that the molecular diffusion plays no part in the dispersion phenomenon at all, a point still in dispute. It seems more plausible that $D_{ik}/D_m = f(R, S, \text{geometry})$ where D_m is the molecular diffusivity, S the Schmidt number and R the particle Reynolds number.

There has been little study of density induced flows in saturated porous media and most is the work of one man.

Wooding (17,3) has studied the mixing zone at the boundary of a buoyant plume in a saturated porous medium and under the justifiable assumption that the lateral dispersion coefficient is constant has found these flows are governed by equations similar to those of laminar incompressible flow for such cases as the Gortler half jet and the Schlichting solutions for a momentum jet from a slit or point source. Mixing along the fresh water sea water interface of the Ghyben-Herzberg lens is also considered by Wooding (3).

The stability of a vertically moving interface between immiscible fluids in a porous medium was studied by Saffman and Taylor (18) and the work has been extended by Wooding (19) to include the influence of the longitudinal dispersion across the interface of two miscible fluids. In addition Wooding (20,21,22) has investigated the gravitational instability of a viscous fluid in a vertical tube containing a porous material, and also the stability of a liquid of variable density in a vertical

Hele-Shaw cell.

The motion and mixing of two fluids of differing density and in horizontal motion one above the other has not been studied previously. It will be the object of this dissertation to investigate the stability and mixing of such a flow, when the heavier fluid is above the lighter.

1.2 The Problem

A flow such as above could be generated in the following way. Consider a line source of strength $2Q_2$ per unit length discharging half of its total flow of density ρ_2 into a homogeneous isotropic porous medium of intrinsic permeability k and confined between two horizontal parallel planes distant a apart. The porous medium also has a uniform flow of velocity U and density ρ_1 and moving from left to right, Figure 1.1. The two fluids are miscible and have kinematic viscosities ν_2 , ν_1 respectively. The problem is to study the mixing of the two fluids by dispersion across the interface, and to study the flow stability.

1.3 The Equations of Motion

In flow in porous media two velocities are generally spoken of. The superficial velocity vector $\vec{v}$ is taken to be the flow rate dQ through an area dS in a direction normal to the flow, i.e. the flow in the direction normal to dS is given by

$$\vec{v} \cdot \vec{n}\, dS = dQ \qquad (1.1)$$

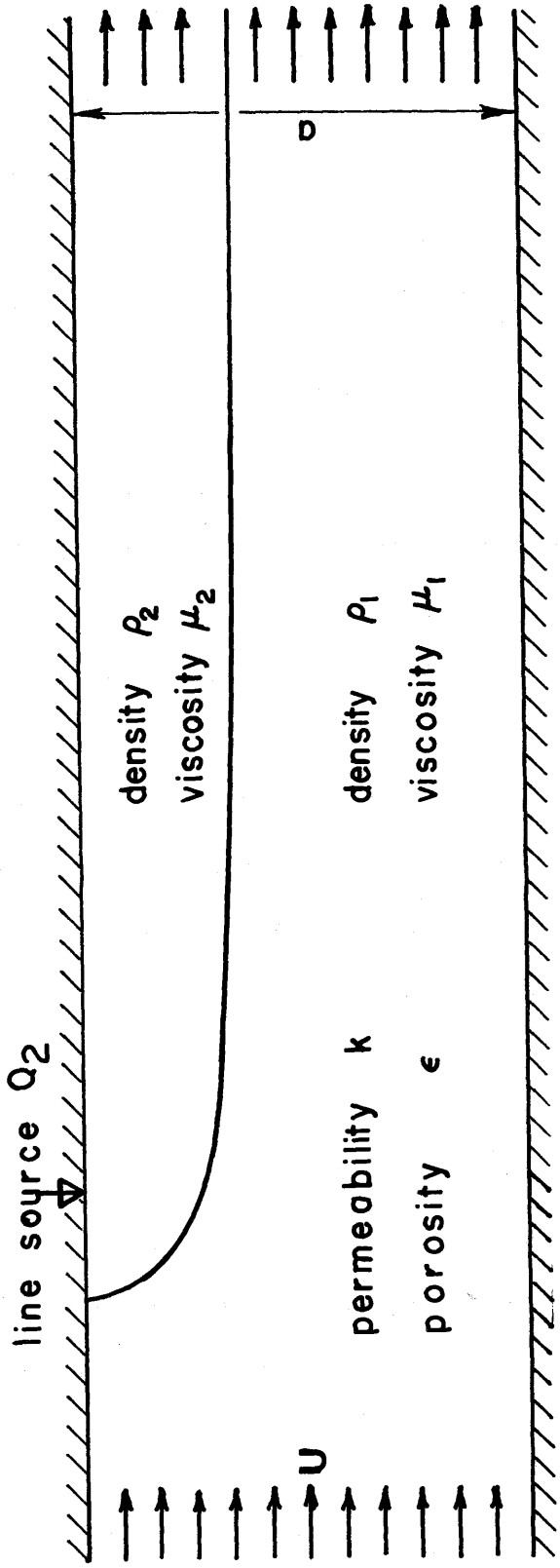

Figure 1.1 The flow geometry.

where $\vec{n}$ is the normal to dS and where dS is assumed to be large compared to the pore size but small compared to the overall flow curvature.

The seepage velocity vector $\vec{q}$ is taken to be the flow rate through a pore area dS_o, that is

$$\vec{q} \cdot \vec{n}\, dS_o = dQ \tag{1.2}$$

where again dS_o is large compared to the individual pore sizes, small compared to the flow curvature. The superficial porosity is defined to be

$$\frac{dS_o}{dS} = m \tag{1.3}$$

and is essentially the same as the volumetric porosity ε (see Polubarinova-Kochina (23)). Thus from (1.1), (1.2) and (1.3) it is seen that

$$\vec{v} = \varepsilon\vec{q}$$

The equations of motion for steady flow in a porous medium are known as Darcy's law and have been shown to be, Reference (23), in Cartesian coordinates,

$$\nabla p + \rho g\vec{k} + \frac{\nu}{k}\rho\vec{v} = 0 \tag{1.4}$$

where p is the pressure, ρ the fluid density, ν the fluid kinematic viscosity, k the intrinsic permeability, g the gravitational constant, $\vec{k}$ a unit vector in the upward vertical direction.

Surprisingly, equation (1.4) is even valid for unsteady flow,

see Reference (23), provided that the changes in ∇p with time are bounded. It is shown that for times $T > k/\nu$ then the term $\partial\vec{v}/\partial t$ may be neglected. So, if for example $k \sim O(10^{-6})$ cm^2, $\nu \sim O(10^{-2})$ cm^2/sec then $\partial\vec{v}/\partial t$ may be ignored for $T > O(10^{-4})$ seconds.

1.4 Equation of Continuity and Dispersion

The equation of continuity is

$$\epsilon \frac{\partial \rho}{\partial t} + \nabla \cdot (\rho\vec{v}) = 0 \qquad (1.5)$$

when there is no diffusion or dispersion of dissolved material in the fluid. However, when there is a dissolved substance present it becomes necessary to add an additional mass transfer term to account for the dispersion.

The net efflux of mass from a closed surface S due to dispersion is

$$-\int_S \epsilon\, (D\nabla C) \cdot \vec{n}\, dS$$

where D is the dispersion tensor as defined in section 1.1, C is the concentration of tracer per unit volume. This implies a dispersion term must be added to equation (1.5)

$$\epsilon \frac{\partial \rho}{\partial t} + \nabla \cdot (\rho\vec{v}) = \nabla \cdot (\epsilon\, D\nabla C)$$

And writing $\vec{v} = \epsilon\vec{q}$

$$\frac{\partial \rho}{\partial t} + \nabla \cdot (\rho \vec{q}) = \nabla \cdot (D \nabla C) \tag{1.6}$$

where D is defined such that it reduces to the molecular diffusivity in a porous medium when $\vec{q}$ becomes zero. The conservation equation for the tracer (the dispersion equation) is (see section 1.1)

$$\frac{\partial C}{\partial t} + \nabla \cdot (\vec{q} C) = \nabla \cdot (D \nabla C) \tag{1.7}$$

Now for small differences in density and concentration the density and concentration per unit volume are connected by an equation of state

$$\rho - \rho_1 = \beta (C - C_1) \tag{1.8}$$

where ρ_1 and C_1 are free stream reference quantities.

Equations (1.6) and (1.7) can be rewritten as

$$\frac{d\rho}{dt} + \rho \nabla \cdot \vec{q} = \nabla \cdot (D \nabla C) \tag{1.9}$$

$$\frac{dC}{dt} + C \nabla \cdot \vec{q} = \nabla \cdot (D \nabla C) \tag{1.10}$$

where

$$\frac{d}{dt} \equiv \left(\frac{\partial}{\partial t} + \vec{q} \cdot \nabla \right)$$

Subtracting (1.10) from (1.9) gives

$$\nabla \cdot \vec{q} = \frac{d(\rho - C)}{dt} \cdot \left(\frac{1}{\rho - C} \right)$$

But from (1.8)

$$d(\rho - C) \sim O(\Delta\rho)$$

$$\rho - C \sim O(\rho)$$

so that if a characteristic velocity U_0 and a characteristic length a are chosen so that a characteristic time is a/U_0 then

$$\nabla \cdot \vec{q} \sim O\left(\frac{U_0}{a}\right)$$

$$\frac{d(\rho - C)}{dt} \cdot \frac{1}{(\rho - C)} \sim O\left(\frac{U_0}{a}\frac{\Delta\rho}{\rho}\right)$$

Thus for $\Delta\rho \ll \rho$

$$\nabla \cdot \vec{q} = 0 \tag{1.11}$$

Furthermore, using (1.11) and (1.8) equation (1.7) can be rewritten

$$\frac{\partial\rho}{\partial t} + \vec{q} \cdot \nabla\rho = \nabla \cdot (D\nabla\rho)$$

To summarize, the equations of motion for a density stratified flow in a saturated homogeneous porous medium can then be written

$$\nabla \cdot \vec{q} = 0 \tag{1.12}$$

$$\nabla p + \rho g\vec{k} + \frac{\varepsilon\nu}{k}\rho\vec{q} = 0 \tag{1.13}$$

$$\frac{\partial\rho}{\partial t} + \vec{q} \cdot \nabla\rho = \nabla(D\nabla\rho) \tag{1.14}$$

Now that the equations of motion have been deduced a study may be made of the mixing process, and the flow stability, for the problem specified in section 1.2.

In the following chapter a solution is developed for the mixing

across the interface shown in Figure 1.1, and in Chapter 3 the stability of the flow is investigated. Two methods are used to find a neutral stability curve in a Rayleigh-number wave-number plane, and the growth rates of unstable waves are investigated also.

Chapter 4 outlines the experimental apparatus and procedure used to confirm the theoretical results developed in Chapter 2, and Chapter 5 details the experimental results from the experimental investigation of the mixing. The results obtained from the stability study and the study of the mixing are discussed in Chapter 6; conclusions are drawn and suggestions for further investigations are made.

CHAPTER TWO

THE MIXING LAYER

2.0 Introduction

There are two major problems associated with the two-dimensional flow system depicted in Figure 1.1. The first is to determine how the two fluids intermix. The approach to solving this problem is to first assume the two fluids are immiscible and compute the shape of the interface between them. A solution of the dispersion equation is then sought in the system of coordinates formed by the streamlines and their orthogonal trajectories.

The second problem is the question of overall stability of one fluid flowing over another of different density in a porous medium. Since the stability behavior will be intimately connected with the mixing characteristics the mixing problem will be studied first and the stability in the next chapter.

2.1 Shape of the Immiscible Interface

The shape of the interface between two immiscible fluids of different density in motion in a homogeneous isotropic porous medium will not depend on the dispersion equation; consequently the equations of motion for each fluid will be just the continuity equation (1.10) and Darcy's Law, equation (1.11)

$$\nabla \cdot \vec{v}_1 = 0 \qquad (2.1)$$

$$\nu_1 \vec{v}_1 = - \frac{k}{\rho_1} \nabla(p_1 - \rho_1 g y) \tag{2.2}$$

$$\nabla \cdot \vec{v}_2 = 0 \tag{2.3}$$

$$\nu_2 \vec{v}_2 = - \frac{k}{\rho_2} \nabla(p_2 - \rho_2 g y) \tag{2.4}$$

where

$$\vec{v}_i = (u_i, v_i)$$

are the superficial velocity vectors and ν_1, ν_2 and ρ_1, ρ_2 are the constant kinematic viscosities and constant densities of the two fluids, and where left-handed Cartesian coordinate axes have been chosen with the source point as origin and the y-axis pointing vertically down.

Now from equations (2.2) and (2.4) it is possible to define velocity potentials φ_1 and φ_2 such that

$$\nu_1 \vec{v}_1 = \nabla \varphi_1 \tag{2.5a}$$

$$\nu_2 \vec{v}_2 = \nabla \varphi_2 \tag{2.5b}$$

where

$$\varphi_1 = - \frac{k}{\rho_1} (p_1 - \rho_1 g y) \tag{2.6a}$$

$$\varphi_2 = - \frac{k}{\rho_2} (p_2 - \rho_2 g y) \tag{2.6b}$$

and

$$\nabla^2 \varphi_1 = \nabla^2 \varphi_2 = 0$$

It will become evident later that if the potentials are defined in this way then one solution can be written down for the entire flow field when the densities, but not the viscosities, are equal.

Since the flow is two-dimensional equations (2.1) and (2.3) imply that there exist stream functions ψ_1 and ψ_2 such that

$$\nu_i u_i = \frac{\partial \varphi_i}{\partial x} = \frac{\partial \psi_i}{\partial y} \tag{2.7a}$$

$$\nu_i v_i = \frac{\partial \varphi_i}{\partial y} = -\frac{\partial \psi_i}{\partial x} \tag{2.7b}$$

where u_i and v_i $(i = 1,2)$ are the horizontal and vertical components of the superficial velocity vector $\vec{v}_i$.

Suppose that the interface can be represented by the equation

$$y = \zeta(x)$$

Then the two boundary conditions on the interface are

(i) That there is no flow across the interface; this can be written in terms of the potentials defined above as

$$\frac{\partial \varphi_i}{\partial y} - \zeta'(x) \frac{\partial \varphi_i}{\partial x} = 0 \tag{2.8}$$

on

$$y = \zeta(x)$$

where the prime denotes differentiation with respect to x .

(ii) That the pressures on each side of the interface are equal. From the definition, equation (2.6), of the potentials this can

be written as

$$\varphi_1 - \frac{\rho_2}{\rho_1}\varphi_2 = -\left(\frac{\rho_2 - \rho_1}{\rho_1}\right) gk\zeta(x) \qquad (2.9)$$

The equations of motion and the boundary conditions may all be suitably non-dimensionalized by choosing appropriate characteristic values of length, a, the depth of the porous bed, and U_o a velocity, defined below.

Then let

$$Q_i = Q_i^* \cdot U_o a$$

$$\vec{v}_i = \vec{v}_i^* \cdot U_o$$

$$(x,y) = (x^*,y^*)\, a$$

$$p_i = p_i^* \cdot \rho_1 g a$$

$$U_o = \frac{gk}{\nu_1}$$

$$\varphi_i = \varphi_i^* \cdot gk a$$

where the non-dimensional values are denoted by an asterisk which is subsequently dropped. The equations of motion then become

$$\vec{v}_1 = -\nabla(p_1 - y) = \nabla\varphi_1 \qquad (2.10a)$$

$$\varphi_1 = -(p_1 - y) \qquad (2.11a)$$

$$\frac{\nu_2}{\nu_1}\vec{v}_2 = -\frac{\rho_1}{\rho_2}\nabla\left(p_2 - \frac{\rho_2}{\rho_1}y\right) = \nabla\varphi_2 \qquad (2.10b)$$

$$\varphi_2 = -\frac{\rho_1}{\rho_2}\left(p_2 - \frac{\rho_2}{\rho_1}y\right) \qquad (2.11b)$$

The boundary conditions become,

$$\varphi_1 - \frac{\rho_2}{\rho_1}\varphi_2 = -\left(\frac{\rho_2 - \rho_1}{\rho_1}\right)\zeta(x) = -\delta\cdot\zeta(x) \qquad (2.12)$$

and

$$\frac{\partial\varphi_i}{\partial y} - \zeta'(x)\frac{\partial\varphi_i}{\partial x} = 0, \quad \text{at} \quad y = \zeta(x); \qquad (2.13a)$$

and

$$\frac{\partial\varphi_i}{\partial y} = 0 \quad \text{at} \quad y = 0 \text{ and } 1 \qquad (2.13b)$$

The boundary condition upstream is obviously

$$\frac{\partial\varphi_1}{\partial x} = Q_1 \qquad (2.14)$$

since there is a uniform flow. The boundary condition at downstream infinity can be investigated in the following way. From equation (2.12) we can write

$$\frac{\partial\varphi_1}{\partial s} - \frac{\rho_2}{\rho_1}\frac{\partial\varphi_2}{\partial s} = -\delta\frac{\partial y}{\partial s} \quad \text{on} \quad y = \zeta(x) \qquad (2.15)$$

where s is the distance along $y = \zeta(x)$ from the stagnation point. Now, suppose the interface has a horizontal tangent at infinity, which indeed it must if continuity is to be preserved, then $\partial y/\partial s = 0$ which

implies

$$u_1(\infty,y) = \frac{\partial\varphi_1}{\partial s} = \frac{\rho_2}{\rho_1}\frac{\partial\varphi_2}{\partial s} = \frac{\nu_2}{\nu_1}\frac{\rho_2}{\rho_1}u_2(\infty,y) \qquad (2.16)$$

The velocity distribution will be uniform in each layer at infinity so that it is possible to write

$$u_1(\infty,y) \cdot (1 - d) = Q_1$$

$$u_2(\infty,y) \cdot d = Q_2$$

where

$$d = \zeta(\infty) .$$

These equations imply that

$$d = \frac{\rho_2\nu_2Q_2}{\rho_1\nu_1Q_1 + \rho_2\nu_2Q_2} \qquad (2.17)$$

$$u_2(\infty,y) = \left(\frac{\rho_2\nu_2Q_2 + \rho_1\nu_1Q_1}{\rho_2\nu_2}\right) = \frac{\nu_1}{\nu_2}\frac{\partial\varphi_2}{\partial x}(\infty,y) \qquad (2.18)$$

$$u_1(\infty,y) = \left(\frac{\rho_2\nu_2Q_2 + \rho_1\nu_1Q_1}{\rho_1\nu_1}\right) = \frac{\partial\varphi_1}{\partial x}(\infty,y) \qquad (2.19)$$

In summary, finding the interface reduces to the following problem in two-dimensional potential theory.

$$\nabla^2\varphi_1(x,y) = 0 \quad \text{in Region I}$$

$$\nabla^2\varphi_2(x,y) = 0 \quad \text{in Region II}$$

with the following boundary conditions on the interface $y = \zeta(x)$

$$\varphi_1(x,\zeta(x)) - \frac{\rho_2}{\rho_1}\varphi_2(x,\zeta(x)) = -\delta\,\zeta(x)$$

and

$$\frac{\partial\varphi_i}{\partial y}(x,\zeta(x)) - \zeta'(x)\frac{\partial\varphi_i}{\partial x}(x,\zeta(x)) = 0$$

and with

$$\frac{\partial\varphi_i}{\partial y}(x,y) = 0 \quad \text{at} \quad y = 0,\ 1$$

$$\frac{\partial\varphi_1}{\partial x}(-\infty,y) = Q_1$$

$$\frac{\nu_1}{\nu_2}\frac{\partial\varphi_2}{\partial x}(\infty,y) = \frac{\rho_2\nu_2Q_2 + \rho_1\nu_1Q_1}{\rho_2\nu_2}$$

$$\frac{\partial\varphi_1}{\partial x}(\infty,y) = \frac{\rho_2\nu_2Q_2 + \rho_1\nu_1Q_1}{\rho_1\nu_1}$$

This is an exceedingly difficult problem to solve since not only is the interface $y = \zeta(x)$ unknown and to be found as part of the solution but the boundary condition at the interface prescribes a jump in the velocity potentials at the interface. The problem is therefore the simultaneous solution of two coupled free surface boundary value problems and since free surface boundary value problems are notoriously difficult to solve the simultaneous solution of two coupled systems would seem to be nearly impossible unless done numerically. However, it may be possible to develop an approximate solution which contains all the essential characteristics of the exact solution.

In the following section (2.2) it is shown that an approximate solution can be obtained by developing regular perturbation series

about the solution when the densities are equal but the viscosities unequal. In this way the behavior of the exact solution can be approximated to within the order of the density difference by taking only the first terms of the perturbation series. In section 2.3 the solution when the densities are equal is investigated and the shape of the interface found; and in section 2.4 the mixing along the interface is studied.

2.2 A Perturbation Solution

In view of the fact that the density difference is small it would seem that a regular perturbation about the solution when the densities are equal would offer some simplification. Furthermore, since δ is small δ should make an ideal parameter for expansion. Thus expansions of the following form are sought for the interface shape and velocity potentials

$$\begin{aligned} \zeta(x) &= \zeta_o(x) + \delta\,\zeta_1(x) + \delta^2\,\zeta_2(x) + \ldots \\ \varphi_1 &= a_o\varphi_{10} + \delta\,\varphi_{11} + \delta^2\,\varphi_{12} + \ldots \\ \varphi_2 &= b_o\varphi_{20} + \delta\,\varphi_{21} + \delta^2\,\varphi_{22} + \ldots \end{aligned} \tag{2.20}$$

where $y = \zeta_o(x)$ is the solution for the shape of the interface when the densities are equal; $\varphi_{10}(x,y)$, $\varphi_{20}(x,y)$ are the corresponding velocity potentials.

These expansions are first substituted into the dynamic boundary condition equation (2.12) and the $\varphi_{ij}(x,y)$ expanded in Taylor series

about $y = \zeta_o(x)$. Collecting terms of equal order in δ

$$O(\delta^o) : a_o\varphi_{10}(x,\zeta_o(x)) - \frac{\rho_2}{\rho_1} b_o\varphi_{20}(x,\zeta_o(x)) = 0 \qquad (2.21a)$$

$$O(\delta) : \varphi_{11}(x,\zeta_o(x)) - \frac{\rho_2}{\rho_1} \varphi_{21}(x,\zeta_o(x)) = - \zeta_o(x) \qquad (2.21b)$$

$$O(\delta^2) : \varphi_{12}(x,\zeta_o(x)) - \frac{\rho_2}{\rho_1} \varphi_{22}(x,\zeta_o(x))$$

$$= - \zeta_1(x) \left[1 + \frac{\partial\varphi_{11}}{\partial y} (x,\zeta_o(x)) + \frac{\rho_2}{\rho_1} \frac{\partial\varphi_{21}}{\partial y} (x,\zeta_o(x))\right] \qquad (2.21c)$$

And from the kinematic boundary condition (2.8)

$$O(\delta^o) : \frac{\partial\varphi_{10}}{\partial y} (x,\zeta_o(x)) - \zeta_o'(x) \frac{\partial\varphi_{10}}{\partial x} (x,\zeta_o(x)) = 0 \qquad (2.22a)$$

$$O(\delta) : \frac{\partial\varphi_{11}}{\partial y} (x,\zeta_o(x)) - \zeta_o'(x) \frac{\partial\varphi_{11}}{\partial x} (x,\zeta_o(x)) = a_o\zeta_1'(x) \frac{\partial\varphi_{10}}{\partial x} (x,\zeta_o(x)). \qquad (2.22b)$$

etc.

and

$$O(\delta^o) : \frac{\partial\varphi_{20}}{\partial y} (x,\zeta_o(x)) - \zeta_o'(x) \frac{\partial\varphi_{20}}{\partial x} (x,\zeta_o(x)) = 0 \qquad (2.23a)$$

$$O(\delta) : \frac{\partial\varphi_{21}}{\partial y} (x,\zeta_o(x)) - \zeta_o'(x) \frac{\partial\varphi_{21}}{\partial x} (x,\zeta_o(x)) = b_o\zeta_1'(x) \frac{\partial\varphi_{20}}{\partial x} (x,\zeta_o(x)) \qquad (2.23b)$$

etc.

Now a_o and b_o are chosen in such a way that $\varphi_{10}(x,y)$ and $\varphi_{20}(x,y)$

are the analytic continuations of each other in Regions I and II

i.e. $\varphi_{10}(x,y) \equiv \varphi_{20}(x,y)$

This is possible, if

$$a_o = \frac{\rho_2}{\rho_1}$$

$$b_o = 1$$

Using these two conditions we can eliminate $\zeta_1'(x)$ from equations (2.22b), (2.23b) and obtain a condition relating the first derivatives of φ_{11}, φ_{21} across $y = \zeta_o(x)$,

$$\frac{\partial \varphi_{11}}{\partial y}(x,\zeta_o(x)) + \zeta_o'(x)\frac{\partial \varphi_{11}}{\partial x}(x,\zeta_o(x))$$

$$= \left(\frac{\rho_2}{\rho_1}\right)\left[\frac{\partial \varphi_{21}}{\partial y}(x,\zeta_o(x)) - \zeta_o'(x)\frac{\partial \varphi_{21}}{\partial x}(x,\zeta_o(x))\right] \qquad (2.24)$$

The boundary conditions at infinity on the first order perturbations are now required. These are obtained by expanding equations (2.18) and (2.19) in powers of $\delta = \rho_2/\rho_1 - 1$, and give

$$O(\delta^o) : \frac{\partial \varphi_{10}}{\partial x}(\infty,y) = (\nu_2 Q_2 + \nu_1 Q_1)/\nu_1 \qquad (2.25a)$$

$$O(\delta^1) : \frac{\partial \varphi_{11}}{\partial x}(\infty,y) = -\frac{\rho_2}{\rho_1} Q_1 \qquad (2.25b)$$

$$O(\delta^2) : \frac{\partial \varphi_{12}}{\partial x}(\infty,y) = \frac{\rho_2}{\rho_1} Q_1 \qquad (2.25c)$$

and similarly

$$O(\delta^0) : \frac{\partial \varphi_{20}}{\partial x}(\infty, y) = (\nu_2 Q_2 + \nu_1 Q_1)/\nu_1 \tag{2.26a}$$

$$O(\delta^1) : \frac{\partial \varphi_{21}}{\partial x}(\infty, y) = - Q_1 \tag{2.26b}$$

$$O(\delta^2) : \frac{\partial \varphi_{22}}{\partial x}(\infty, y) = Q_1 \tag{2.26c}$$

This completes the formulation of the problem for calculating the first order perturbations, and summarizing the first order quantities

$$\nabla^2 \varphi_{11} = 0 \quad \text{in Region I}$$

$$\nabla^2 \varphi_{21} = 0 \quad \text{in Region II}$$

$$\varphi_{11}(x, \zeta_o(x)) - \frac{\rho_2}{\rho_1} \varphi_{21}(x, \zeta_o(x)) = - \zeta_o(x)$$

$$\frac{\partial \varphi_{11}}{\partial y}(x, \zeta_o(x)) + \zeta_o'(x) \frac{\partial \varphi_{11}}{\partial x}$$

$$= \frac{\rho_2}{\rho_1} \left[\frac{\partial \varphi_{21}}{\partial y}(x, \zeta_o(x)) - \zeta_o'(x) \frac{\partial \varphi_{21}}{\partial y}(x, \zeta_o(x)) \right]$$

$$\frac{\partial \varphi_{11}}{\partial x}(\infty, y) = - \frac{\rho_2}{\rho_1} Q_1$$

$$\frac{\partial \varphi_{21}}{\partial x}(\infty, y) = - Q_1$$

$$\frac{\partial \varphi_i}{\partial y}(x,y) = 0 \quad \text{at} \quad y = 0, 1$$

$$\frac{\partial \varphi_{11}}{\partial x}(-\infty,y) = 0$$

Since $\zeta_o(x)$ is given by the solution of the zeroth order problem when the densities are equal the first order potential perturbations can then be calculated to within a constant since Neumann boundary conditions are given. This arbitrariness can be resolved by placing $\varphi_{11}(-h,0) = \varphi_{21}(-h,0) = 0$. (For definition of h see Fig. 2.1.)

Once $\varphi_{11}(x,y)$ and $\varphi_{21}(x,y)$ are known it then becomes possible to compute the first order perturbation to the interface shape, for from equation (2.22b)

$$\zeta_1'(x) = \frac{\frac{\partial \varphi_{11}}{\partial y}(x,\zeta_o(x)) - \zeta_o'(x)\frac{\partial \varphi_{11}}{\partial x}(x,\zeta_o(x))}{\frac{\rho_2}{\rho_1}\cdot\frac{\partial \varphi_{10}}{\partial x}(x,\zeta_o(x))} \tag{2.27}$$

and thus $\zeta_1'(x)$ can be calculated. It should be noted that at $x = -h$

$$\frac{\partial \varphi_{10}}{\partial x}(-h,0) = 0 \,, \quad \zeta_o'(-h) = \infty$$

thus it would appear that $\zeta_1'(-h) = \infty$ also. Hence to first order the interface has a vertical tangent at $x = -h$.

From equation (2.17)

$$\zeta(\infty) = d = \frac{\rho_2 \nu_2 Q_2}{\rho_1 \nu_1 Q_1 + \rho_2 \nu_2 Q_2}$$

and this may be expanded in powers of δ as follows

$$\zeta(\infty) = \zeta_o(\infty) + \zeta_1(\infty)\,\delta + \zeta_2(\infty)\,\delta^2 + \ldots .$$

$$= d_o + (1 - d_o)\,d_o\,\delta + (1 - d_o)\,d_o^2\,\delta^2 + \ldots .$$

where

$$d_o = \frac{\nu_2 Q_2}{\nu_1 Q_1 + \nu_2 Q_2}$$

is the half body width when the densities are equal. Hence it is seen that

$$\zeta_1(\infty) = (1 - d_o)\,d_o$$

and that the correction to the interface from the first order term will be of $O(\delta)$.

It appears therefore that the zeroth order solution is at least correct to within $O(\delta)$ and for all practical purposes there may be no need to compute the perturbations, especially as even the problem of computing the perturbations is not an easy one.

The strategy will be to compute the zeroth order solution and then compute the dispersion as if the zeroth order solution were the exact solution and check with experimental results; if good agreement is reached then it will not be necessary to compute the terms of $O(\delta)$.

2.3 The Zeroth Order Solution

It has been shown that a perturbation solution can be found to the problem when the densities are different provided that a solution

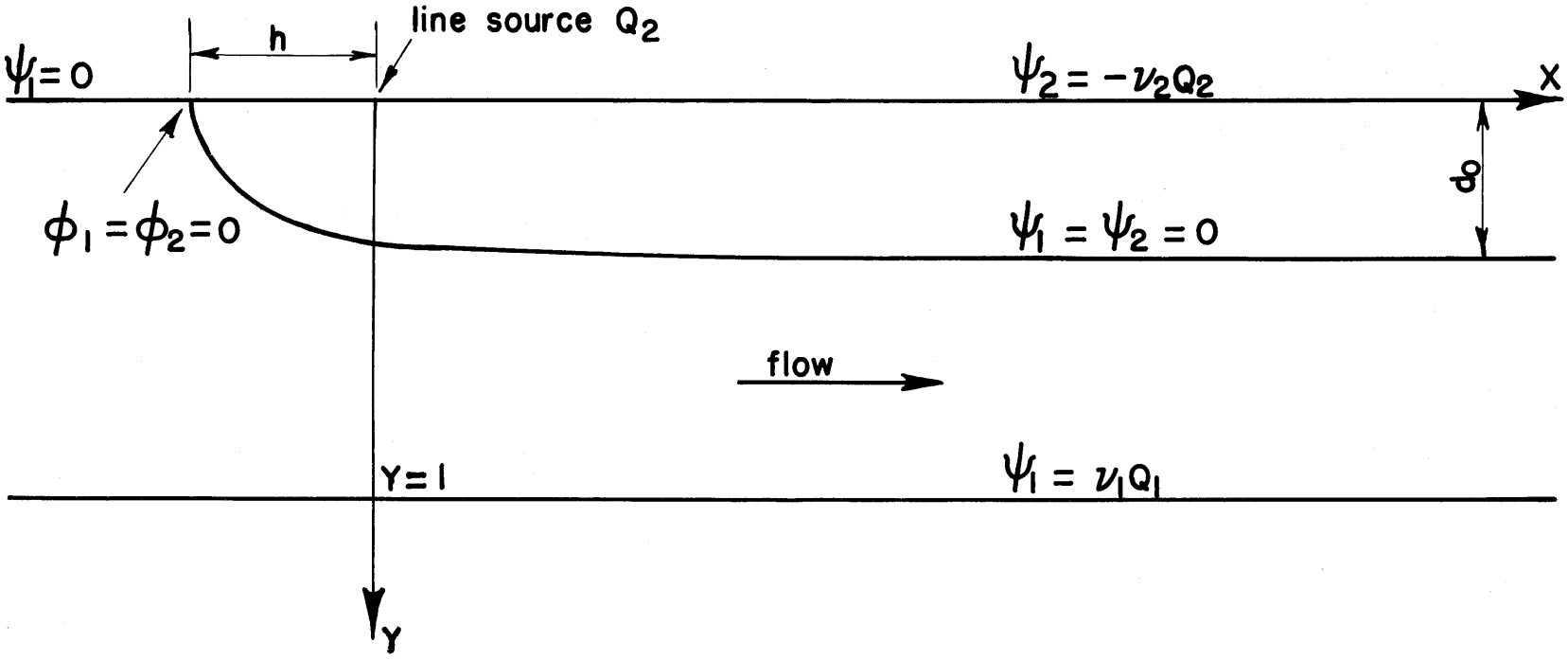

Figure 2.1 Boundary conditions for the zeroth order problem.

is known for equal densities. This zeroth order solution can be found in a straightforward manner (using image methods or conformal mapping) provided that non-dimensional velocity potentials and stream functions are defined as below

$$u_1 = \frac{\partial \varphi_{10}}{\partial x} = \frac{\partial \psi_{10}}{\partial y}$$

$$v_1 = \frac{\partial \varphi_{10}}{\partial y} = -\frac{\partial \psi_{10}}{\partial x}$$

$$\frac{\nu_2}{\nu_1} u_2 = \frac{\partial \varphi_{20}}{\partial x} = \frac{\partial \psi_{20}}{\partial y}$$

$$\frac{\nu_2}{\nu_1} v_2 = \frac{\partial \varphi_{20}}{\partial y} = -\frac{\partial \psi_{20}}{\partial x}$$

The problem is that defined in Figure 2.1.

The line source is represented by a logarithmic singularity of strength $2\nu_2 Q_2/\nu_1$. The solution for both φ_{10} and φ_{20} is given by the complex velocity potential

$$w(z) = \left(Q_1 + \frac{\nu_2 Q_2}{2\nu_1}\right)(z + h) + \frac{\nu_2 Q_2}{\pi \nu_1} \log \left(\frac{\sinh \frac{\pi z}{2}}{\sinh \frac{\pi h}{2}}\right) - \frac{i\nu_2 Q_2}{\nu_1} \qquad (2.28)$$

where the point $z = -h$ has been arbitrarily chosen to have

$$\text{Re } w(z) = \varphi_{10} = \varphi_{20} = 0$$

The shape of the interface is then given by $\psi_{10} = \psi_{20} = \text{Im } w(z) = 0$

which gives

$$\left(Q_1 + \frac{\nu_2 Q_2}{2\nu_1}\right) y + \frac{\nu_2 Q_2}{\pi \nu_1} \tan^{-1}\left(\coth \frac{\pi x}{2} \tan \frac{\pi y}{2}\right) - \frac{\nu_2 Q_2}{\nu_1} = 0 \quad (2.29)$$

which can be rewritten as

$$y - \zeta_o(x) = e^{-\pi x} - \frac{\sin\left[\pi y \coth \frac{\pi h}{2} + 1\right]}{\sin\left[\pi y \coth \frac{\pi h}{2} - 1\right]} = 0 \quad (2.30)$$

where

$$\frac{\pi h}{2} = \coth^{-1}\left(\frac{2\nu_1 Q_1}{\nu_2 Q_2} + 1\right), \quad (2.31)$$

as determined by placing

$$\frac{\partial \varphi}{\partial x}(-h, 0) = 0 \,..$$

The slope of the free surface can easily be determined and is given by

$$\zeta_o'(x) = \tan\theta = \zeta_o'\left(\zeta_o^{-1}(y)\right)$$

$$= \frac{\cos(\pi y) - \cos(\pi y \coth \frac{\pi h}{2})}{\sin(\pi y) \coth(\frac{\pi h}{2}) - \sin(\pi y \coth \frac{\pi h}{2})} \quad (2.32)$$

A velocity discontinuity exists across the interface for since there is a common pressure gradient on the dividing streamline it is obvious that

$$\nu_1 v_{1s} = \nu_2 v_{2s}$$

where v_{1s} and v_{2s} are the respective velocities along the streamline. It can easily be shown that

$$v_{1s} = \frac{\nu_2 Q_2}{2\nu_1 \sin \pi y}\left(\left[\sin(\pi y) \cdot \coth \frac{\pi h}{2} - \sin\left(\pi y \coth \frac{\pi h}{2}\right) \right]^2 + \left[\cos(\pi y) - \cos\left(\pi y \coth \frac{\pi h}{2}\right) \right]^2 \right) \qquad (2.33)$$

These results are now used to investigate the mixing along the interface.

2.4 Solution of the Dispersion Equation

As a result of being concerned only with steady flow the dispersion equation (1.13) can be written

$$\vec{q} \cdot \nabla C = \nabla \cdot (D \nabla C) \qquad (2.34)$$

Now for two dimensional flow with streamline coordinates equation (2.34) can be written

$$q(s) \cdot \frac{\partial C}{\partial s} = \frac{\partial}{\partial n}\left(D_T \frac{\partial C}{\partial n}\right) + \frac{\partial}{\partial s}\left(D_L \frac{\partial C}{\partial s}\right) \qquad (2.35)$$

provided that the radius of curvature of the streamlines is large, Wooding (3), Li (24).

D_L and D_T, the longitudinal and lateral coefficients of dispersion respectively, are functions of the seepage velocity q provided that the particle Reynolds number qd/ν is large enough ($> 10^{-2}$, Pfannkuch (10)) where d is the mean particle size. D_L and D_T are

constant at the molecular diffusion rate in a porous medium for very low Reynolds numbers.

Near the stagnation point the velocity is small, for it may be shown from equation (2.33) that $q \sim O(s)$ near this point; consequently D_L is almost constant and $\partial D_L/\partial s$ is approximately zero. Furthermore, $\partial^2 C/\partial s^2$ will be small compared to $\partial^2 C/\partial n^2$ since the diffusion zone will be very thin across the interface. The term

$$\frac{\partial}{\partial s}\left(D_L \frac{\partial C}{\partial s}\right)$$

is therefore ignored near the stagnation point.

Downstream, $q(s)$ becomes almost constant since the flow becomes uniform, so again D_L is constant and $\partial D_L/\partial s$ is zero $\partial^2 C/\partial s^2$ is again small for the same reason above.

Hence in a first approximation the longitudinal dispersion term

$$\frac{\partial}{\partial s}\left(D_L \frac{\partial C}{\partial s}\right)$$

is ignored compared to the lateral dispersion term

$$\frac{\partial}{\partial n}\left(D_T \frac{\partial C}{\partial n}\right)$$

Since the transverse dispersion coefficient D_T depends on q and to a first approximation q is constant within the band of dispersion (i.e. independent of the coordinate n), it is possible to write

$$q(s)\,\frac{\partial C}{\partial s} = D_T(s)\,\frac{\partial^2 C}{\partial n^2} \qquad (2.35)$$

The boundary conditions are that

$$C(0,n) = 1 \qquad (0 \le n < \infty)$$

$$C(0,n) = 0 \qquad (-\infty < n \le 0)$$

$$\frac{\partial C}{\partial n} = 0 \qquad (n = \pm\infty \text{ for all } s > 0)$$

The validity of the approximations made in writing this equation will become evident when the experimental results are presented later in Chapter 5.

Equation (2.35) can be solved easily by assuming there exists a function $h(s)$ such that a similarity solution may be found,

$$C = F\left(\frac{n}{h(s)}\right) = F(\eta) \qquad (2.36)$$

Now substituting equation (2.36) into equation (2.35) it is seen that (2.36) is a solution of

$$F''(\eta) + \eta\, F'(\eta) = 0 \qquad (2.37)$$

provided that

$$h'(s) \cdot h(s) = \frac{D_T(s)}{q(s)}$$

i.e.

$$h(s) = \left[2 \int^{s} \frac{D_T(s)}{q(s)}\, ds\right]^{\frac{1}{2}} \tag{2.38}$$

Now with the given boundary conditions equation (2.37) is easily solved to give

$$C(s,n) = \frac{1}{\sqrt{\pi}} \int_{-\infty}^{\eta/\sqrt{2}} e^{-t^2}\, dt = \frac{1}{2} + \frac{1}{2}\, \mathrm{erf}\left(\frac{\eta}{\sqrt{2}}\right) \tag{2.39}$$

where

$$\eta = \frac{n}{\left[2 \int^{s} \frac{D_T(s)}{q(s)}\, ds\right]^{\frac{1}{2}}} . \tag{2.40}$$

From section 2.3 it is possible to write

$$s = \int_{o}^{y} \left[1 + \left(\frac{dx}{dy}\right)^2\right]^{\frac{1}{2}} dy \tag{2.41}$$

where

$$\frac{dx}{dy} = \frac{\sin \pi y . \coth \frac{\pi h}{2} - \sin(\pi y \coth \frac{\pi h}{2})}{\cos(\pi y) - \cos(\pi y \coth \frac{\pi h}{2})} \tag{2.42}$$

and

$$q(s) = \frac{v_{ls}}{\epsilon}$$

where v_{ls} is given by equation (2.33) and the interface by equation (2.29).

It has been shown in this chapter that the shape of the interface in the two fluid system depicted in Figure 1.1 can be approximated

to within the order of the density difference. Furthermore, the mixing of the two fluids along the interface has been investigated using this approximate solution.

In Chapter 5 these results will be related to an experimental study and the validity of the approximations confirmed.

CHAPTER THREE

STABILITY OF THE INTERFACE

3.0 The Stability Equation

Experiments (see Chapter Five) have shown that it appears to be possible to have a more dense fluid in stable horizontal motion above a less dense fluid, a situation which cannot occur if the two fluids are at rest or in uniform vertical motion (Wooding, (19)). In other words, the horizontal motion of the interface between the two fluids appears to have a stabilizing effect.

In the previous chapter the mixing between two fluids when one was injected into the other was investigated. It was seen that the flow downstream tended to a uniform motion with one fluid on top of the other with a mixing layer between. Thus the stability of this system will be governed by much the same mechanism as if the two fluids had always been in parallel motion. The following system is therefore considered here.

A viscous fluid of density ρ_2 is assumed to be in uniform horizontal motion, in a homogeneous porous medium of intrinsic permeability k and porosity ϵ, with seepage velocity U in the positive x-direction overlying a similar fluid of density $\rho_1 (< \rho_2)$, also in uniform horizontal motion with the same velocity and in the same direction. The two flows are assumed to have been divided for $-\infty < x < 0$ and mixing begins to occur at the point $x = 0$. A stability investigation will be carried out by perturbing the equations of motion to

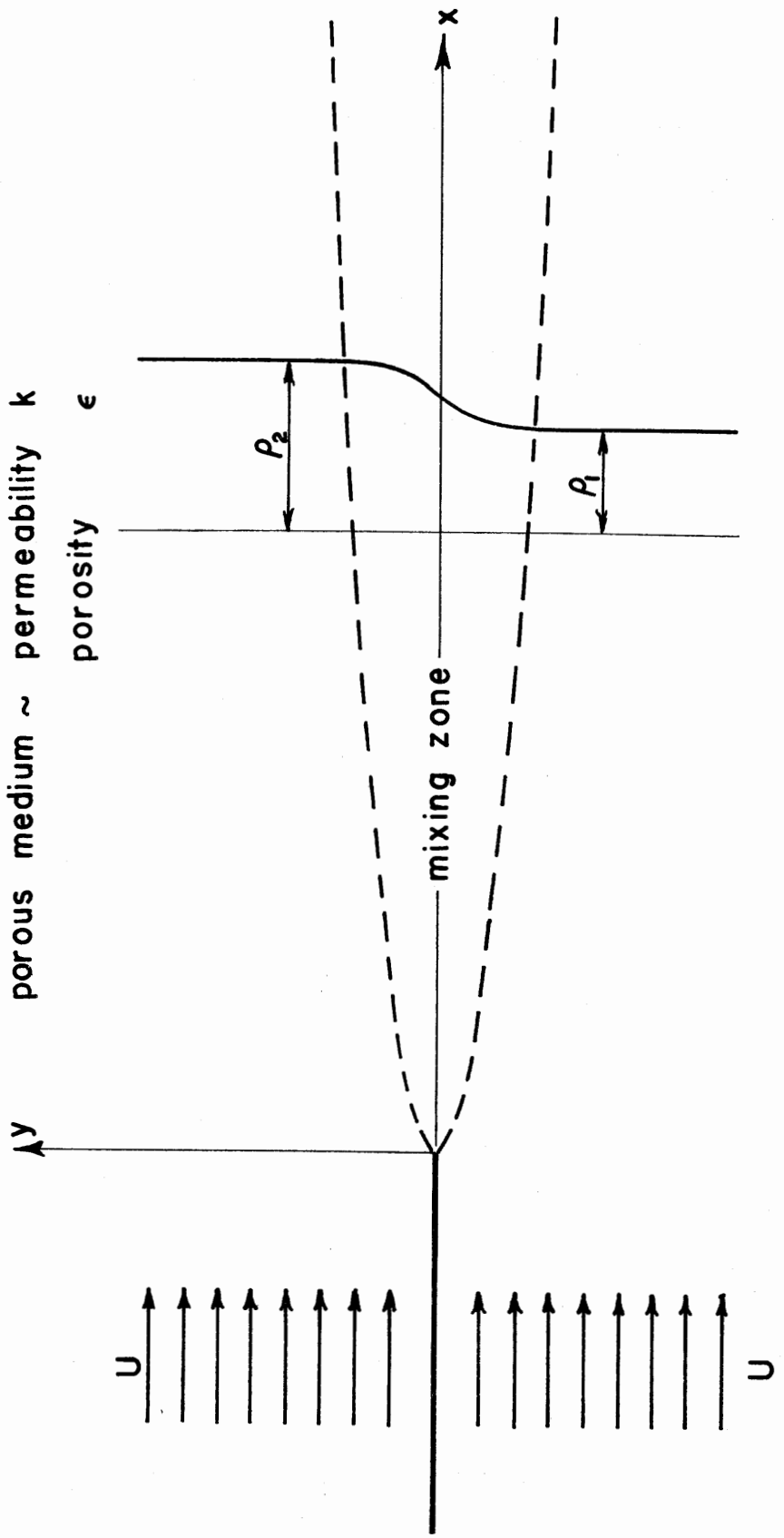

Figure 3.1 The flow geometry for the stability problem.

obtain a linear fourth order partial differential equation analogous to the Orr-Sommerfeld equation. The flow geometry is pictured in Figure 3.1.

The equations of motion are (see section 1.4)

$$\nabla \cdot \vec{q} = 0 \tag{3.1}$$

$$\nabla p + \rho g \vec{k} + \frac{\epsilon\mu}{k} \vec{q} = 0 \tag{3.2}$$

$$\frac{\partial \rho}{\partial t} + \vec{q} \cdot \nabla \rho = \nabla \cdot (D \nabla \rho) \tag{3.3}$$

Now introduce the non-dimensional quantities denoted below by asterisks and assuming constant viscosity

$$p = p^* (\rho_2 - \rho_1) g\ell \tag{3.4a}$$

$$(x,y) = (x^*,y^*) \ell \tag{3.4b}$$

$$\rho = \rho^* (\rho_2 - \rho_1) \tag{3.4c}$$

$$\vec{q} = \vec{q}^* U_o \tag{3.4d}$$

$$U_o = \frac{gk (\rho_2 - \rho_1)}{\epsilon\mu} \tag{3.4e}$$

where ℓ is a characteristic length yet to be defined and $u = U/U_o$.

The equations (3.4) are substituted into equations (3.3), (3.2), and (3.1) to give, after dropping asterisks,

$$\nabla \cdot \vec{q} = 0 \tag{3.5}$$

$$\nabla p + \rho \vec{k} + \vec{q} = 0 \tag{3.6}$$

$$\frac{\partial \rho}{\partial t} + \vec{q} \cdot \nabla \rho = \frac{\partial}{\partial x}\left(\frac{1}{\lambda_L}\frac{\partial \rho}{\partial x}\right) + \frac{\partial}{\partial y}\left(\frac{1}{\lambda_T}\frac{\partial \rho}{\partial y}\right) \tag{3.7}$$

and

$$\lambda_T = \frac{gk\,\ell\,(\rho_2 - \rho_1)}{\epsilon\, D_T\, \mu}\,, \tag{3.8}$$

$$\lambda_L = \frac{gk\,\ell\,(\rho_2 - \rho_1)}{\epsilon\, D_L\, \mu} \tag{3.9}$$

are the lateral and longitudinal Rayleigh numbers respectively.

The density ρ, pressure p, and velocities are now perturbed by small amounts denoted by a prime which is subsequently dropped when the orders of δ are collected.

$$p = P + \delta p' \tag{3.10a}$$

$$\rho = \Theta + \delta\theta' \tag{3.10b}$$

$$u = \mathcal{U} + \delta u' \tag{3.10c}$$

$$v = \delta v' \tag{3.10d}$$

As a first approximation it is assumed that the rate of growth of the mixing layer can be taken to be very small over some length so that it may be assumed that Θ is a function of y alone. This is tantamount to assuming the "sides" of the mixing zone are parallel and is the normal assumption in considering the stability of jets. It will be shown later that

$$\frac{\partial \Theta}{\partial x} \sim \frac{e^{-y^2/x}}{x^{3/2}}$$

which rapidly becomes small, compared to $\partial\Theta/\partial y$.

Equations (3.10) are substituted into equations (3.5), (3.6), and (3.7) and the order of δ collected to give

$$\frac{\partial u}{\partial x} + \frac{\partial v}{\partial y} = 0 \tag{3.11}$$

$$\frac{\partial p}{\partial x} + u = 0 \tag{3.12}$$

$$\frac{\partial p}{\partial y} + \theta + v = 0 \tag{3.13}$$

$$\frac{\partial \theta}{\partial t} + u \frac{\partial \theta}{\partial x} + v \frac{\partial \theta}{\partial y} = \frac{\partial}{\partial x}\left(\frac{1}{\lambda_L}\frac{\partial \theta}{\partial x}\right) + \frac{\partial}{\partial y}\left(\frac{1}{\lambda_T}\frac{\partial \theta}{\partial y}\right) \tag{3.14}$$

Since only two-dimensional disturbances are considered equation (3.11) implies the existence of a stream function such that

$$u = \frac{\partial \psi}{\partial y} \qquad v = -\frac{\partial \psi}{\partial x}$$

Elimination of p from (3.12) and (3.13) gives

$$\frac{\partial u}{\partial y} - \frac{\partial v}{\partial x} = \frac{\partial \theta}{\partial x} ,$$

i.e. $$\nabla^2 \psi = \frac{\partial \theta}{\partial x} \tag{3.15}$$

Equations (3.14) may be differentiated with respect to x to give

$$\frac{\partial}{\partial t}\left(\frac{\partial \theta}{\partial x}\right) + \mathcal{U}\frac{\partial}{\partial x}\left(\frac{\partial \theta}{\partial x}\right) - \frac{\partial^2 \psi}{\partial x} \cdot \frac{\partial \Theta}{\partial y} = \frac{\partial^2}{\partial x^2}\left(\frac{1}{\lambda_L}\frac{\partial \theta}{\partial x}\right) + \frac{\partial^2}{\partial y \partial x}\left(\frac{1}{\lambda_T}\frac{\partial \theta}{\partial y}\right) \qquad (3.16)$$

Now since $\mathcal{U}$ is assumed constant and λ_L and λ_T depend only on $\mathcal{U}$, equation (3.16) may be rewritten using (3.15) to give

$$\nabla^2 \frac{\partial \psi}{\partial t} + \mathcal{U}\nabla^2 \frac{\partial \psi}{\partial x} - \frac{\partial^2 \psi}{\partial x^2} \cdot \frac{\partial \Theta}{\partial y} = \frac{\partial^2}{\partial x^2}\left(\frac{1}{\lambda_L}\nabla^2 \psi\right) + \frac{\partial^2}{\partial y^2}\left(\frac{1}{\lambda_T}\nabla^2 \psi\right) \qquad (3.17)$$

Now suppose that arbitrary sinusoidal disturbances are represented by

$$\psi = \psi(y)\, e^{i(\alpha x - \alpha c t)}$$

where α is the non-dimensional wave number

$$\alpha = \frac{2\pi \ell}{L}$$

and where L is the wavelength of the disturbance;

$$c = c_r + i c_i$$

is the non-dimensional complex wave velocity and x and t are non-dimensional distance and time as defined previously. Then equation (3.17) becomes

$$\frac{1}{\lambda_T}\psi^{iv}(y) - \alpha^2 \psi''(y)\left(\frac{1}{\lambda_T} + \frac{1}{\lambda_L}\right) + \frac{\alpha^4}{\lambda_L}\psi(y) = i\alpha(\mathcal{U} - c)[\psi''(y) - \alpha^2 \psi(y)] + \alpha^2 \Theta' \psi(y) \qquad (3.18)$$

Note that making the assumption that λ_L and λ_T are independent of x is consistent with the approximation that Θ is independent of x, and therefore justifiable in a first approximation.

The equation (3.18) is rather similar to the Orr-Sommerfeld equation: This is not surprising, as it has already been mentioned that Wooding (17,3) has found that the equations governing the motion of a buoyant plume in a saturated porous medium are similar to those of a laminar momentum jet in incompressible flow. It would appear the dispersion plays a similar role with regard to mass transfer as viscosity does to momentum transfer in incompressible flow.

Equation (3.18) may be multiplied through by $\bar{\psi}(y)$, the complex conjugate of $\psi(y)$, and integrated from $-\infty$ to ∞. The boundary conditions on $\psi(y)$, namely that

$$\psi(\pm\infty) = 0 \tag{3.19a}$$

$$\psi'(\pm\infty) = 0 \tag{3.19b}$$

are equally true for $\bar{\psi}(y)$; hence when (3.18) is integrated, the result is

$$\int_{-\infty}^{\infty} \left(\frac{|\psi''(y)|^2}{\lambda_T} + \left(\frac{1}{\lambda_T} + \frac{1}{\lambda_L}\right) |\psi'(y)|^2 + \frac{\alpha^4}{\lambda_L} |\psi(y)|^2 \right) dy$$

$$= -i\alpha(\mathcal{U} - c) \int_{-\infty}^{\infty} \left(|\psi'(y)|^2 + \alpha^2 |\psi(y)|^2 \right) dy + \alpha^2 \int_{-\infty}^{\infty} \Theta' \cdot |\psi(y)|^2 \, dy \tag{3.20}$$

A similar operation may be carried out on the conjugate operator for $\bar{\psi}(y)$, multiplying through by $\psi(y)$, and this leads to equation (3.21)

$$\int_{-\infty}^{\infty} \left(\frac{|\psi''(y)|^2}{\lambda_T} + \left(\frac{1}{\lambda_T} + \frac{1}{\lambda_L} \right) |\psi'(y)|^2 + \frac{\alpha^4}{\lambda_L} |\psi(y)|^2 \right) dy$$

$$= + i\alpha(\mathcal{U} - \bar{c}) \int_{-\infty}^{\infty} \left(|\psi'(y)|^2 + \alpha^2 |\psi(y)|^2 \right) dy + \alpha^2 \int_{-\infty}^{\infty} \Theta' |\psi(y)|^2 \, dy \tag{3.21}$$

Subtracting (3.20) from (3.21) implies

$$2(\mathcal{U} - c_r) \int_{-\infty}^{\infty} \left(|\psi'(y)|^2 + \alpha^2 |\psi(y)|^2 \right) dy = 0$$

which implies that

$$\mathcal{U} = c_r$$

since the term under the integral is positive definite.

Thus any waves that might appear must have a phase velocity equal to the velocity of flow. Furthermore, equation (3.18) can be re-written

$$\frac{\psi^{iv}(y)}{\lambda_T} - \alpha^2 \psi''(y) \left(\frac{1}{\lambda_T} + \frac{1}{\lambda_L} \right) + \frac{\alpha^4}{\lambda_L} \psi(y)$$

$$= \alpha c_i [\psi''(y) - \alpha^2 \psi(y)] + \alpha^2 \Theta' \psi(y) \quad . \tag{3.22}$$

This equation plus the boundary conditions (3.19) defines an

eigenvalue problem which will now be investigated.

3.1 The Neutral Stability Curve

The equation (3.22) governing the stability can be rewritten

$$\psi^{iv}(y) - (\alpha^2(1 + \varkappa) + \lambda_T \alpha c_i)\psi''(y) + (\alpha^4 \varkappa + \lambda_T \alpha^3 c_i)\psi(y) - \lambda_T \alpha^2 \Theta' \psi(y) = 0 \tag{3.23}$$

and the boundary conditions

$$\psi(\pm \infty) = 0 \tag{3.24a}$$

$$\psi'(\pm \infty) = 0 \tag{3.24b}$$

where

$$\varkappa = \frac{\lambda_T}{\lambda_L} .$$

The neutral stability curve is the curve in the Rayleigh number - wave number plane (λ_T, α) which corresponds to disturbances which neither grow nor decay with time. Since equation (3.23) has real coefficients and has real boundary conditions then the neutral stability curve will be generated by the solutions of (3.23) with $c_i = 0$. In other words, the principle of exchange of stabilities is valid. Equation (3.23) (with $c_i = 0$) is of fourth order and has four linearly independent solutions and

$$\psi(y) = \sum_{i=1}^{4} A_i \psi_i(y) \tag{3.25}$$

By substituting (3.25) into the boundary conditions (3.24) four

homogeneous equations in four unknowns (A_i) are generated. For these four homogeneous equations to have non-trivial solutions for the A_i the determinant of the coefficients must vanish. This is the so called secular determinant and it generates the neutral stability curves in the (λ_T , α) plane with κ as a parameter.

However, it is generally not necessary to solve the equation (3.23) to generate the neutral stability curve. A well-known variational method due to S. Chandrasekhar (25) is now employed.

3.2 A Variational Method

Prior to proceeding with the development of the Chandrasekhar method consider Θ which is the steady state density distribution in the interfacial zone (see section 2.4)

$$\Theta = \frac{1}{\sqrt{\pi}} \int_{-\infty}^{\frac{\ell y}{2(DX/U)^{\frac{1}{2}}}} e^{-s^2} \, ds + \frac{\rho_1}{\rho_2 - \rho_1}$$

where D, X, and U are dimensional quantities, and X is the distance from the start of the mixing zone.

The two coordinates X and x can be regarded as a geographical coordinate and a local coordinate respectively. The aim of the stability analysis will be to investigate local stability in the region of the coordinate X and the approximation made will be that while Θ depends on X it is independent of κ . This is equivalent to assuming the mixing zone has parallel sides locally and is the usual approximation in

considering the stability of laminar jets etc.

Thus

$$\Theta'(y) = \frac{\ell}{2(\pi DX/U)^{\frac{1}{2}}} e^{-\frac{(\ell y)^2 U}{4DX}}$$

Now choose ℓ so that

$$\Theta'(0) = \frac{1}{2} ,$$

then

$$\ell = \left(\frac{\pi DX}{U}\right)^{\frac{1}{2}} \tag{3.26}$$

and

$$\Theta'(y) = \frac{1}{2} e^{-\frac{\pi y^2}{4}} \tag{3.27}$$

It is seen that ℓ depends on the geographical coordinate X but is supposed to be independent of the local coordinate x .

The assumption that the mixing zone has parallel sides can be checked here

$$\frac{\partial \Theta}{\partial X} \sim \frac{e^{-\frac{y^2}{X}}}{X^{\frac{3}{2}}}$$

and thus becomes small when X becomes large, hence the larger X the better the approximation.

Thus for neutral stability $(c_i = 0)$ we have

$$\psi^{iv}(y) - \alpha^2(1 + \varkappa)\psi''(y) + \alpha^4 \varkappa \psi(y) - \frac{\lambda\alpha^2}{2} e^{-\frac{\pi}{4} y^2} \psi(y) = 0 \tag{3.28}$$

where we have now written

$$\lambda = \lambda_T$$

and

$$\psi(\pm \infty) = 0 \tag{3.29a}$$

$$\psi'(\pm \infty) = 0 \ . \tag{3.29b}$$

The essence of the Chandrasekhar method is to expand the function $\psi(y)$ in orthogonal functions which satisfy the boundary conditions. The orthogonal functions on the doubly infinite range implicit in (3.24) are Hermite polynomials, Morse and Feshbach (26), thus we write

$$\psi(\zeta) = e^{-\zeta^2} \sum_{n=o}^{\infty} A_n H_n(\zeta) \tag{3.30}$$

where

$$\zeta = \sqrt{\frac{\pi}{4}} \cdot y \tag{3.31}$$

and

$$H_n(\zeta) = (-1)^n e^{\zeta^2} \frac{d^n\left|e^{-\zeta^2}\right|}{d\zeta^n}$$

Then

$$\psi''(\zeta) = e^{-\zeta^2} \sum_{n=o}^{\infty} A_n H_{n+2}(\zeta) \tag{3.32}$$

$$\psi^{iv}(\zeta) = e^{-\zeta^2} \sum_{n=o}^{\infty} A_n H_{n+4}(\zeta) \tag{3.33}$$

Substituting (3.30), (3.31), (3.32) and (3.33) into equation (3.28) leads to

$$\sum_{n=0}^{\infty} A_n e^{-\zeta^2} \left(\frac{H_{n+4}}{16}(\zeta) - \frac{(1+n)\alpha^2}{4\pi} H_{n+2}(\zeta) \right.$$

$$\left. + \frac{\alpha^4 n}{\pi^2} H_n(\zeta) - \frac{\lambda\alpha^2}{2\pi^2} e^{-\zeta^2} H_n(\zeta) \right) = 0 \qquad (3.34)$$

Now multiply equation (3.34) through by $H_m(\zeta)$ and use the orthogonality integral for Hermite polynomials

$$\int_{-\infty}^{\infty} H_m(\zeta) \cdot H_n(\zeta) e^{-\zeta^2} d\zeta = \delta_{mn} \cdot 2^n \cdot n! \sqrt{\pi}$$

This leads to

$$\sum_{n=0}^{\infty} a_{mn} A_n = 0 \qquad m = 0, 1, 2, \ldots \qquad (3.35)$$

and since

$$\int_{-\infty}^{\infty} e^{-2\zeta^2} H_m(\zeta) \cdot H_n(\zeta) d\zeta$$

$$= (-1)^{\frac{m-n}{2}} \cdot 2^{\frac{m+n-1}{2}} \cdot \Gamma\left(\frac{m+n+1}{2}\right) \chi_{(m,n)}$$

where

$$\chi_{(m,n)} = \begin{cases} 0 \text{ if } m+n \text{ is odd} \\ 1 \text{ if } m+n \text{ is even} \end{cases}$$

then

$$|a_{mn}| = \left| \frac{\delta_{mn+4}\, 2^{n+4}(n+4)!}{16} - \frac{\alpha^2(1+\varkappa)\,\delta_{mn+2}\, 2^{n+2}(n+2)!}{4\pi} \right.$$

$$\left. + \frac{\alpha^4 \varkappa}{\pi^2}\,\delta_{mn} \cdot 2^n \cdot n! - \frac{\lambda\alpha^2}{2\pi^{\frac{3}{2}}}\,(-1)^{\frac{m-n}{2}} \cdot 2^{\frac{m+n-1}{2}}\,\Gamma\left(\frac{m+n+1}{2}\right)\chi_{(m,n)} \right| \tag{3.36}$$

where $m,n = 0, 1, 2, \ldots$

Equation (3.35) can be regarded as an infinite number of homogeneous equations in an infinite number of unknowns A_n. For non-trivial solutions for A_n, $|a_{mn}| = 0$; thus equation (3.36) generates the neutral stability curve.

3.3 Variational Theory Results

In this section results are given from which a graph of Rayleigh number

$$\lambda = \frac{gk\ell\,(\rho_2 - \rho_1)}{\epsilon\, D_T\, \mu}$$

can be drawn as a function of α, the non-dimensional wave number, for neutrally stable disturbances.

To compute this curve, leading minors of the determinant (3.36) are successively put equal to zero. This then defines an intrinsic relation between λ, α and $\varkappa$. If values of $\varkappa$ and α are given and the lowest value of λ found at which the determinant vanishes then this gives a point on the neutral stability curve.

This Chandrasekhar process is often rapidly convergent in that only a low order leading minor need be taken in order to get a fairly

precise answer. However, in this case it was necessary to take the leading minor of order 10 to get sufficient accuracy. Furthermore, as the value of $\varkappa$ decreased the convergence became even slower as it also did for λ large.

The numerical calculations were carried out on the IBM 7094 in the Booth Computing Center at the California Institute of Technology. The determinants were evaluated using a standard library subroutine available for this purpose. The results are given for $\varkappa = 0.5$ and $\varkappa = 0.9$ and are the dashed lines on Figure 3.2.

Several interesting points are brought out by the results. The most obvious result is that the flow is always unstable when the Rayleigh number is positive, that is when $\rho_2 > \rho_1$. This is not surprising as the analogous incompressible flow, a free shear layer, is also always unstable, Tatsumi and Gotoh (27). However, there do exist waves which are not unstable at a given Rayleigh number. Another interesting result is that at a given Rayleigh number, an increase in the longitudinal dispersion will be stabilizing, that is the spectrum of unstable wave numbers is narrower. According to Harleman and Rumer (16) $\varkappa = \lambda_T/\lambda_L = D_L/D_T \sim U^{0.5}$ and $D_T \sim U^{0.7}$ and since $\ell \sim U^{-0.5}$ the effect of increasing the flow velocity will be to decrease the Rayleigh number and increase $\varkappa$. Thus increasing the flow velocity will reduce the spectrum of unstable wave numbers, or have a stabilizing effect. Thus the higher the velocity the longer the unstable waves.

3.4 An Approximate Solution

The density profile as specified by

$$\Theta(y) = \frac{1}{\sqrt{\pi}} \int_{-\infty}^{\frac{\sqrt{\pi}y}{2}} e^{-t^2}\, dt + \frac{\rho_1}{\rho_2 - \rho_1}$$

can be approximated by the profile

$$\Theta(y) = 1 + \frac{\rho_1}{\rho_2 - \rho_1}, \qquad y \geq 1$$

$$\Theta(y) = \frac{y + 1}{2} + \frac{\rho_1}{\rho_2 - \rho_1}, \qquad |y| \leq 1$$

$$\Theta(y) = \frac{\rho_1}{\rho_2 - \rho_1} \qquad y \leq -1$$

Then

$$\Theta'(y) = \begin{cases} 0, & |y| > 1 \\ \frac{1}{2} & |y| < 1 \end{cases} \tag{3.37}$$

and the equations of motion become

$$\psi^{iv}(y) - (1 + \varkappa)\alpha^2\psi''(y) + \alpha^4\varkappa\psi(y) = \lambda\alpha c_i[\psi''(y) - \alpha^2\psi(y)], \quad |y| > 1 \tag{3.38}$$

$$\psi^{iv}(y) - (1 + \varkappa)\alpha^2\psi''(y) + \alpha^4\psi(y) = \lambda\alpha c_i[\psi''(y) - \alpha^2\psi(y)] + \frac{\lambda\alpha^2}{2}\psi(y), \quad |y| < 1 \tag{3.39}$$

and these equations are easily solved. It will be noted that c_i has not been put equal to zero this time as it is desired to investigate the growth rates of unstable waves. The boundary conditions are given

in equations (3.24). However, these boundary conditions only apply to the outer equations (3.38) and matching conditions must be determined by which the solutions of the inner (3.39) and outer (3.38) equations can be related. These matching conditions are required at the points $y = \pm 1$ and are obtained by integrating equation (3.23) between $1 - \epsilon$ and $1 + \epsilon$ and taking the limit as $\epsilon \to 0$; similarly between $-1 - \epsilon$ and $-1 + \epsilon$ (Esch, (28)). This gives, considering the first case

$$[\psi'''(y)]_{1-\epsilon}^{1+\epsilon} - \alpha^2(1 + \kappa)[\psi'(y)]_{1-\epsilon}^{1+\epsilon} + \alpha^4 \kappa \int_{1-\epsilon}^{1+\epsilon} \psi(y)\, dy$$

$$= \lambda\alpha c_i[\psi(y)]_{1-\epsilon}^{1+\epsilon} - \alpha^2 \int_{1-\epsilon}^{1+\epsilon} \psi(y)\, dy + \lambda\alpha^2 \int_{1-\epsilon}^{1+\epsilon} \Theta'(y)\psi(y)\, dy \quad .$$

Now suppose $\psi(y)$ is continuous, then we can write

$$\lim_{\epsilon\to 0} \int_{1-\epsilon}^{1+\epsilon} \Theta'\psi(y)\, dy = \lim_{\epsilon\to 0} [\Theta\psi(y)]_{1-\epsilon}^{1+\epsilon} - \lim_{\epsilon\to 0} \int_{1-\epsilon}^{1+\epsilon} \Theta\psi'(y)\, dy$$

$$= - \lim_{\epsilon\to 0} \int_{1-\epsilon}^{1+\epsilon} \Theta\psi'(y)\, dy = \lim_{\epsilon\to 0} A \int_{1-\epsilon}^{1+\epsilon} \psi'(y)\, dy$$

$$\longrightarrow 0$$

since $\Theta \to A =$ constant at $y = 1 \pm \epsilon$. Thus if $\psi(y)$ is continuous then $\psi'(y)$, $\psi''(y)$ and $\psi'''(y)$ are continuous at $y = 1$ also. A similar argument applies at $y = -1$.

The solutions of (3.38) can be written down as

$$\psi(y) = A_1 e^{-\alpha y} + A_2 e^{-\beta y} + A_3 e^{\alpha y} + A_4 e^{\beta y} , \quad |y| > 1$$

where

$$\beta = \sqrt{\alpha^2 \kappa + \lambda \alpha c_i} \tag{3.40}$$

But the boundary conditions (3.24) imply that

$$\psi(y) = A_1 e^{-\alpha y} + A_2 e^{-\beta y} , \quad y > 1 \tag{3.41}$$

$$\psi(y) = A_3 e^{\alpha y} + A_4 e^{\beta y} , \quad y < -1 \tag{3.42}$$

For $|y| < 1$ there are three solutions which must be considered separately and they correspond to the three cases implied by

$$\lambda \gtrless \frac{2\alpha^2 \kappa}{1 - 2\alpha c_i}$$

Case I

$$\lambda > \frac{2\alpha^2 \kappa}{1 - 2\alpha c_i} \tag{3.43}$$

The solution of equation (3.39) can be written as

$$\psi_I(y) = B_1 e^{\gamma y} + B_2 e^{-\gamma y} + B_3 e^{\delta y} + B_4 e^{-\delta y} , \quad |y| < 1 \tag{3.44}$$

where

$$\gamma = \left(\frac{\alpha^2(1+\kappa) + \lambda\alpha c_i}{2} - \left[\left(\frac{\alpha^2}{2}(1-\kappa) - \frac{\lambda\alpha c_i}{2} \right)^2 + \frac{\lambda\alpha^2}{2} \right]^{\frac{1}{2}} \right)^{\frac{1}{2}} \tag{3.45}$$

$$\delta = \left(\frac{\alpha^2(1+\kappa) + \lambda\alpha c_i}{2} + \left[\left(\frac{\alpha^2}{2}(1-\kappa) - \frac{\lambda\alpha c_i}{2} \right)^2 + \frac{\lambda\alpha^2}{2} \right]^{\frac{1}{2}} \right)^{\frac{1}{2}} \tag{3.46}$$

Case II

When

$$\lambda = \frac{2\alpha^2\kappa}{1 - 2\alpha c_i} \tag{3.47}$$

then

$$\gamma = 0$$

and equation (3.39) has a solution

$$\psi_{II}(y) = B_1 + B_2 y + B_3 e^{\delta y} + B_4 e^{-\delta y} \tag{3.48}$$

Case III

When

$$\lambda < \frac{2\alpha^2\kappa}{1 - 2\alpha c_i} \tag{3.49}$$

equation (3.39) has the solution

$$\psi_{III}(y) = B_1 \cos \gamma y + B_2 \cosh \delta y + B_3 \sin \gamma y + B_4 \sinh \delta y \tag{3.50}$$

where

$$\gamma = \left(\left(\left(\frac{\alpha^2(1-\kappa)}{2} - \frac{\lambda\alpha c_i}{2} \right)^2 + \frac{\lambda\alpha^2}{2} \right)^{\frac{1}{2}} - \frac{\alpha^2(1+\kappa) + \lambda\alpha c_i}{2} \right)^{\frac{1}{2}} \tag{3.51}$$

Each one of these three cases must be investigated separately. The four matching conditions at $y = \pm 1$ will give eight homogeneous equations in 8 unknowns, the four A_i and four B_i. For these eight equations to have non-trivial solutions the determinant of the coefficients of the A_i, B_i must vanish. This will generate the secular equation and there will be three such secular equations, corresponding to the three cases above, to investigate. Each of these will involve simplifying an 8 x 8 determinant, but fortunately the labor is not excessive.

i) Case I $\quad \lambda < \dfrac{2\alpha^2\kappa}{1 - 2\alpha c_i}$

The determinant obtained from the matching conditions at $y = \pm 1$ is

$$\begin{vmatrix}
1 & 1 & 0 & 0 & e^{\gamma} & e^{\delta} & -e^{-\gamma} & -e^{-\delta} \\
0 & 0 & 1 & 1 & e^{-\gamma} & e^{-\delta} & -e^{\gamma} & -e^{\delta} \\
-\alpha & -\beta & 0 & 0 & \gamma e^{\gamma} & \delta e^{\delta} & \gamma e^{-\gamma} & \delta e^{-\delta} \\
0 & 0 & \alpha & \beta & \gamma e^{-\gamma} & \delta e^{-\delta} & \gamma e^{\gamma} & \delta e^{\delta} \\
\alpha^2 & \beta^2 & 0 & 0 & \gamma^2 e^{\gamma} & \delta^2 e^{\delta} & -\gamma^2 e^{-\gamma} & -\delta^2 e^{-\delta} \\
0 & 0 & \alpha^2 & \beta^2 & \gamma^2 e^{-\gamma} & \delta^2 e^{-\delta} & -\gamma^2 e^{\gamma} & -\delta^2 e^{\delta} \\
-\alpha^3 & -\beta^2 & 0 & 0 & \gamma^3 e^{\gamma} & \delta^3 e^{\delta} & \gamma^3 e^{-\gamma} & \delta^3 e^{-\delta} \\
0 & 0 & \alpha^3 & \beta^3 & \gamma^3 e^{-\gamma} & \delta^3 e^{-\delta} & \gamma^3 e^{\gamma} & \delta^3 e^{\delta}
\end{vmatrix} = 0$$

This determinant simplifies to (the details are given in Appendix B),

$$(\gamma + \alpha)^2 (\gamma + \beta)^2 (\delta + \alpha)^2 (\delta + \beta)^2 (\gamma - \delta)^2$$

$$8\gamma\delta (\delta^2 - \alpha^2) (\delta^2 - \beta^2) (\gamma^2 - \alpha^2)(\gamma^2 - \beta^2) e^{-2(\gamma + \delta)}$$

$$-e^{-4\gamma} (\delta + \alpha)^2 (\delta + \beta)^2 (\gamma - \alpha)^2 (\gamma - \beta)^2 (\gamma + \delta)^2$$

$$-e^{-4\delta} (\delta - \alpha)^2 (\delta - \beta)^2 (\gamma + \alpha)^2 (\gamma + \beta)^2 (\gamma + \delta)^2 \qquad = \quad 0$$

This intrinsic relation for α, c_i, ν and λ was investigated numerically to determine if any positive roots for λ existed when α, c_i and ν were given. The determinant appeared to be a positive monotonically increasing function of α for all values of λ, c_i and ν chosen and an intensive search found no roots on the (λ, α) plane. It was concluded no roots of any physical significance exist for Case I.

ii) Case II $\qquad \lambda = \dfrac{2\alpha^2\nu}{1 - 2\alpha c_i}$

The determinant can easily be written down using the matching conditions and solutions (3.48), (3.41) and (3.42)

$$\begin{vmatrix}
1 & 1 & 0 & 0 & 1 & 1 & e^{\delta} & e^{-\delta} \\
0 & 0 & 1 & 1 & 1 & -1 & e^{-\delta} & e^{\delta} \\
-\alpha & -\beta & 0 & 0 & 0 & 1 & \delta e^{\delta} & -\delta e^{-\delta} \\
0 & 0 & \alpha & \beta & 0 & 1 & \delta e^{-\delta} & -\delta e^{\delta} \\
\alpha^2 & \beta^2 & 0 & 0 & 0 & 0 & \delta^2 e^{\delta} & \delta^2 e^{-\delta} \\
0 & 0 & \alpha^2 & \beta^2 & 0 & 0 & \delta^2 e^{-\delta} & \delta^2 e^{\delta} \\
-\alpha^3 & -\beta^3 & 0 & 0 & 0 & 0 & \delta^3 e^{\delta} & -\delta^3 e^{-\delta} \\
0 & 0 & \alpha^3 & \beta^3 & 0 & 0 & \delta^3 e^{-\delta} & -\delta^3 e^{\delta}
\end{vmatrix} = 0$$

The determinant can be simplified to

$$\left| e^{\delta}(\delta + \alpha)\,(\delta + \beta)\,[\delta(\alpha\beta + \alpha + \beta) - \alpha\beta] \right.$$

$$\left. + e^{-\delta}\,(\delta - \alpha)\,(\delta - \beta)\,[\delta(\alpha\beta + \alpha + \beta) + \alpha\beta] \right| \ .$$

$$\left| e^{\delta}(\delta + \alpha)\,(\delta + \beta) - e^{-\delta}(\delta - \alpha)\,(\delta - \beta) \right| = 0 \qquad (3.52)$$

and since $r = 0$ and $\lambda = 2\alpha^2\kappa/(1 - 2\alpha c_i)$

$$\beta = \alpha\sqrt{\frac{\kappa}{1 - 2\alpha c_i}}$$

$$\delta = \alpha\sqrt{1 + \frac{\kappa}{1 - 2\alpha c_i}}$$

The behavior for $c_i = 1/2\alpha$ is disregarded for the moment and will be discussed later, (see page 56).

A simple investigation of the roots of (3.52) when $c_i = 0$ shows that there are only negative values of λ when α and κ are real and positive. There is no indication of any positive roots for λ even when $c_i \neq 0$.

iii) Case III $\qquad \lambda > \dfrac{2\alpha^2\kappa}{1 - 2\alpha c_i}$

The determinant is again easily evaluated using solution $\psi_{III}(y)$ (equation (3.50)) and solutions (3.41) and (3.42) and the matching conditions at $y = \pm 1$. The determinant is

$$\begin{vmatrix} 1 & 1 & 0 & 0 & -\cos\gamma & -\cosh\delta & -\sin\gamma & -\sinh\delta \\ 0 & 0 & 1 & 1 & -\cos\gamma & -\cosh\delta & \sin\gamma & \sinh\delta \\ -\alpha & -\beta & 0 & 0 & \gamma\sin\gamma & -\delta\sinh\delta & -\gamma\cos\gamma & -\delta\cosh\delta \\ 0 & 0 & \alpha & \beta & -\gamma\sin\gamma & \delta\sinh\delta & -\gamma\cos\gamma & -\delta\cosh\delta \\ \alpha^2 & \beta^2 & 0 & 0 & \gamma^2\cos\gamma & -\delta^2\cosh\delta & \gamma^2\sin\gamma & -\delta^2\sinh\delta \\ 0 & 0 & \alpha^2 & \beta^2 & \gamma^2\cos\gamma & -\delta^2\cosh\delta & -\gamma^2\sin\gamma & \delta^2\sinh\delta \\ -\alpha^3 & -\beta^3 & 0 & 0 & -\gamma^3\sin\gamma & -\delta^3\sinh\delta & \gamma^3\cos\gamma & -\delta^3\cosh\delta \\ 0 & 0 & \alpha^3 & \beta^3 & \gamma^3\sin\gamma & \delta^3\sinh\delta & \gamma^3\cos\gamma & -\delta^3\cosh\delta \end{vmatrix} = 0$$

and can be simplified with some labor to two factors

$$\delta\sin\gamma\left|\alpha\beta(\gamma^2+\delta^2) - (\gamma^2\delta^2 - \alpha^2\beta^2) + \gamma^2(\alpha^2+\beta^2)\right|$$

$$+ \gamma\cos\gamma\tanh\delta\left|\alpha\beta(\gamma^2+\delta^2) + (\gamma^2\delta^2 - \alpha^2\beta^2) + \delta^2(\alpha^2+\beta^2)\right|$$

$$+ \sin\gamma\tanh\delta\cdot\alpha\beta(\alpha+\beta)(\gamma^2+\delta^2) + \cos\gamma\cdot(\alpha+\beta)\gamma\delta(\gamma^2+\delta^2) = 0 \qquad (3.53)$$

and

$$\gamma\sin\gamma\left|\alpha\beta(\gamma^2+\delta^2) + \delta^2(\alpha^2+\beta^2) + \gamma^2\delta^2 - \alpha^2\beta^2\right|$$

$$-\delta\cos\gamma\cdot\tanh\delta\left|\alpha\beta(\gamma^2+\delta^2) + \gamma^2(\alpha^2+\beta^2) - (\gamma^2\delta^2 - \alpha^2\beta^2)\right|$$

$$+ \gamma\delta\sin\gamma\tanh\delta\cdot(\alpha+\beta)(\gamma^2+\delta^2) - \cos\gamma\cdot(\alpha+\beta)\alpha\beta(\gamma^2+\delta^2) = 0 \qquad (3.54)$$

where γ is defined by equation (3.51), δ by equation (3.46) and β by (3.40).

The roots of these two factors are investigated numerically and

the results given in a later section.

With the use of these approximate solutions that have been developed it is possible to determine not only the neutral stability curves but curves of constant c_i in the (λ, α) plane. These curves determine the growth rate of any instability that occurs.

Considering again the case where

$$\lambda = \frac{2\alpha^2 \kappa}{1 - 2\alpha c_i}$$

it appears that the growth rate may be bounded at $\alpha c_i = \frac{1}{2}$ and since the amplification of unstable disturbances, $e^{\alpha c_i t}$, depends on αc_i it appears that the amplification of unstable waves may be bounded.

3.5 Results from Approximate Theory

In this section detailed computed results are given for the shape of the neutral stability curve and the maximum growth rates of unstable waves. It has already been stated that there are no apparent roots for Case I or Case II when

$$\lambda \leq \frac{2\alpha^2 \kappa}{1 - 2\alpha c_i} \quad .$$

For Case III,

$$\text{i.e.} \quad \lambda > \frac{2\alpha^2 \kappa}{1 - 2\alpha c_i}$$

there is one obvious root of equation (3.53) namely $\gamma = 0$. However, this is Case II for which the solution to the differential equations

is different from Case III. It so happens that when $\gamma = 0$ the determinant in Case II is not identically zero so $\gamma = 0$ is an extraneous root of Case III. The correct roots are plotted in Figure 3.2 to show the comparison with the results of the variational theory. It is seen that the variational theory gives somewhat more stable results. Since it is known that variational methods of the Rayleigh-Ritz family generally overestimate the stability of a given system it would seem that the results of linearizing the profile are quite reasonable.

The neutral stability curves for four values of κ are also plotted on logarithmic graph paper on Figure 3.3, where it appears that the neutral stability curves are asymptotic to $\lambda = 2\alpha^2\kappa$ when α becomes large. It will be recalled that

$$\lambda = 2\alpha^2\kappa$$

with $c_i = 0$ corresponds to $\gamma = 0$. This result then explains the extraneous root $\gamma = 0$ in Case III; it is actually an asymptote to the correct result.

Curves of constant amplification rates can be computed from equations (3.53) and (3.54) by choosing a fixed positive value of c_i in the definitions of γ (equation (3.51)), δ, equation (3.46) and β, equation (3.40) and then evaluating the roots for λ when α and κ are given. The results of such a computation are shown in Figures 3.4, 3.5 and 3.6 which gives curves of constant c_i in the (λ, α) plane for values $\kappa = 0.1, 0.9, 5.0$ respectively.

From these results it is possible to draw curves of α versus

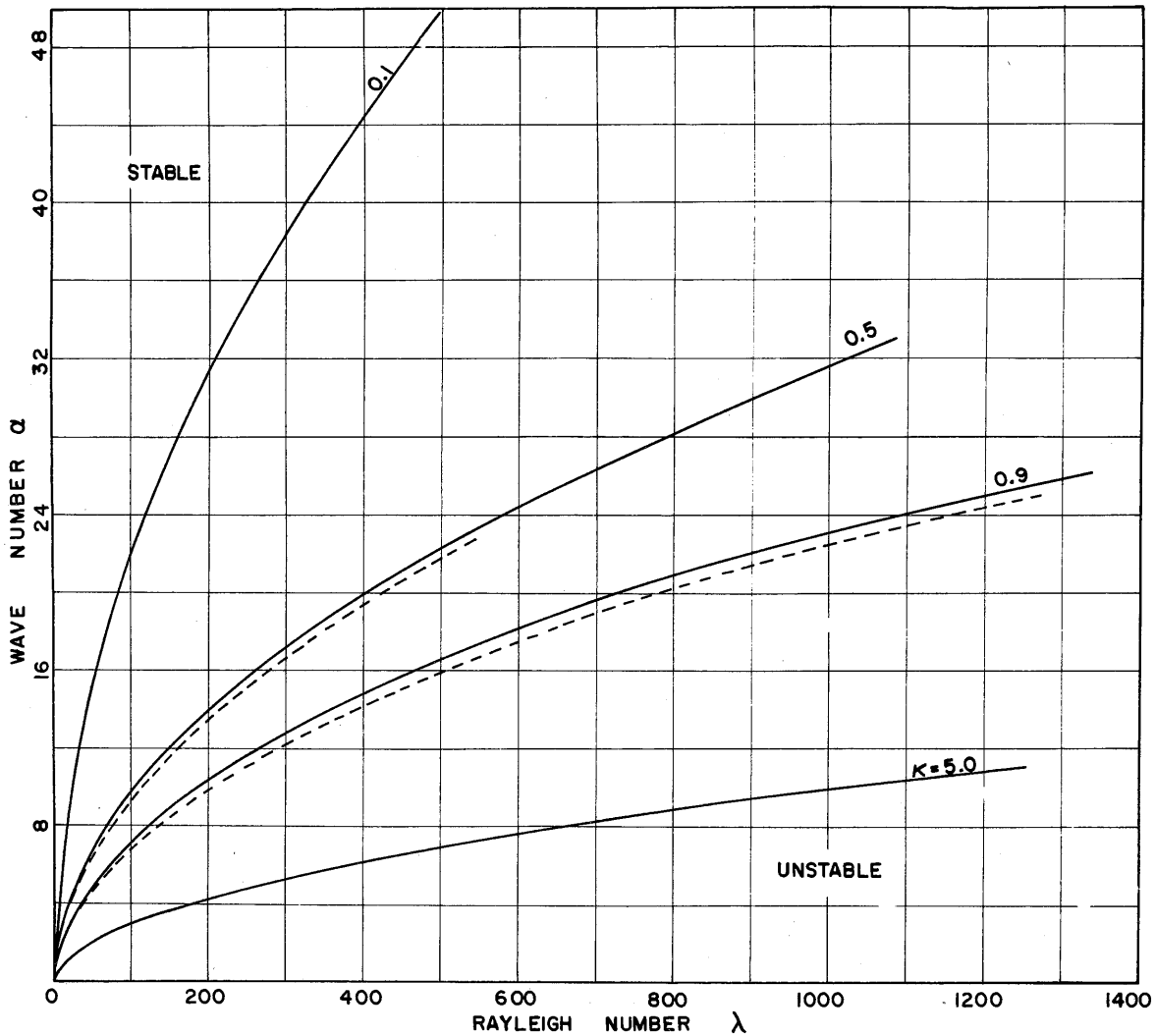

Figure 3.2 Neutral stability curves (full line-linearized density profile, broken line - exact density profile).

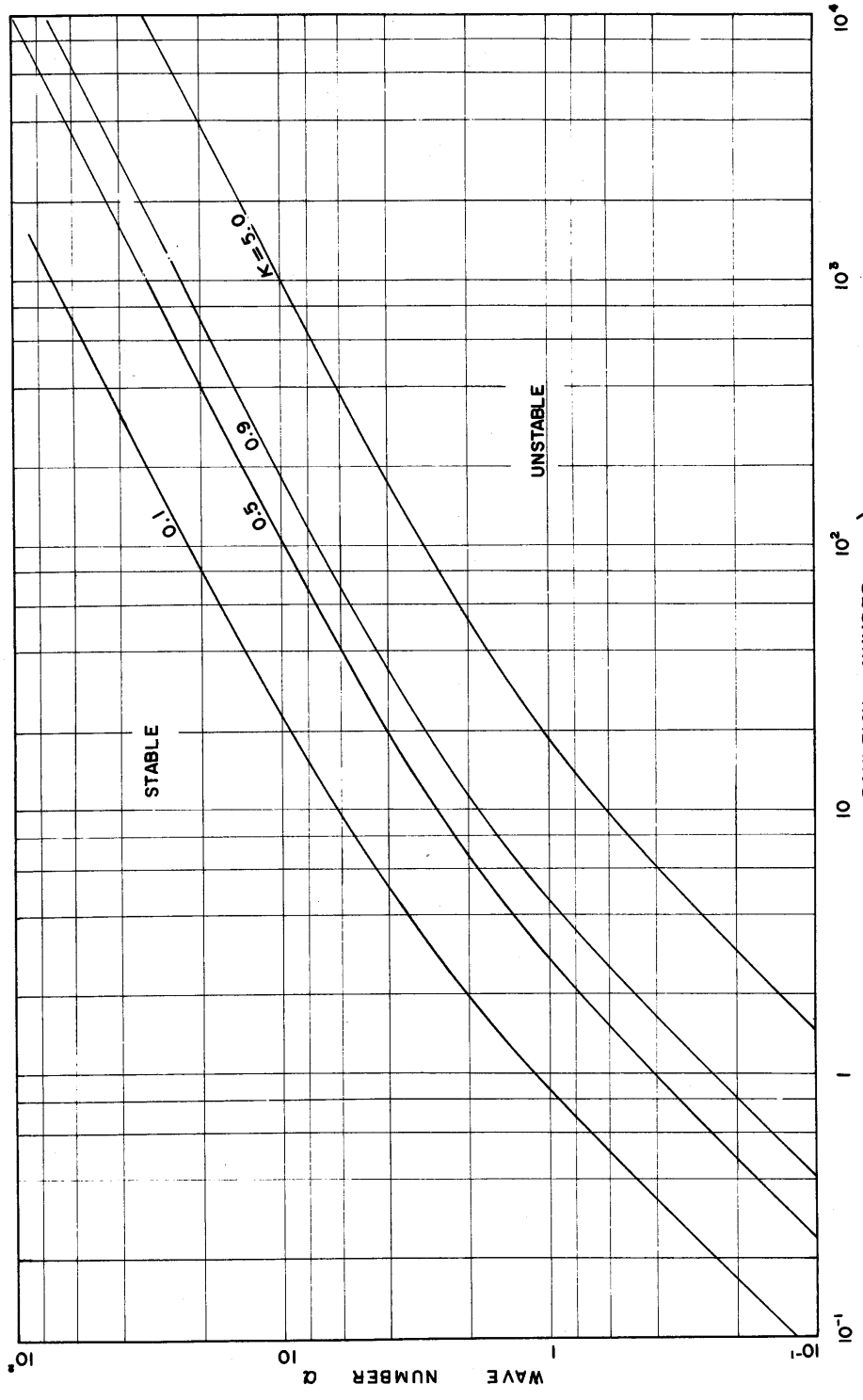

Figure 3.3 Neutral stability curves plotted on logarithmic paper.

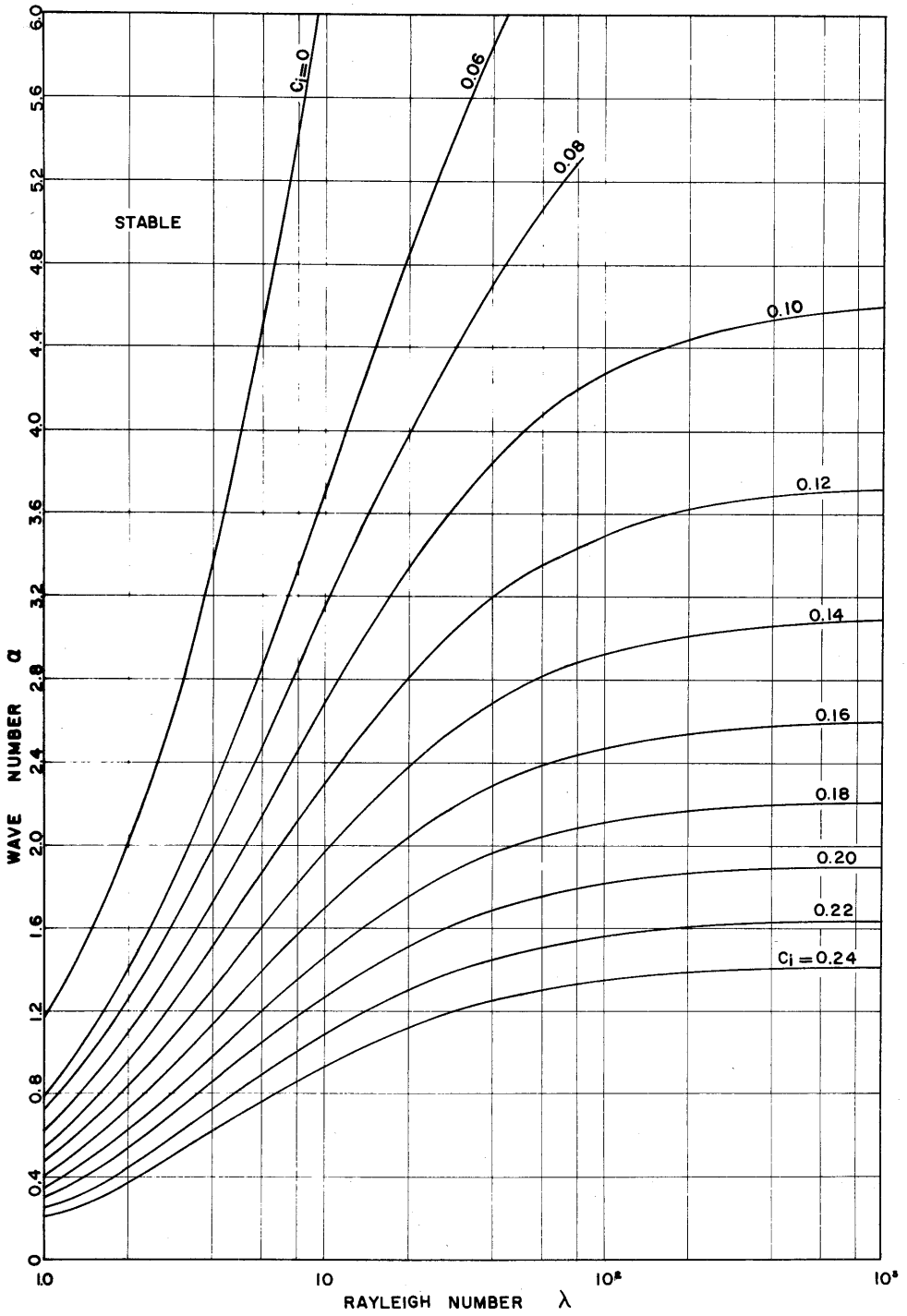

Figure 3.4 Curves of constant c_i for $\varkappa = 0.1$.

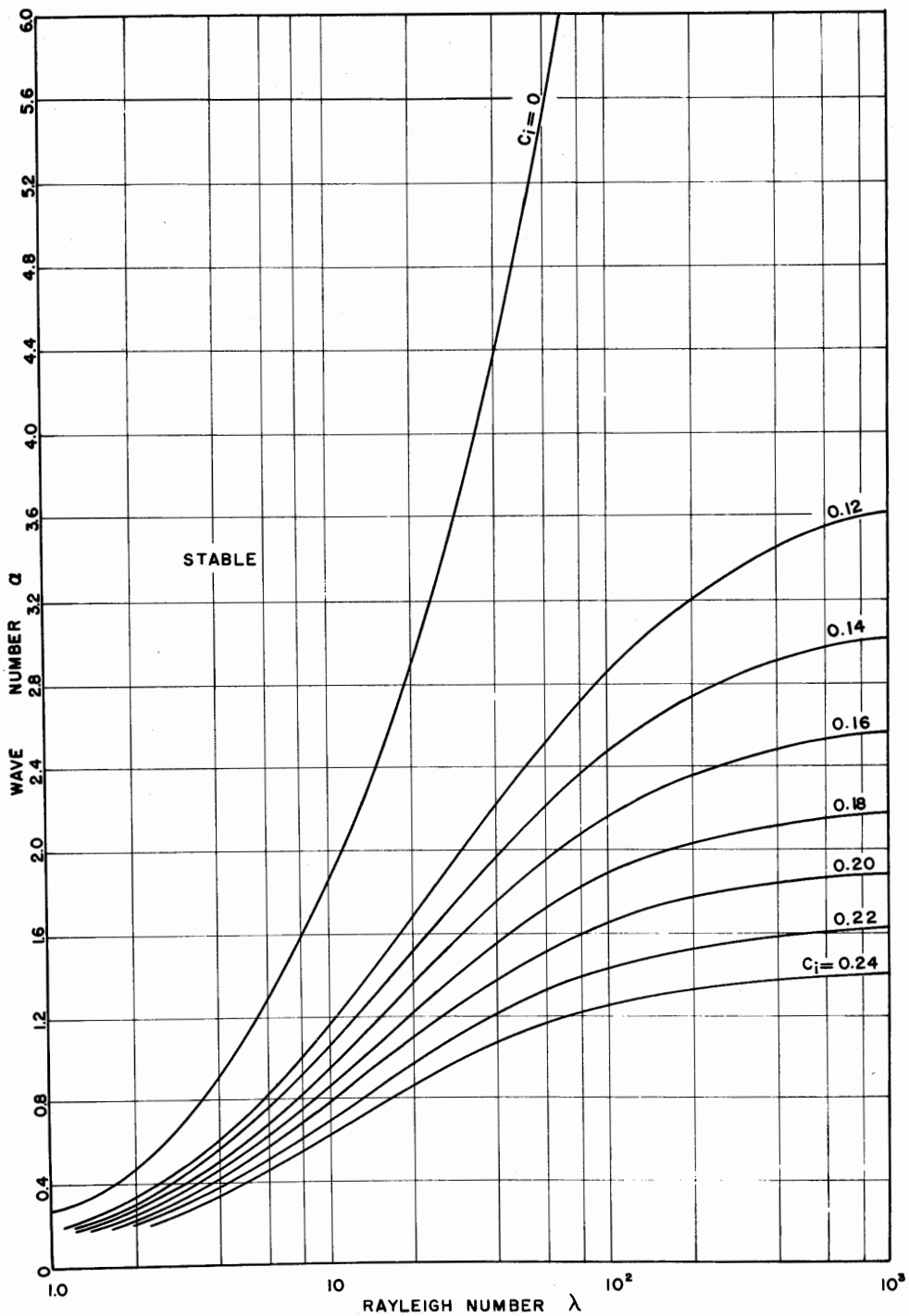

Figure 3.5 Curves of constant c_i for $\varkappa = 0.9$.

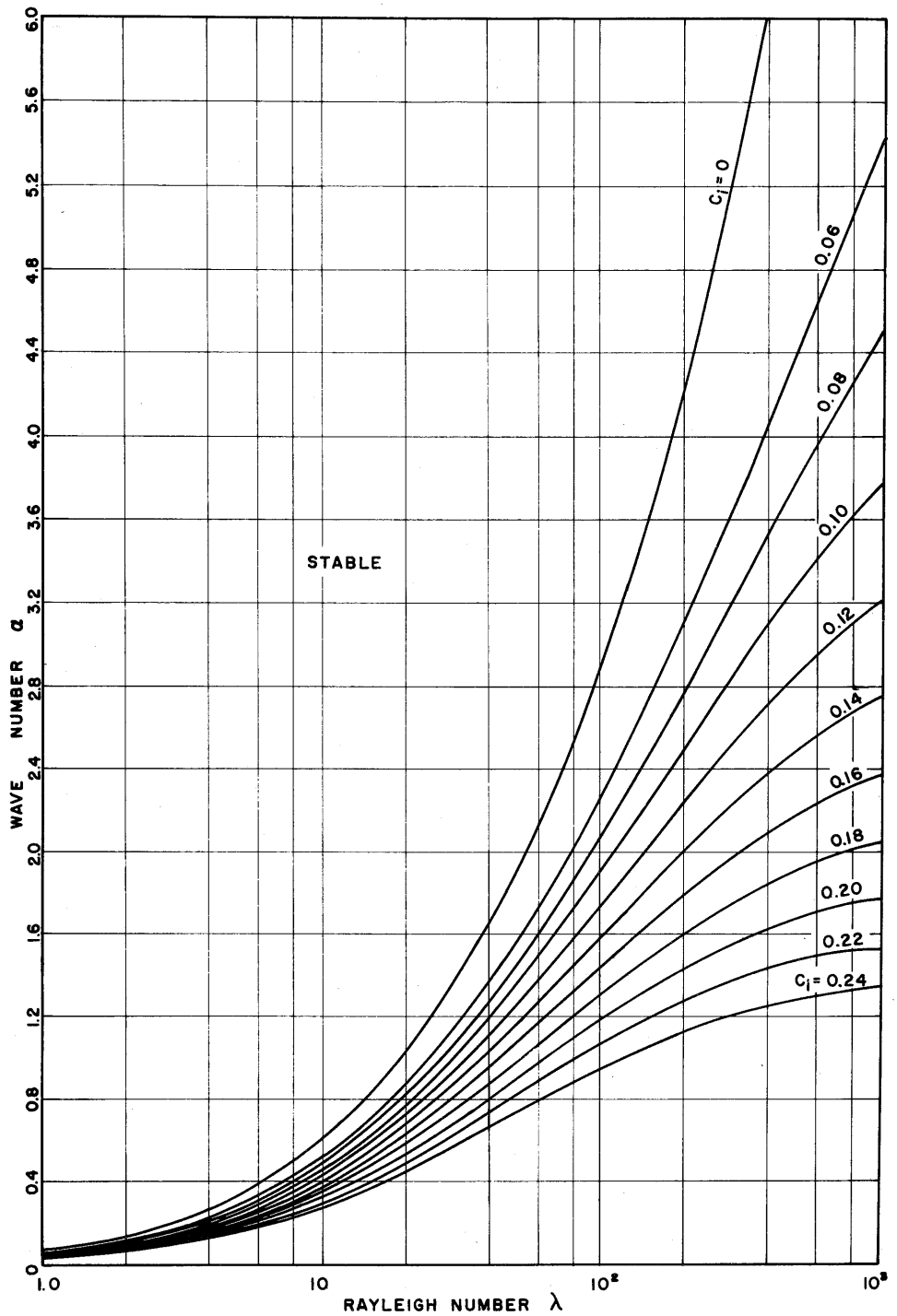

Figure 3.6 Curves of constant c_i for $\mu = 5.0$.

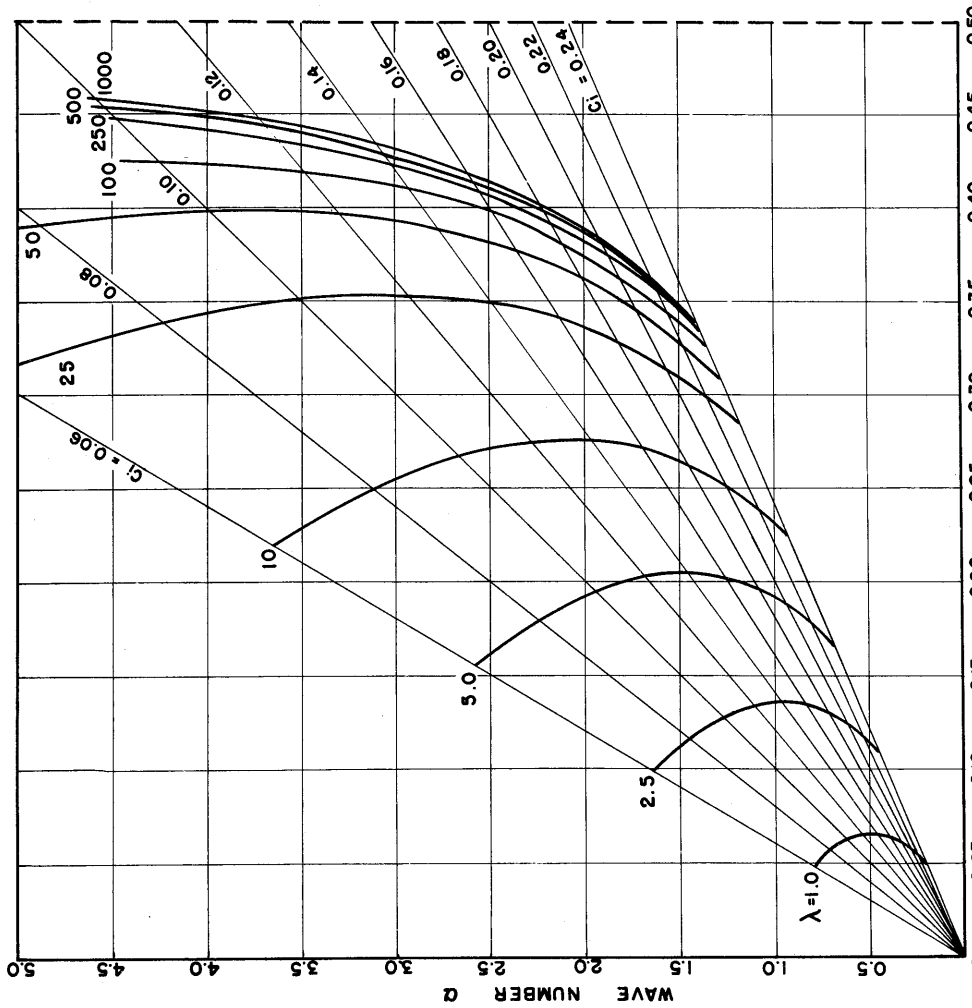

Figure 3.7 Growth rate factors at constant Rayleigh number for $\mathcal{M} = 0.1$.

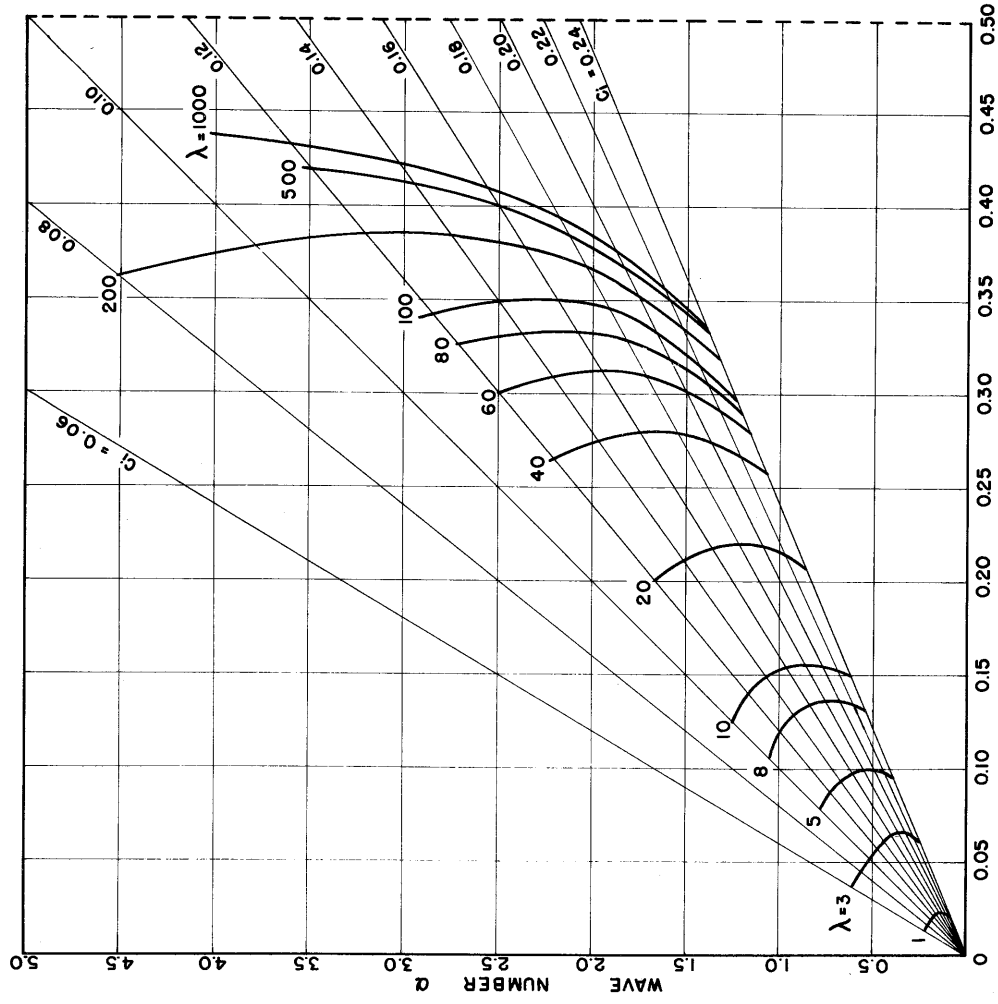

Figure 3.8 Growth rate factors at constant Rayleigh number for $\kappa = 0.9$.

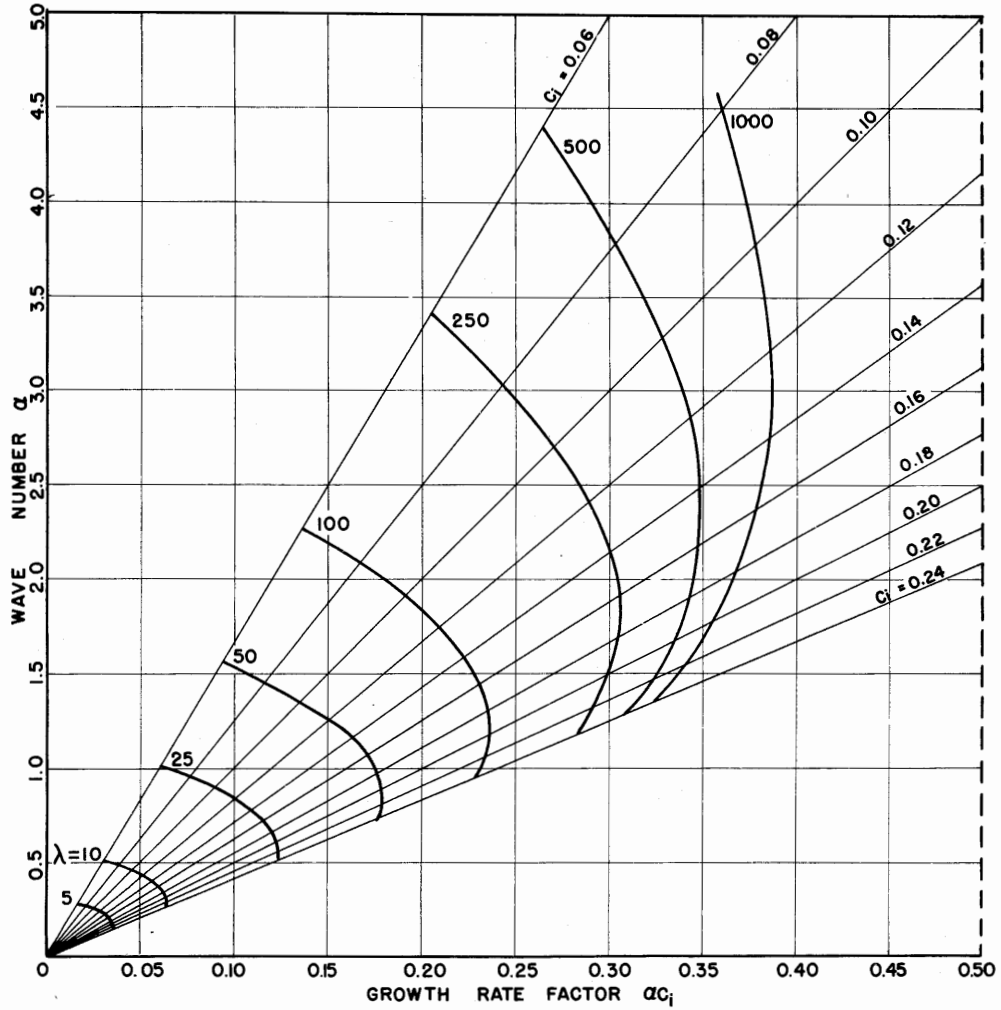

Figure 3.9 Growth rate factors at constant Rayleigh number for $\pi = 5.0$.

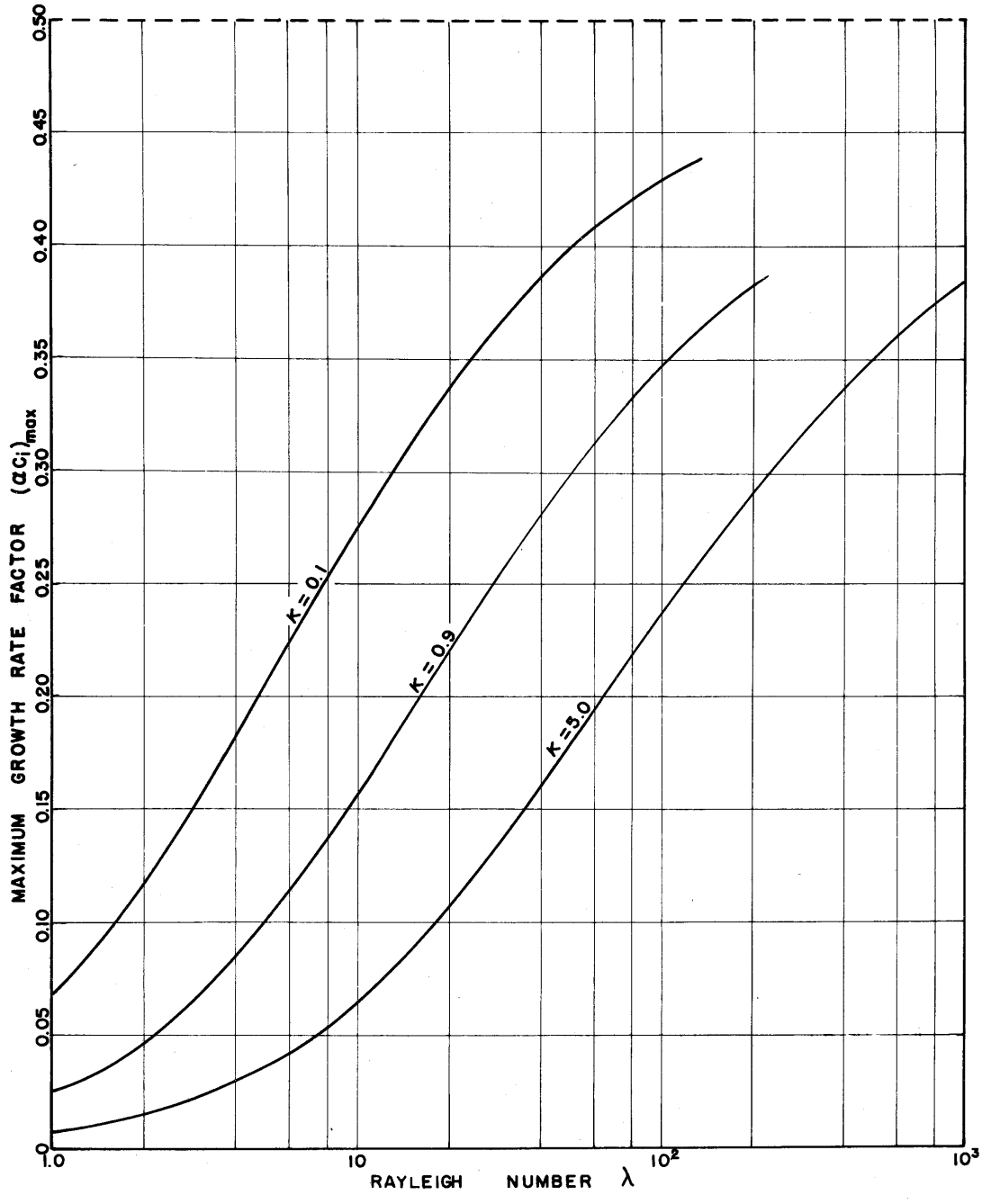

Figure 3.10 Maximum growth rate factors as a function of Rayleigh number.

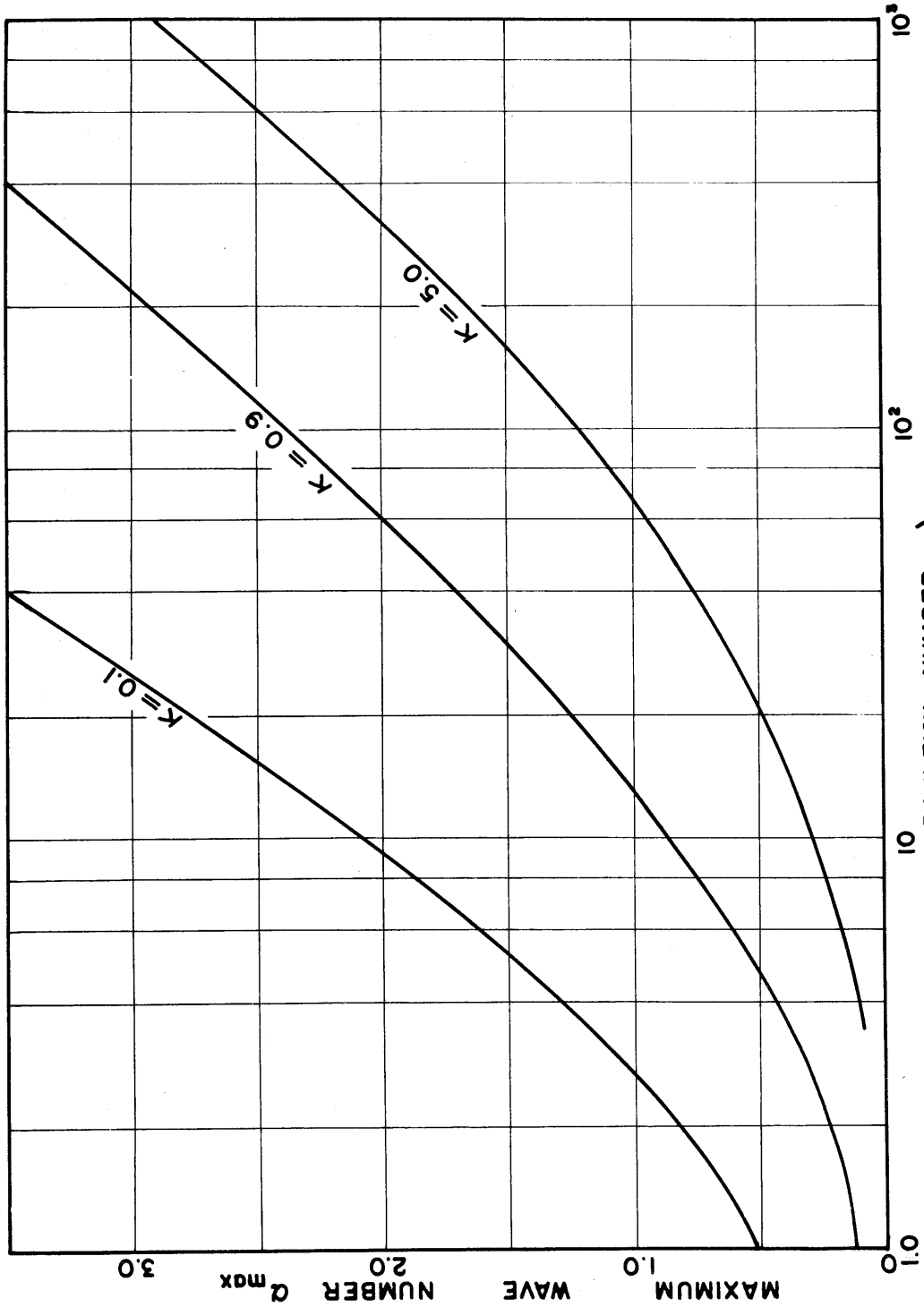

Figure 3.11 Wave numbers for waves with the maximum growth rate as a function of Rayleigh number.

αc_i at constant Rayleigh number, λ, and determine the maximum value of αc_i. The corresponding value of α (called α_{max}) will be the most unstable or fastest growing wave, according to this approximate linear theory. This most unstable wave will amplify with time according to

$$\mathcal{A} = e^{(\alpha c_i)_{max} t} .$$

The curves of α versus αc_i for constant λ and $\varkappa$ are given in Figures 3.7, 3.8, and 3.9. It is seen on these graphs that growth rate factor αc_i is bounded at $\alpha c_i = 0.5$. The maximum values of αc_i and α are plotted against the Rayleigh number in Figures 3.10 and 3.11.

Figure 3.10 gives the growth rate of the fastest growing unstable wave. If L is the wavelength of such a wave then

$$\alpha = \frac{2\pi\ell}{L}$$

and thus the wavelength is easily determined.

From Figure 3.10 it is observed that the rate of growth decreases as the longitudinal dispersion coefficient increases (i.e. $\varkappa$ increasing). Thus not only is the spectrum of unstable wave numbers narrower with increasing velocity (see section 3.1) but the rate of growth of unstable waves is decreased.

It should be emphasized here that this is only a local theory assuming that locally the width of the dispersion zone is not increasing with x, consequently the growth rates predicted are only local growth rates. To determine the wave most likely to be seen at any point is a far more difficult problem. In order to solve this one would have to

consider the variation with x of the dispersion zone and then solve an initial value problem; that is give an arbitrary disturbance at $x = 0$ and see how it grows or decays as it is swept downstream. The wave most likely to be seen at any location is then the wave having the maximum growth rate. This problem is intended for later study.

However as an example of the local growth rates consider the amplification of a disturbance in the time taken for the flow to travel a distance 5ℓ. The non-dimensional time taken will be

$$t^* = \frac{U_o}{\ell} \cdot \frac{5\ell}{U}$$

Now

$$U_o = \frac{gk(\rho_2 - \rho_1)}{\epsilon \mu}$$

and for example suppose $U_o \sim O(10^{-4})$, $U \sim O(5 \times 10^{-3})$ then $t^* = 10^{-1}$

$$\mathcal{A} = e^{\left|(\alpha c_i)_{max}\right| /10}$$

and since according to this linear theory the upper bound for $(\alpha c_i)_{max}$ is 0.5 the maximum amplification would be

$$e^{0.05} = 1.05 \ ,$$

which is a 5% increase in amplitude.

Furthermore, since $(\alpha c_i)_{max}$ is bounded (Figure 3.10) there can be no sudden growth of instability such as occurs when laminar flow becomes turbulent. This bounded growth rate of instability implies the existence of a quasi-stable flow, that is a flow which will appear

stable but will ultimately display growing waves along the density interface. This result is borne out experimentally and will be described in more detail in Chapters 5 and 6.

CHAPTER FOUR

APPARATUS AND PROCEDURE

4.0 Introduction

An experimental investigation was undertaken to determine the rates of dispersion and to observe the stability along a moving density interface. The experimental setup was intended to model the flow pattern shown diagrammatically in Figure 1.1. The experimental procedure will first be described in an overall way and particular details discussed later.

Horizontal flow through a sand bed was established in a closed Lucite tank 250 cm long, 15 cm wide, and 35 cm deep. The tank was filled with sand and a lid screwed onto the top giving in effect a box full of sand through which a uniform flow of deaired distilled water could be run. A flow of deaired saline water was introduced, through a transverse slit in the top of the box, into the uniform flow of distilled water. The flow pattern shown schematically in Figure 1.1 was thereby generated.

Salt concentrations at points in the flow were determined from electrical conductivity measurements taken by conductivity probes which were passed through the sand bed top to bottom. The probes were sealed at the top and bottom of the tank in such a way that they could be moved up and down without fluid escaping from the tank. They were connected to a recorder which measured the electrical conductivity of the salt solution introduced through the slit in the top. By moving the probes

slowly through the tank it was possible to record a profile of electrical conductivity of the moving water in the tank and thus determine a concentration profile by calibration curves relating electrical conductivity to concentration per unit mass. The shape of the concentration profile across the tank was then used to determine dispersion coefficients. The experimental setup is shown schematically in Figure 4.1.

4.1 The Experimental Tank

A tank 250 cm long, 15 cm wide and 35 cm deep was constructed of 1/2 inch thick Lucite according to the diagrammatic plan shown in Figure 4.2 and shown photographically in Figure 4.3. The bottom of the tank had six tapped holes 40 cms apart and located as shown in Figure 4.2. Stainless steel "Swagelok" fittings (nominal size 1/4 inch) were screwed into the holes and the conductivity probes passed up through the fittings and located temporarily with straps across the top of the tank. At each end were screens (65 meshes per inch) to retain the sand and help produce uniform flow of water through the sand. Three inlet pipes fitted with diffusers (visible in Figure 4.3b) were placed in the upstream end of the tank to help produce a uniform flow through the tank.

One thousand pounds of Ottawa Flint Shot sand were sieved to give the sand used in the tank. This sieved sand had a grading curve as shown in Figure 4.4 and a mean diameter of 0.530 mm and $\sigma_g = 1.10$. The tank, with the probes held in position by temporary straps across the top, was filled with sand by siphoning through a 5/8 inch diameter

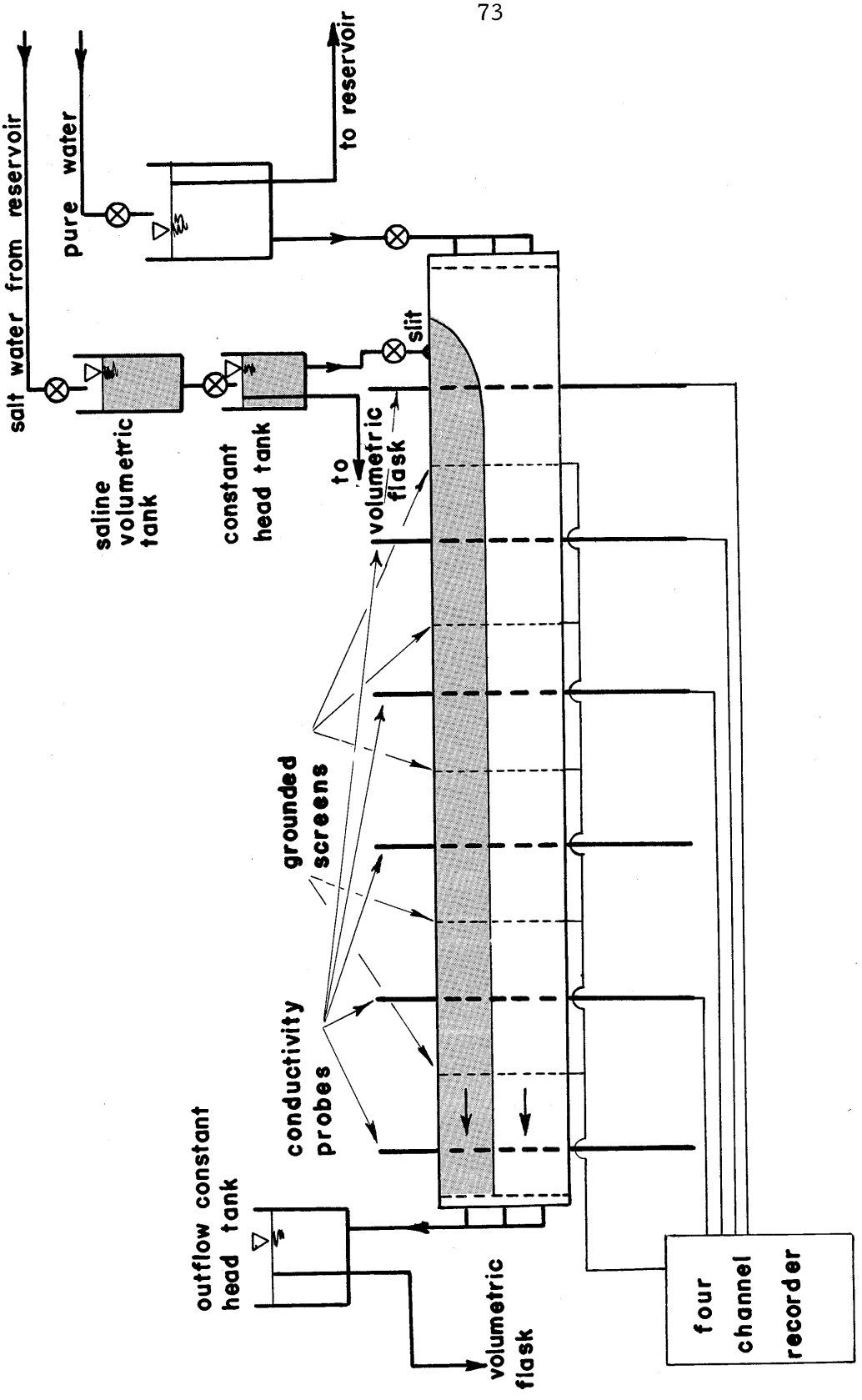

Figure 4.1 Diagrammatic representation of the experimental set up.

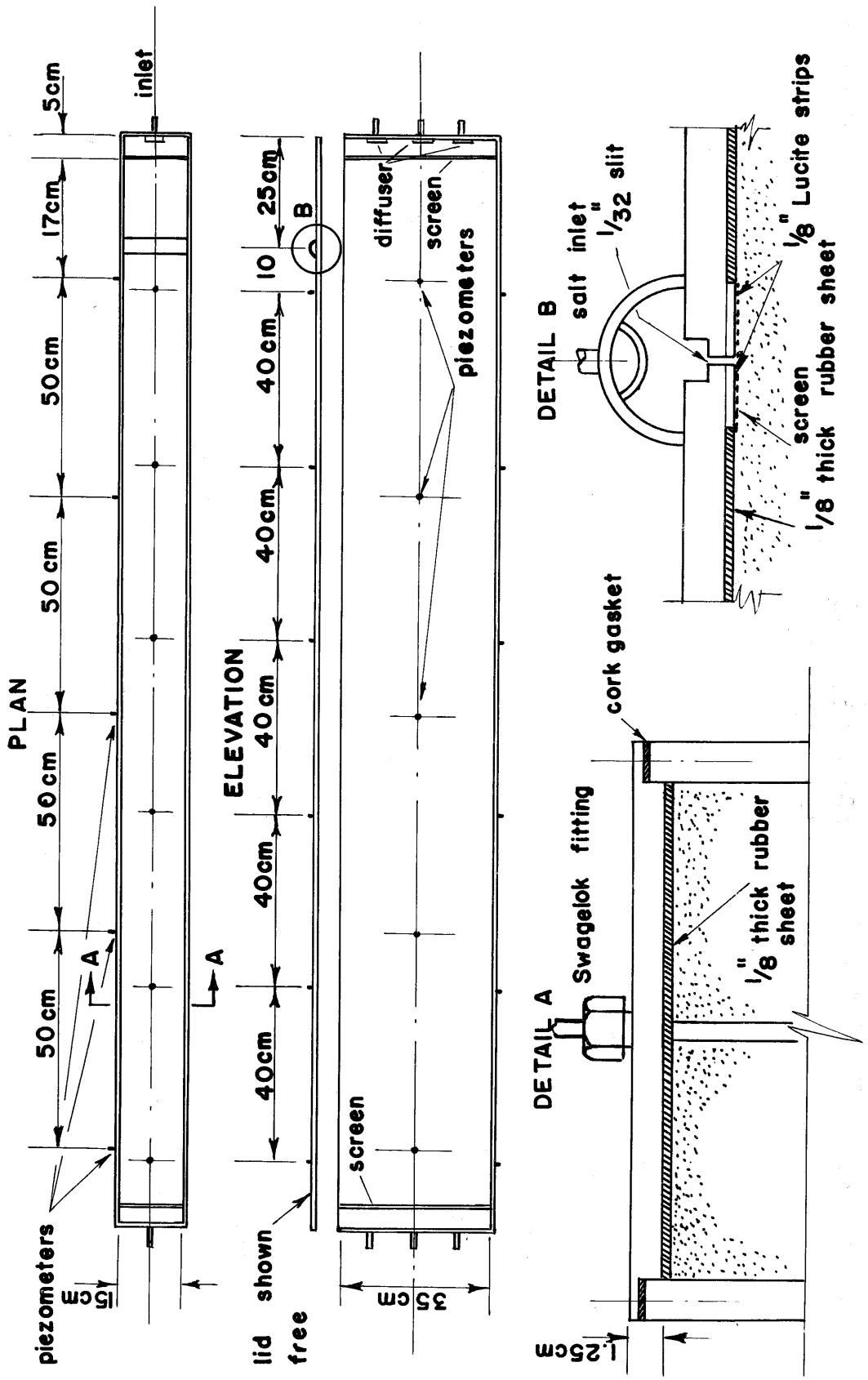

Figure 4.2 Details of the flow tank.

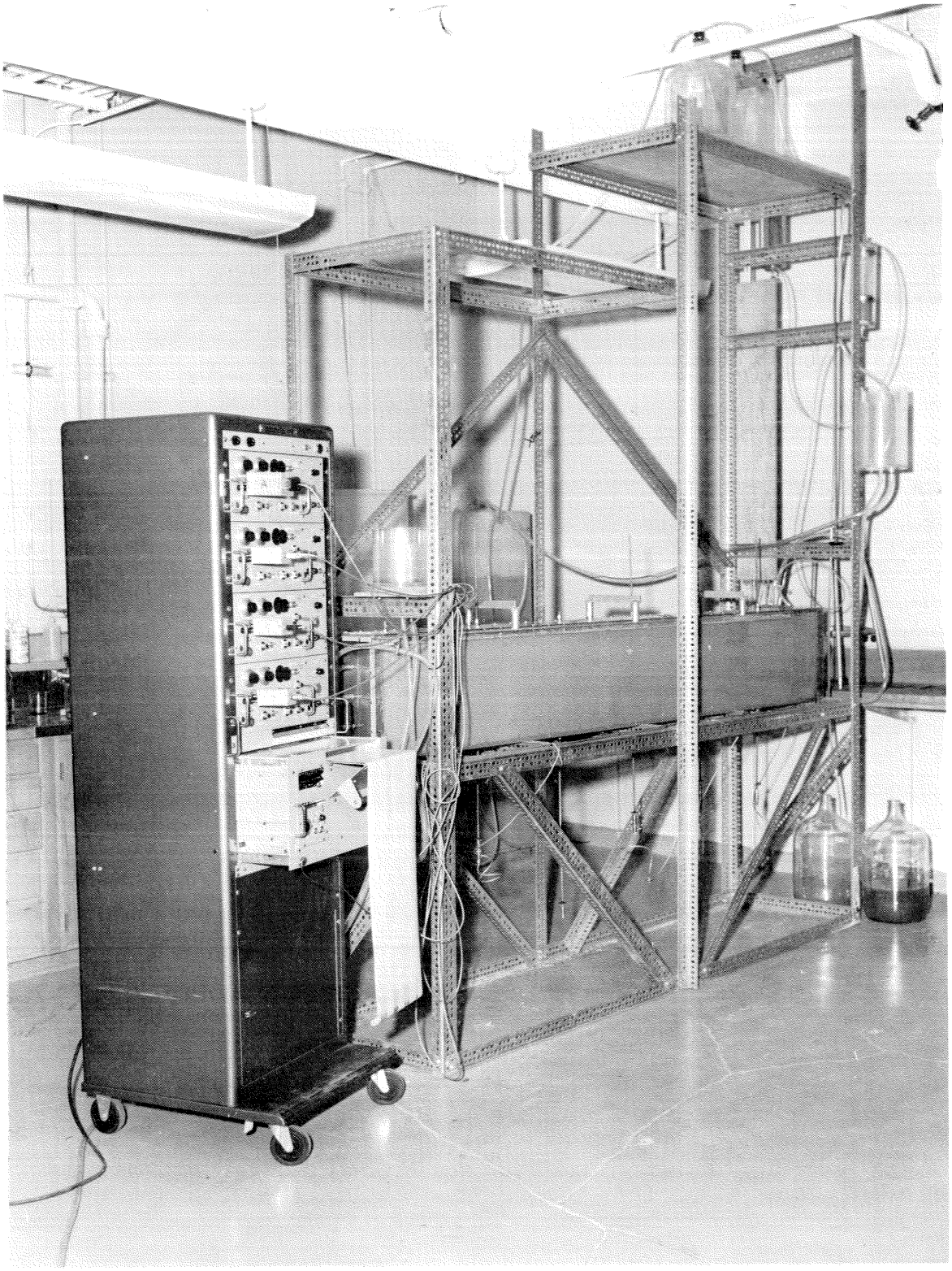

Figure 4.3a The experimental set up.

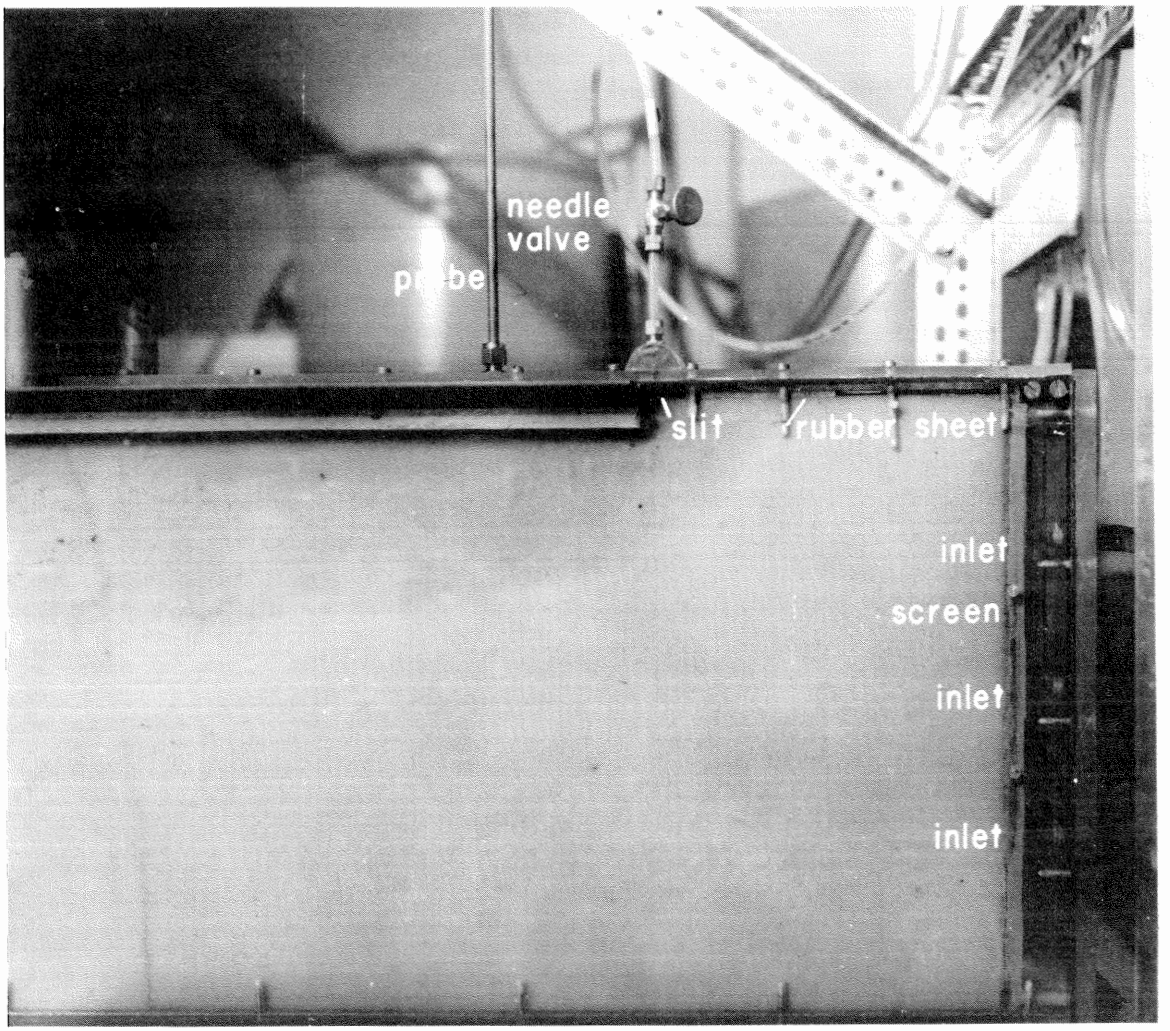

Figure 4.3b Details of the apparatus.

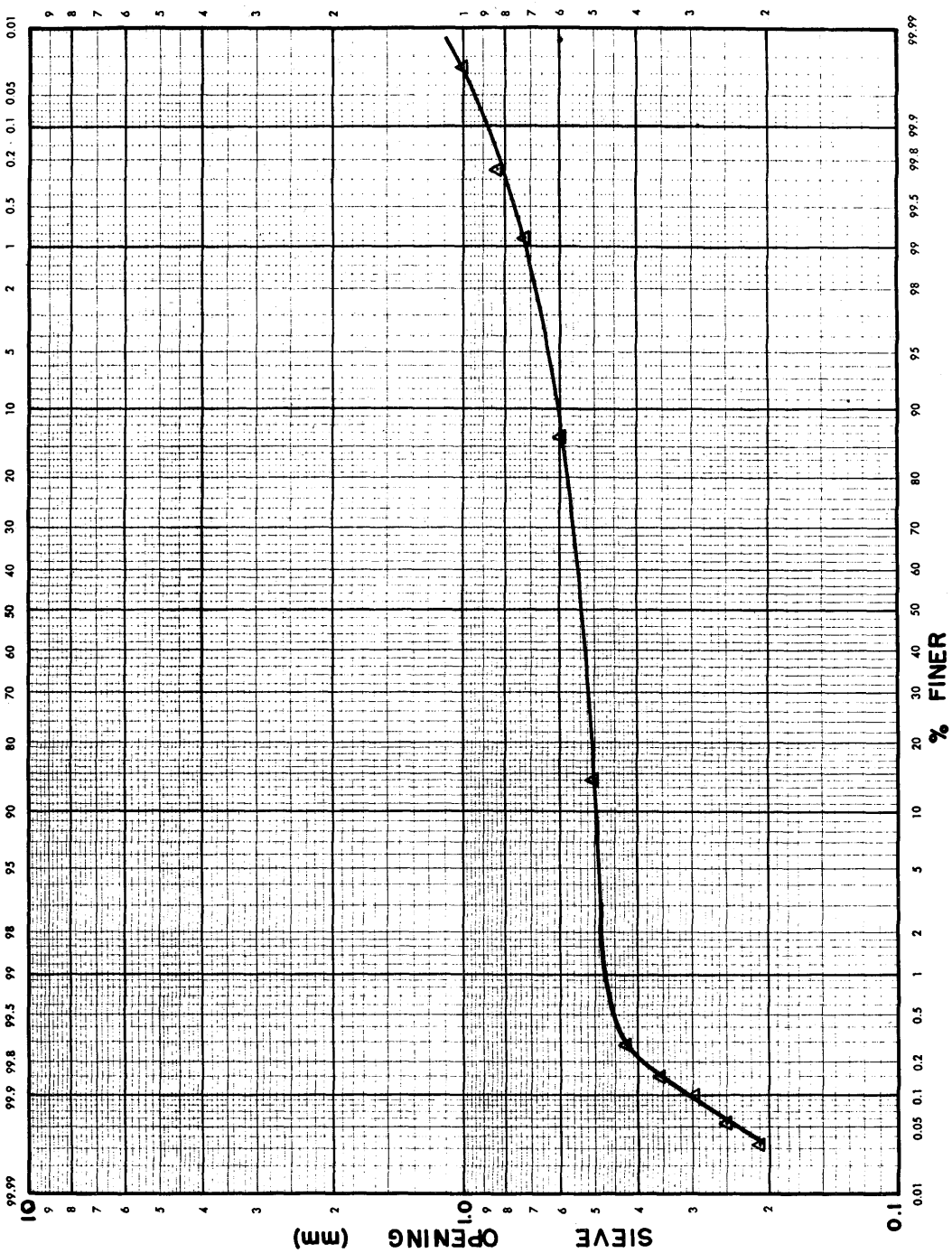

Figure 4.4 Sand grading curve.

plastic tube. First the tank was quarter filled with water and then a slurry of sand and water siphoned in from a supply tank. In this way the sand was placed under water without any air bubbles being caught in the sand. Approximately two inches of sand would be placed and then the sand was compacted by the vibration of the tank with an air hammer and the process repeated until the sand, when levelled off with a specially made screed, was 8 mm from the top edge of the tank. The locating straps for the tops of the probes were then removed as the tightly compacted sand now held them in place.

At this stage a 1/8 inch thick soft "Neoprene" sheet 15 cm wide, with holes cut for the probes and the slit in the lid, was placed on top of the sand (see Figure 4.2). When the lid was placed on the tank this compressed onto the top of the sand and helped to prevent short circuiting of the flow between the lid and the top of the sand. The sealing was completed by placing a thin bead (1/8 inch in diameter) of "Sealastic" on top of the rubber sheet and against each wall of the tank. (When the lid was screwed down the "Sealastic" filled any remaining gaps between the neoprene, lid, and walls.) The lid was now carefully placed on the tank, and the tips of the probes projecting from the Neoprene sheet guided into the fittings in the lid. The lid was then screwed down.

4.2 The Conductivity Probes and Recorder

The conductivity probes (Figure 4.5) were made by binding two platinum wires 0.020 inches in diameter into two grooves cut 2.5 mm

apart near one end of a 1/4 inch diameter phenolic resin tube approximately 18 inches long. The wire was then pulled through small holes drilled in the bottom of the grooves and led out the end through the 1/8 inch hollow center of the tube. This tube was then spliced to another of the same length by a slotted dowel rod 1/8 inch in diameter, the slots being necessary to allow the lead wires to pass up the tube. The hollow tube so formed was pumped full of polyester resin to form a solid rod with two platinum rings 2.5 mm apart near the center of the rod. A microphone connector to which the lead wires were attached was then glued to the end of the rod, and the two platinum rings polished flush with the surface of the rod. The construction is shown diagrammatically in Figure 4.5, along with a photograph of the finished article.

A Sanborn Four-Channel Recorder (Model 154-100B) with 1100 AS Carrier Amplifiers was used for the measurement of the conductivity. A circuit diagram showing the half bridge elements used in conjunction with the conductivity probes is given in Figure 4.6. Grounded screens between each probe were necessary to prevent interactions. These were provided by stainless steel screens (28 meshes per inch) of the same cross-sectional area as the tank and placed midway between probes. The probes were grounded by a machine screw connection up through the bottom of the tank.

4.3 Measurement of Salinity Profiles

Preparatory to running each series of experiments it was

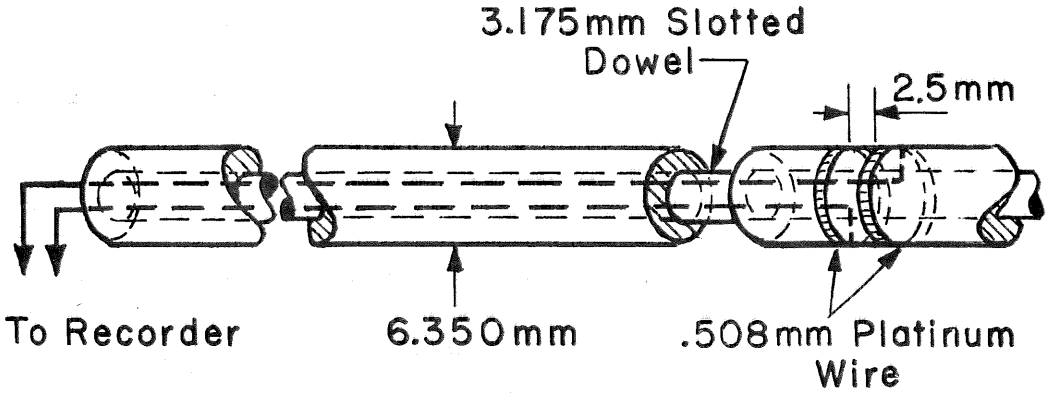

PROBE BEFORE ASSEMBLY

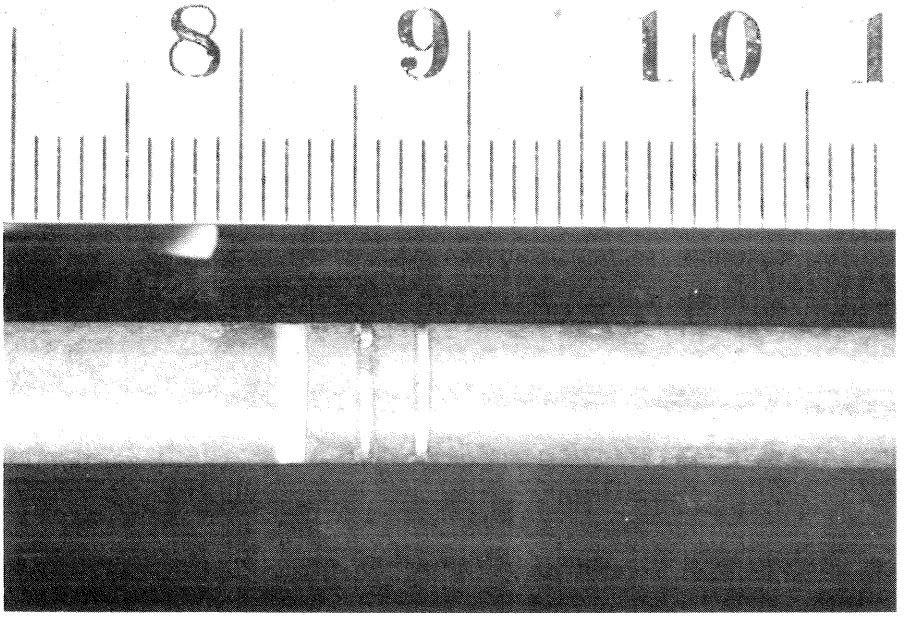

Figure 4.5 The conductivity probes.

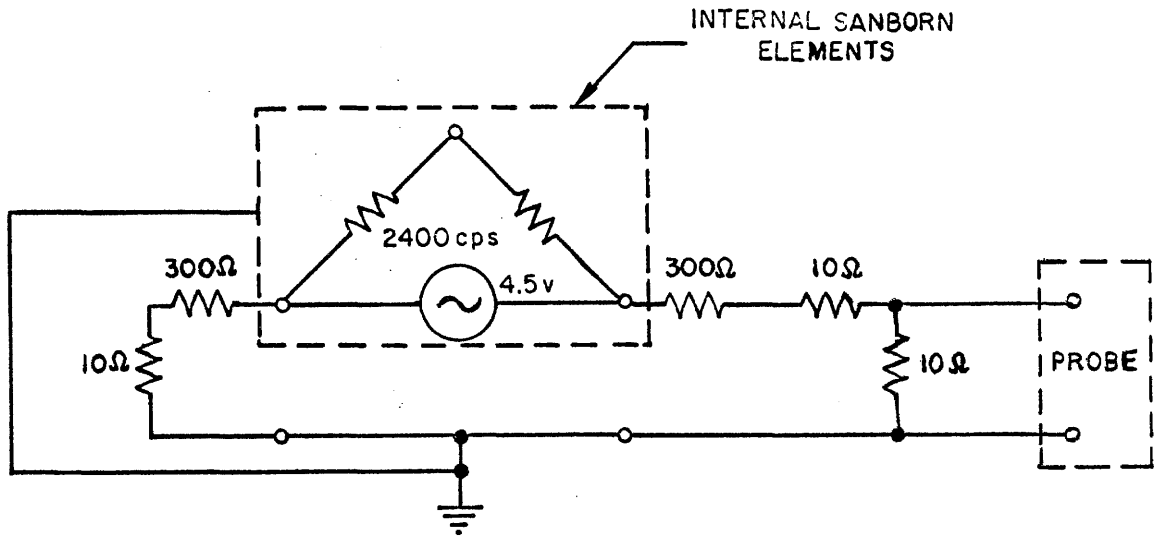

Figure 4.6 The bridge circuit used in conjunction with the Sanborn recorder for the measurement of the conductivity.

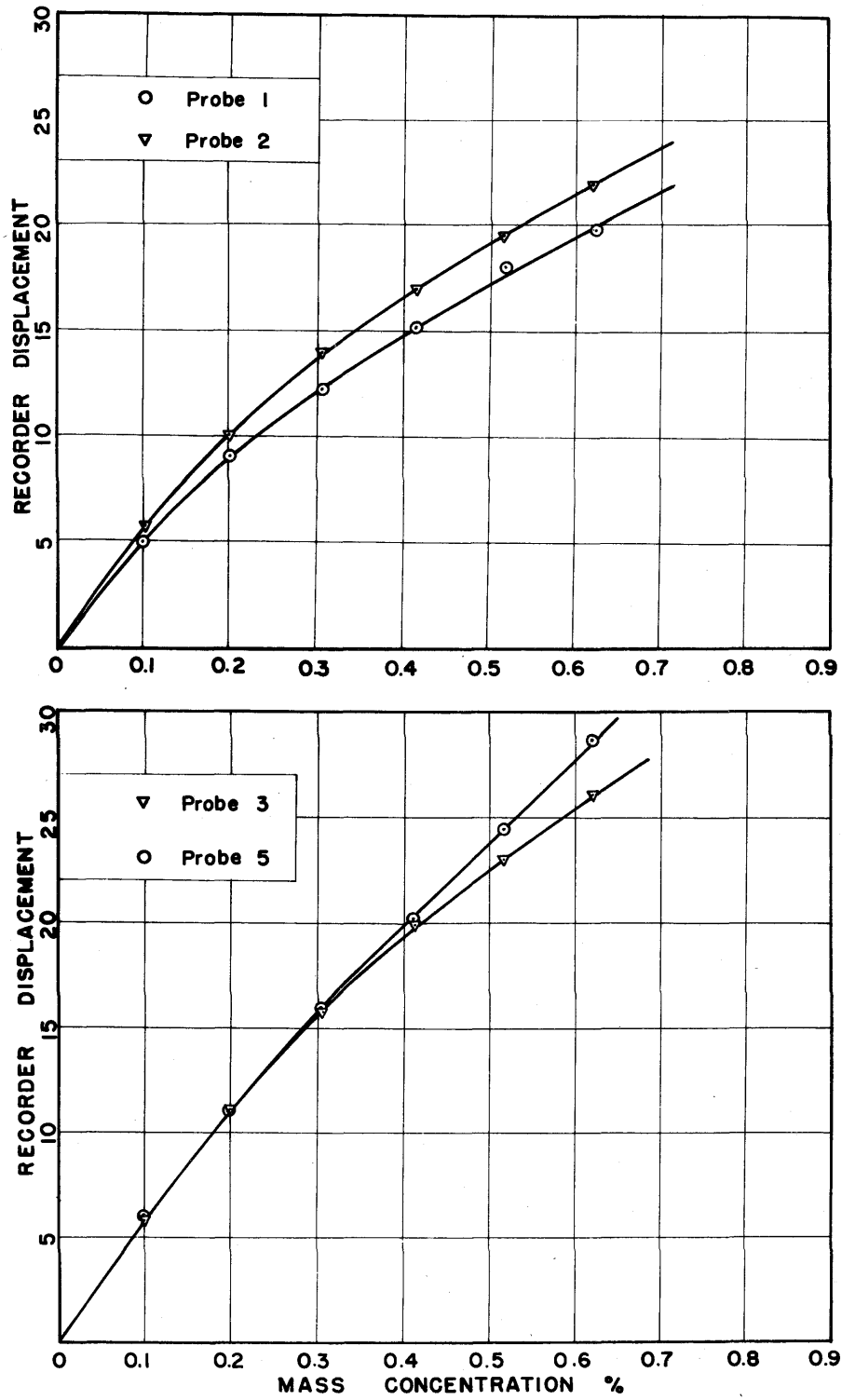

Figure 4.7 Typical calibration curves for the conductivity probes. (D-series)

necessary to calibrate the conductivity probes in situ. This was accomplished by making up solutions of sodium chloride (Morton food grade "999") of known concentration and passing approximately 5 gallons of each through the apparatus and recording the relative conductivity. A curve was then drawn of concentration per unit mass against Sanborn reading, the amplifiers having been balanced and the recorder zeroed to deaired distilled water at the start of the calibration. Typical calibration curves (D-series) for probes are shown in Figure 4.7. With curves like this for each of the probes in use for particular run to be carried out it then became a simple matter to measure the actual concentration profile.

Having calibrated the probes to be used by successive flushings with known solutions, the last calibration solution would be flushed out by running deaired distilled water through the apparatus until the recorder had returned to a zero reading. The approximate flow rate for the main flow in the experiment would then be set by adjusting the height of the inflow constant head tank. The injected flow would then be started and adjusted to the required value by operating the needle valve above the entrance to the slit. Both flows would then be permitted to run until a steady half-body shape could be observed. The injected flow contained a very small amount of a nonconducting nonadsorbable dye (Krieger, Fl. 6.8 Pink concentrate Color No. B-3-G-6). At this point the probes would be moved up sequentially until measurements indicated the platinum rings were almost at the dye line and the distance between the top of the tank and the end of the probe recorded. The probes

would then be moved up approximately 1 mm each and the elevation noted against the respective track on the recorder paper. The position of the two rings with respect to the top of the sand bed was determined in the following manner. The probes had been constructed so that it was exactly 50 cm from the upper end (the end without the connector) of the probe to the point midway between the rings. It was possible to measure the distance from the end of a probe to the top of the tank to within ± 0.25 mm and the distance between the top of the sand bed and the top of the tank was known to ± 0.5 mm. Thus the location of the rings with respect to the top of the sand bed was known to ± 0.75 mm and the relative distance between points on the conductivity profile to within ± 0.5 mm. This accuracy is quite sufficient for even at a uniform concentration of solution the sand grain packing about the probes caused a fluctuation of approximately one half a division on the Sanborn recorder scale. At low concentrations this causes a high error, for example, for 2½ recorder divisions this is an error of 20%. Consequently some scatter can be expected in the results especially at the low concentration end of the profile.

4.4 Measuring the Flow Rate

The main flow inlet, main flow outlet and the salt water inlet were all connected to constant head reservoirs (Figure 4.1). The supply of fresh water came from two five gallon glass jars, on the very top of the apparatus, which in turn were supplied by a Jabsco plastic impeller pump from a 55 gallon reservoir. The salt-water supply to the constant

head tank came from a volumetric tank which in turn was supplied by another Jabsco pump from another 55 gallon reservoir.

The saline flow rate was measured by recording the elevations in the saline volumetric tank and measuring the overflow from the saline constant head tank for a given time lapse. The maximum probable error in this flow measurement was approximately ± 0.04 mℓ per second, giving a maximum per centage error of ± 4%. However, it will be seen later that this error could be as high as ± 10% and still not influence the results as the computation involving the flow ratio depends remarkably little on the flow ratio.

The mean total flow was measured volumetrically at the overflow from the outlet constant head tank. The estimated maximum absolute error was within ± 0.04 mℓ/sec and the maximum per centage error within ± 0.4%. The results quoted in Table 5.1 are the mean of several measurements.

4.5 Determining the Concentration of Solutions

The solutions used to calibrate the probes were made up by weighing out the approximate amount of sodium chloride which when dissolved in 5 gallons of distilled water would give approximately the concentration of solution desired. At the time of making the calibrations for the experimental run a sample was taken from the calibrating solution for later gravimetric analysis.

The gravimetric analysis consisted of carefully drying a 100 mℓ. flask and rubber stopper for approximately 24 hours in a silica gel

dessicator. The dried bottle and stopper were then weighed to within ± 0.00005 gm in a dried atmosphere on a "Right-a-weigh" single pan balance manufactured by Wm. Ainsworth and Sons. About 20 mℓ of the calibration solution was then quickly added to the flask and the stopper replaced and weighed again. The stopper was then removed to the dessicator and the weighed solution transferred to an oven at 90°C. When it appeared that all evaporation had taken place, about 24 hours later, the flask was then returned to the dessicator for approximately four hours and then the stopper replaced in the flask and the flask and stopper again weighed in a dried atmosphere. In this way the salt present in approximately 20 gms of solution could be determined to within ± 0.0002 gms on repetition. This gives a maximum per centage error of a 0.01% solution of 10% and 2% on a 0.05% concentration. These low concentrations were only used for the E-series (see Chapter 5) and the error is comparable with the error that occurs with the Sanborn recorder especially at low concentrations (see section 4.3). Furthermore, since the per centage error decreases at higher concentrations and the calibration curves are linear at low concentrations this error is minimized.

The Sanborn recorder had a tendency to "drift" in the time between calibration and on experiment. This was corrected for by rezeroing before an experiment and checking the maximum deflection of the recorder during any experiment with the known concentrations being passed through the tank. Small corrections were often necessary.

4.6 Homogeneity of the Medium

The homogeneity of packing of the sand was checked in two ways.

The packing along the tank could be checked by the pressure loss recorded between piezometers (see Figure 4.2) placed in one side of the tank at mid-depth and located at five equally spaced positions along the tank. If the packing were longitudinally homogeneous then the pressure gradients recorded between equally spaced piezometers should be equal, and this is in fact so (see below).

To check the uniformity of packing with depth a vertical dye front was run through the tank and the shape of the front near the other end of the tank recorded. The black curved line in the photographs of the tank in Chapter Five shows the shape of the dye front. It would appear that the permeability decreases with height being slightly higher at the bottom. The curve appears smooth and it would seem that this is a result of the manner in which the sand is packed in the tank. The maximum percentage difference in permeability can be estimated by taking the difference in the distance traveled at top and bottom divided by the overall distance. This is approximately 5% at the very worst.

The results of a determination of the permeability of the sand bed and its longitudinal uniformity are given below. For uniform flow Darcy's Law states that the velocity of flow v is given by

$$v = K \cdot i$$

where K is the hydraulic conductivity

i is the pressure head gradient.

To measure K it is only necessary to measure the total flow rate and the head loss ΔH between any two stations. If Q is plotted against ΔH then the slope of the line should be constant and equal to KA/L

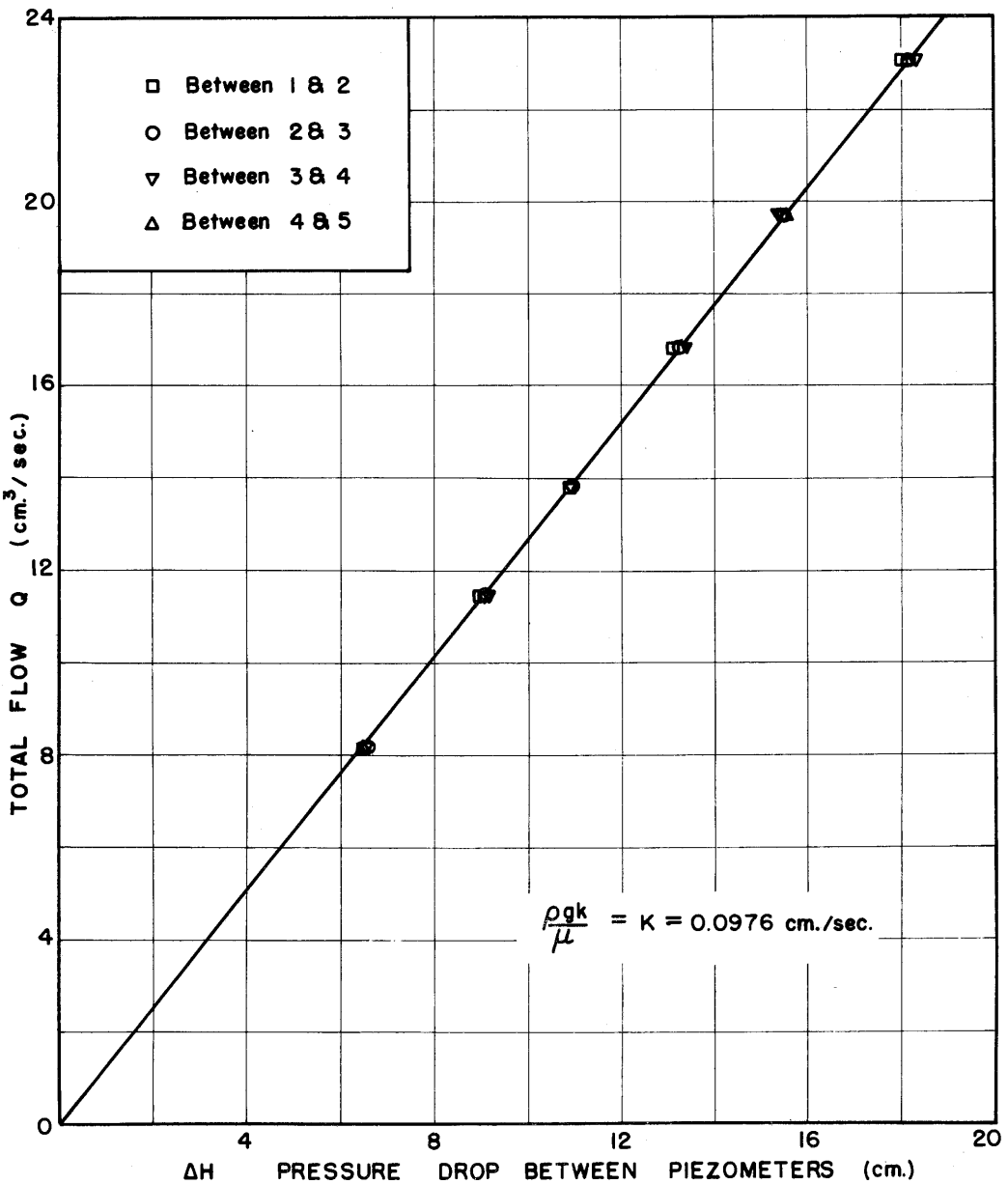

Figure 4.8 Confirmation of longitudinal homogeneity and Darcy's law for the sand bed.

where A is the cross sectional area of the tank, L the distance between piezometers. The results are given in Figure 4.8 below. From Figure 4.8 it is very obvious that Darcy's Law is true for the experiment and that the permeability between piezometers is quite uniform for the entire length of the sand bed. The hydraulic conductivity K was found to be 0.098 cm/sec, at the temperature at the time of the determination, (21.4°C). The intrinsic permeability

$$k = \frac{\mu K}{\rho g}$$

$$= 0.97 \times 10^{-4} \text{ cm}^2 .$$

A direct determination of the porosity was not possible. However an estimate may be made by determining the average rate of advance of a fluid front to give the seepage velocity within the tank; since the superficial flow velocity is known from volumetric measurement then

$$\epsilon = \frac{v}{q}$$

The porosity was found to be 0.34 as a mean of eight trials with an error of ± 0.006.

CHAPTER FIVE

EXPERIMENTAL RESULTS

5.0 Objectives

The basic objectives of the experiments were to observe if a stable two layer flow could be developed with the denser fluid on top and if such a stable flow did exist then to determine whether or not the lateral dispersion coefficient was greatly influenced by the density difference.

It was shown in Chapter 2 that the shape of the interface, a free surface, could be approximated to within the order of the density difference. Furthermore, it was shown how a solution for the mixing along such an interface could be developed. Chapter 3 showed that although the flow as always unstable the growth rate of unstable waves was bounded and very low, thus leading to a quasi-stable flow. The experiments will attempt to confirm this and also to investigate the validity of the mixing theory developed in Chapter 2.

5.1 Basic Experimental Parameters

The details of the experimental runs are given in Table 5.1; an explanation of the data columns is as follows.

Column 1 gives the run number of the experiment. The letter refers to an experimental set of constant salt concentration and the number to a constant flow ratio.

Column 2 gives the salt concentration in grams per gram of solution for the injected flow.

Experiment Number	Salt Conc.%	Flow Ratio	Mean Downstream Velocity in cm/sec	Probes Operated				Density Difference in gm/mℓ	Kinematic Viscosity in $cm^2/sec \times 10^{-2}$	
				I	II	III	V		ν_1	ν_2
A1	0.215	-	0.0420		x	x	x	0.0018	0.940	0.975
A2	0.215	-	0.0225		x	x	x	0.0021	0.920	0.979
A3	0.215	-	0.0326		x	x	x	0.0019	0.938	0.980
B1	0.104	-	0.0305		x	x	x	0.0079	0.923	0.964
B2	0.104	-	0.0314		x	x	x	0.0074	0.930	0.964
B3	0.104	-	0.0302		x	x	x	0.0079	0.949	0.976
B4	0.104	-	0.0241		x	x	x	0.0077	0.927	0.976
C1	0.0594	0.061	0.0392		x	x	x	0.00047	0.927	0.995
C2	0.0594	0.162	0.0405		x	x	x	0.00047	0.927	0.995
C3	0.0594	0.302	0.0402		x	x	x	0.00042	0.960	0.990
C4	0.0594	0.675	0.0318		x	x	x	0.00042	0.969	0.992
C5	0.0594	0.408	0.0355		x	x	x	0.00043	0.956	1.000
D1	0.489	0.188	0.0300	x	x	x	x	0.0043	0.915	0.981
D2	0.489	0.426	0.0328	x	x	x	x	0.0048	0.871	0.981
D3	0.489	0.273	0.0171	x	x	x	x	0.0042	0.926	0.994
D4	0.489	0.453	0.0258	x	x	x	x	0.0038	0.968	0.995
D5	0.489	0.355	0.0307	x	x	x	x	0.0039	0.955	0.995
E1	1.005	0.338	0.0355	x		x	x	0.0100	0.965	0.985
E2	1.005	0.687	0.0267	x		x	x	0.0100	0.941	0.985
E3	1.005	0.845	0.0155	x		x	x	0.0101	0.956	0.985
E4	1.005	0.121	0.0341	x		x	x	0.0100	0.934	0.990
E5	1.005	0.584	0.0264	x		x	x	0.0100	0.949	0.990

Table 5.1 Experimental parameters.

Column 3 gives the ratio of the saline flow to pure water flow. It will be noted that no flow ratios are given for the A and B series experiments. This is the result of an experimental error invalidating the saline flow measurements for these two series.

Column 4 gives the mean superficial flow velocity in centimeters per second through the sand bed and is the total flow rate through the tank divided by the cross-sectional area of the tank normal to the direction of flow (520 sq. cm.).

Columns 5 through 9 give the locations at which conductivity profiles were measured. The Roman numerals correspond to the following distances in centimeters downstream from the entrance slit:

PROBE :	I	II	III	IV	V
DISTANCE:	10 cm	50 cm	90 cm	130 cm	170 cm

Not all four channels were in operation all the time due to intermittent amplifier failures, and probe breakages.

Column 10 gives the density difference in grams per milliliter of the two solutions at the measured temperatures and concentrations. The values are taken from The International Critical Tables, Volume III.

Columns 11 and 12 are the kinematic viscosities (in centistokes) of pure water and salt solutions at the measured temperatures. The values are taken from the International Critical Tables, Volume III and The Handbook of Chemistry and Physics, 42nd Edition.

5.2 Relating Experiment to Theory

In Chapter 2 the equation governing the mixing was shown to be

of the form

$$q \frac{\partial C}{\partial s} = D_T \frac{\partial^2 C}{\partial n^2} \qquad (5.1)$$

in dimensional variables, where q is the seepage velocity, and C the relative concentration in grams of salt per unit volume of solution. However, the concentration measured experimentally is concentration in grams of tracer per gram of solution, and

$$\rho C_m = C_v$$

where ρ is the density of the solution and C_m and C_v are the concentrations per unit mass and unit volume respectively. It will be within the experimental error to use these interchangeably, and this will be done from now on, and the concentration will be called C.

Two methods will be used to relate the experimental data to the mixing theory. The first one, given in this section, will cover the mixing from the stagnation point on downstream and will require a knowledge of the flow ratios. The second method where the flow ratio is not required is only applicable downstream of the salt water inlet and will be given in a later section.

Now, it is generally accepted (see section 1.1) that the dispersion coefficient is proportional to the flow velocity. However, as with all exceedingly complex phenomenon this is only true in a broad sense, consequently attempts have been made to describe the dispersion by means of a semiempirical law such as

$$\frac{\epsilon D_T}{\nu} = r \left(\frac{vd}{\nu}\right)^{\omega} = r R^{\omega} \qquad (5.2)$$

where r and ω are constants

v is the superficial flow velocity

d is the mean particle size.

Such formulas ignore any influence changes in the Schmidt number, ν/D_m, where D_m is the molecular diffusivity, may have on the dispersion coefficient.

Now, according to Harleman and Rumer (16)

$$\left.\begin{aligned} r &= 0.0265 \\ \omega &= 0.7 \end{aligned}\right\} \quad 0.04 < R < 1.10$$

and since their experiments were carried out with a constant density salt solution the Schmidt number can be regarded as constant, although no mention is made of constant temperatures and therefore constant viscosity.

In considering the mixing from the stagnation point on downstream the dispersion coefficient will be assumed to be given by an equation of the form of equation (5.2). This is not strictly true for two reasons (apart from the general validity of such a form).

First, it has already been stated (see Chapter 1) that a formula such as (5.2) can only be true for a particle Reynolds large enough (i.e. $> O(10^{-2})$) since as the velocity becomes low enough it will give dispersion coefficients less than the molecular diffusivity in a porous medium. However, this should not influence the results too much as it

can be shown from equations (2.33), (2.41) and (2.42) that in the neighborhood of the stagnation point the superficial velocity along the streamline, $v(s)$ is given by

$$v(s) \simeq 2\pi \left(\frac{\nu_1 Q_1 + \nu_2 Q_2}{\nu_2 Q_2} \right) s$$

In these experiments

$$d = 0.053 \text{ cm}$$

$$\nu \sim 0.01 \text{ cm}^2/\text{sec}$$

and the maximum value of $\nu_2 Q_2 / \nu_1 Q_1$ used was 0.87. Thus for

$$\frac{vd}{\nu} > 0.04$$

$$s > 0.0006$$

which is a very short distance along the dividing streamline.

Second, since the density variations in the experiments arise both from temperature differences and differences in salt concentration the Schmidt number will not be constant for all experiments; however, the maximum variation is sufficiently small (10%) that it should not have an affect any larger than the normal experimental scatter.

It is also to be remembered that in writing equation (5.1) for the mixing along the streamline terms of order $1/R$, where R is the radius of curvature of the interface, have been neglected.

The procedure will now be to take Harleman and Rumer's (5.2) result and apply the mixing theory developed in Chapter 2 and use experimental results obtained to find a value of r.

When (5.2) is incorporated into (5.1) and lengths nondimensionalized by the depth of the tank a, and velocities by the mean upstream flow velocity U then

$$B\, v^{1-\omega} \frac{\partial C}{\partial s} = \frac{\partial^2 C}{\partial n^2} \tag{5.3}$$

where

$$B = \left(\frac{Ud}{\nu}\right)^{1-\omega} \cdot \frac{a}{rd} \tag{5.4}$$

It has already been shown in Chapter 2 that the solution to (5.3) is

$$2C - 1 = \operatorname{erf}\left(\frac{n}{2\left[\int_0^s \frac{ds}{B\, v^{1-\omega}}\right]^{\frac{1}{2}}}\right) \tag{5.5}$$

so that it is possible to write

$$n = \frac{2}{B^{\frac{1}{2}}} F(s)\, \operatorname{erf}^{-1}(2C - 1) \tag{5.6}$$

where

$$F(s) = \left(\int_0^s \frac{ds}{v(s)^{1-\omega}}\right)^{\frac{1}{2}} \tag{5.7}$$

and erf^{-1} = inverse error function.

Following Harleman and Rumer (16) ω is chosen as 0.7 and r will be determined experimentally.

In the experiments it is possible to measure the conductivity

profile and hence the concentration profile by means of the probes and equipment described in the previous chapter. However, it will be noticed that the probes actually measure the profile normal to the top and bottom of the sand bed and not normal to the interface. Thus where the inclination of the interface to the horizontal is small at Probes II, III, V, the error should be slight and it will be possible to write

$$n \approx -(y - y_o)$$

where y_o is the elevation of the interface. At Probe I the error can easily be corrected for by taking

$$n = -(y - y_o) \cos\theta$$

where θ is the inclination of the interface to the horizontal; however, the maximum computed angle at Probe I is 11^o (Run E3) and the correction is within the experimental errors and thus ignored. Thus from the experimental observations it will be possible to plot curves of y against $\text{erf}^{-1}(1 - 2C)$ and these should be straight lines according to equation (5.6). Furthermore the slope of these lines, S, is given by

$$S = \frac{2\,F(s)}{B^{\frac{1}{2}}} \qquad (5.8)$$

Hence an experimental determination of $2F(s)/B^{\frac{1}{2}}$ is possible.

However, $F(s)$ depends only on the shape of the interface and in Chapter 2 the shape of the interface was found to within the order of the density difference, so it becomes possible to compute $F(s)$ from

equation (5.7).

From Chapter 2 equation (2.33) we have

$$v(s) = \frac{\nu_2 Q_2}{\nu_1 Q_1} \cdot \frac{1}{2 \sin \pi y} \left[\left(\sin (\pi y) \cdot \coth \frac{\pi h}{2} - \sin (\pi y \coth \frac{\pi h}{2}) \right)^2 + \left(\cos \pi y - \cos (\pi y \coth \frac{\pi h}{2}) \right)^2 \right] \tag{5.9}$$

where v, s, y, x, and h have been non-dimensionalized as previously noted. (It will be recalled that the viscosity and density difference between the two fluids implies that there is a velocity discontinuity of order

$$u_2(\infty,y) - u_1(\infty,y) = (\mu_1 - \mu_2) \left(\frac{\mu_2 Q_2 + \mu_1 Q_1}{\mu_1 \mu_2} \right)$$

This must contribute to the lateral dispersion directly by forming a mixing layer and it also gives rise to the complication that D_T varies across the mixing zone. However, since this effect is of the order of the viscosity difference it should be small compared to the mixing produced by the mean convective velocity U. That is $\partial D_T/\partial n$ will be small compared with $\partial^2 C/\partial n^2$ and can be ignored.)

And

$$s = \int_0^y \left(1 + \left(\frac{dx}{dy} \right)^2 \right)^{\frac{1}{2}} dy \tag{5.10}$$

where

$$\frac{dx}{dy} = \frac{\sin(\pi y)\coth\frac{\pi h}{2} - \sin\left(\pi y \coth\frac{\pi h}{2}\right)}{\cos \pi y - \cos \pi y \coth\frac{\pi h}{2}} \tag{5.11}$$

and

$$\coth\frac{\pi h}{2} = 2\frac{\nu_1 Q_1}{\nu_2 Q_2} + 1 \tag{5.12}$$

The interface shape is given by

$$e^{-\pi x} = \frac{\sin\left[\pi y\left(\coth\frac{\pi h}{2} + 1\right)\right]}{\sin\left[\pi y\left(\coth\frac{\pi h}{2} - 1\right)\right]} \tag{5.13}$$

The method of computing $F(s)$ is as follows:

(i) Compute y_{max} $(= \zeta_o(\infty))$ the maximum elevation of the interface

$$y_{max} = \frac{\nu_2 Q_2}{\nu_2 Q_2 + \nu_1 Q_1} \tag{5.14}$$

(ii) Let

$$y_j = \frac{j\, y_{max}}{800}$$

and compute the corresponding x_j from formula (5.13). The (x_j, y_j) define the interfacial shape.

(iii) Compute $(dx/dy)_j$ from (5.11) and this defines the inverse slope of the interface.

(iv) Compute v_j from (5.9).

(v) Compute s_j from (5.10) by using a Simpson's Rule numerical integration process with a step length $y_{max}/800.0$.

The function $v(s)$ is then defined in terms of the discrete variables v_j and s_j and thus it is possible to compute $F(s)$ using (5.7) and integrating numerically. Two problems occur, however, since the y_j were taken in equal increments the s_j have unequal step lengths and

$$\Delta_j = s_j - s_{j-1} < \Delta_{j+1} \quad .$$

This problem is overcome by using a 5 point Lagrange interpolation formula to find $v_{j+\frac{1}{2}}$ at $s_{j+\frac{1}{2}}$ midway between s_j and s_{j+1} and then using Simpson's Rule on the three ordinates v_j, $v_{j+\frac{1}{2}}$, v_{j+1} with a step length $\frac{1}{2}(s_{j+1} - s_j)$. The accuracy of this process should be good since the step lengths are very small where $1/v_j^{0.3}$ is rapidly changing and get larger as $1/v_j^{0.3}$ tends to its asymptotic limit of

$$1/\left(1 + \frac{\nu_2 Q_2}{\nu_1 Q_1}\right)^{0.3}$$

The other problem is that when

$$s \to 0 \qquad v(s) \to 0$$

which implies that the numerical integration process cannot be used when $j = 1$. To circumvent this difficulty it is possible to expand v in powers of y in equation (5.9) and s in powers of y in (5.10). It is found that for small y

$$F(s) = \left(\left(\frac{\nu_2 Q_2}{2\pi (\nu_1 Q_1 + \nu_2 Q_2)} \right)^{0.3} \frac{s^{0.7}}{0.7} \right)^{\frac{1}{2}}$$

Using the methods described above a high speed digital computer was programmed to compute the results and print them in the following format

x	y	s	v(s)	F(s)
..	..	..	..	..
..	..	..	..	..

The tabulated results could then be used to determine F(s) at the required probe location.

The next section gives the results of the experiments and computations.

5.3 Experimental Results

The experimental results are given first for experiments C1 through E5, runs A1 through B4 will be considered in the next section.

The experimentally determined concentration profiles across the fluid interface are plotted on linear graph paper as curves of y (dimensional) versus $\text{erf}^{-1}(1 - 2C)$. It was shown in the previous section that these curves should be straight lines with slope

$$S = \frac{2a}{B^{\frac{1}{2}}} F(s) \qquad (5.15)$$

where

$$B = \left(\frac{Ud}{\nu}\right)^{0.3} \cdot \frac{a}{rd} \qquad (5.16)$$

(the a now occurs on the right hand side of (5.15) since dimensional y is plotted)

and

a = depth of the sand bed

U = dimensional upstream mean velocity

ν = kinematic viscosity

ϵ = porosity of the sand bed

d = mean diameter of sand particles

r = a constant to be determined

These concentration profiles are plotted on Figures 5.1 through 5.15. The straight lines have been fitted by eye and the agreement is seen to be very good in most cases. There are some exceptions however, notably at Probe I on runs E3, E4 and E5 (Figures 5.13, 5.14, 5.15), where the curve becomes very steep at the upper part of the profile i.e. close to the top of the tank. The reason for this behavior is not apparent. It is also seen on Figure 5.13 (run E3) that there is quite a distinct break in the line at all probes. This will be explained later.

Equations (5.15) and (5.16) can be combined to write

$$r = \left(\frac{Ud}{\nu}\right)^{0.3} \cdot \frac{1}{4ad} \cdot \left(\frac{S}{F(s)}\right)^2 \qquad (5.17)$$

and r should be the same constant for all probes for all experiments. The tabulated values of r are given in Table 5.3 below.

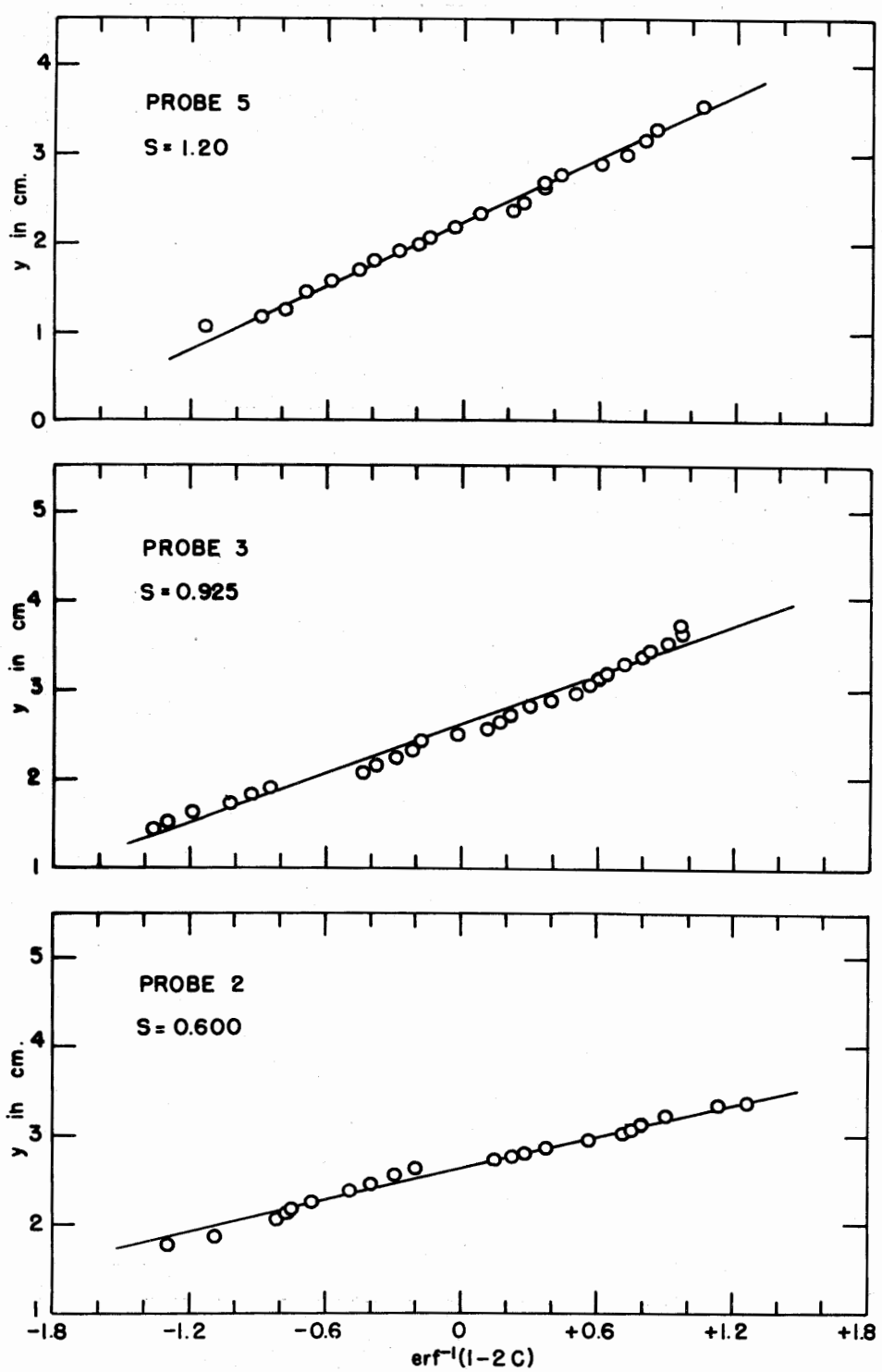

Figure 5.1 Concentration profiles at various stations for run C1.

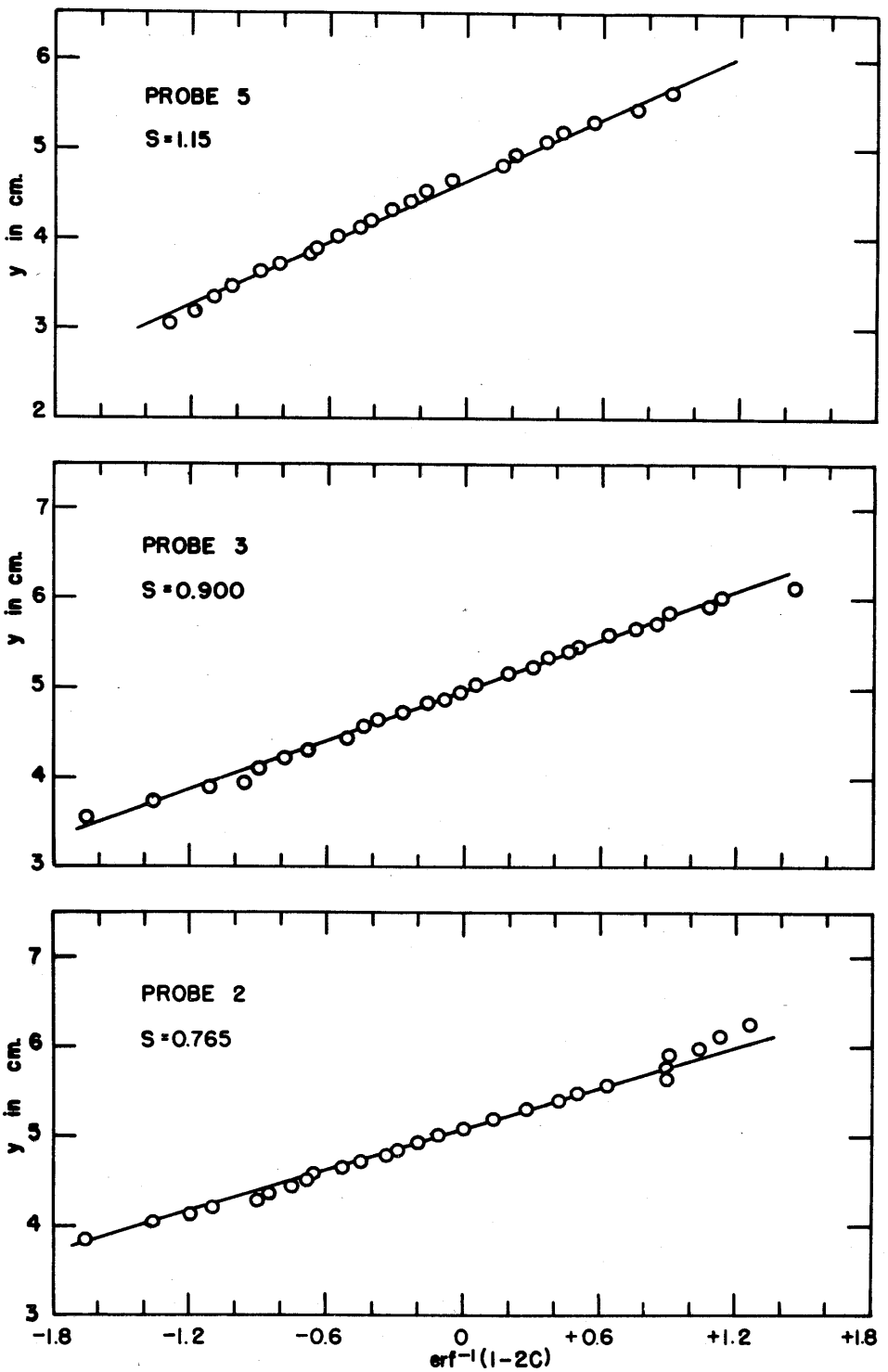

Figure 5.2 Concentration profiles at various stations for run C2.

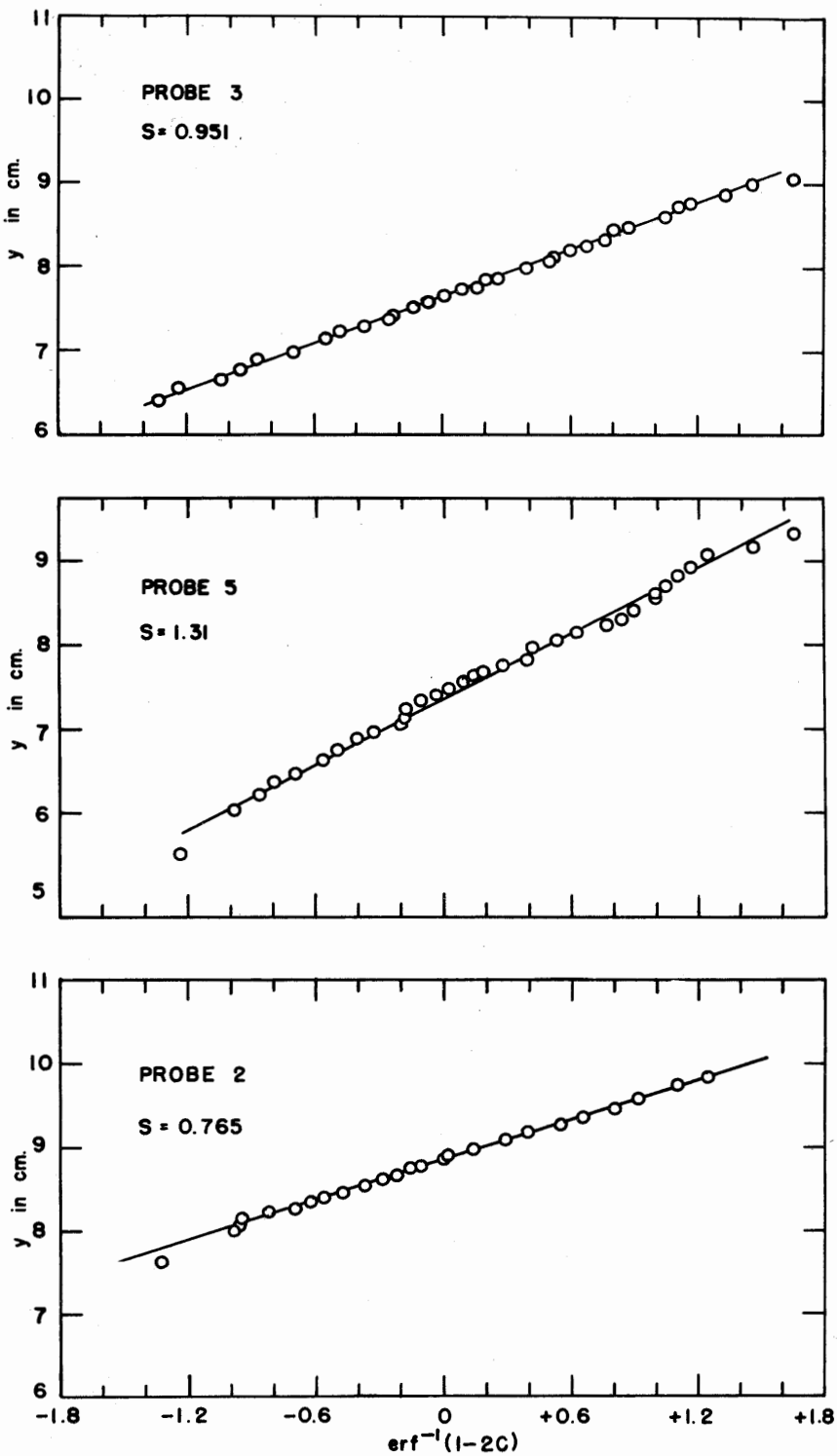

Figure 5.3 Concentration profiles at various stations for run C3.

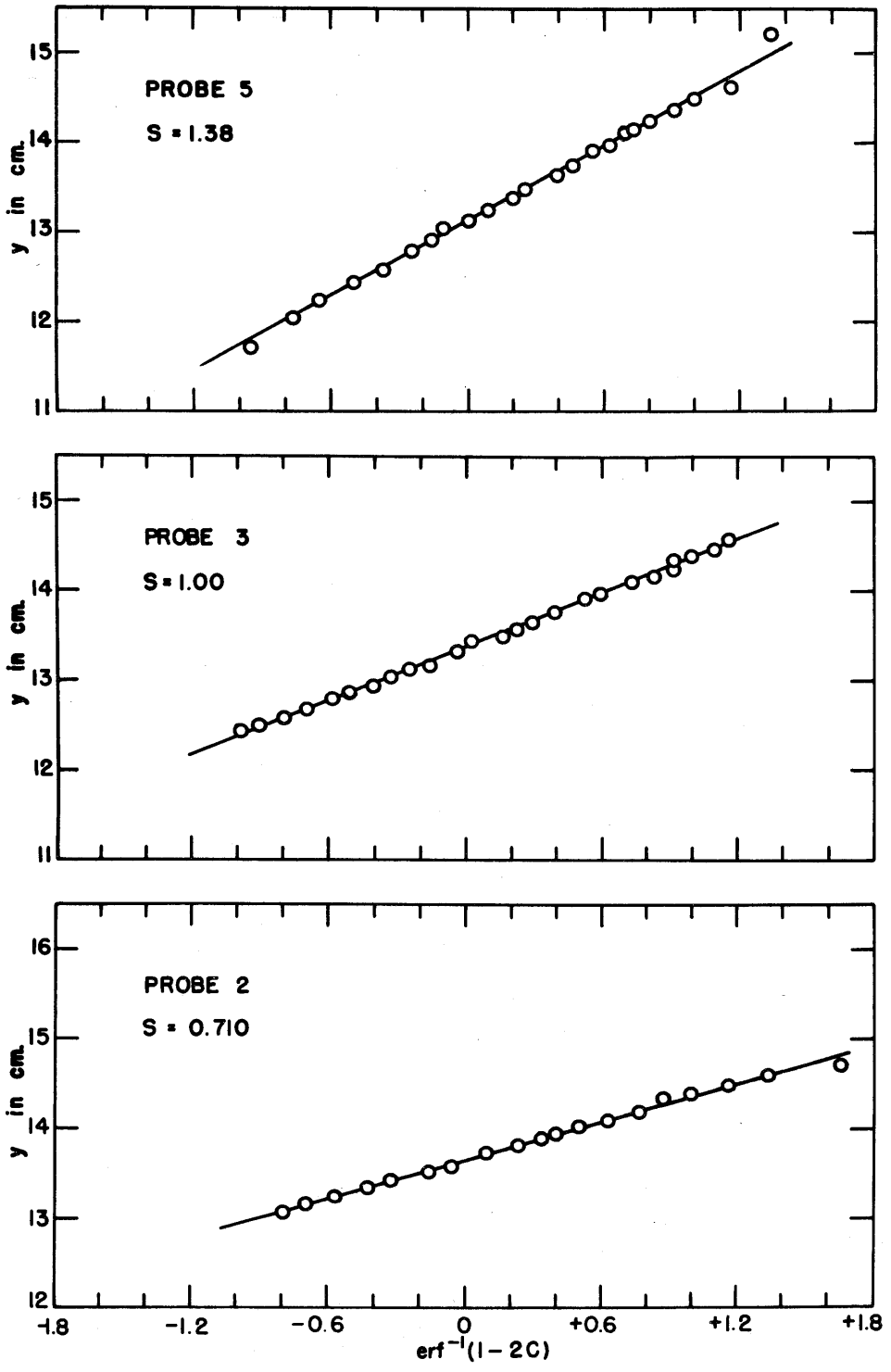

Figure 5.4 Concentration profiles at various stations for run C4.

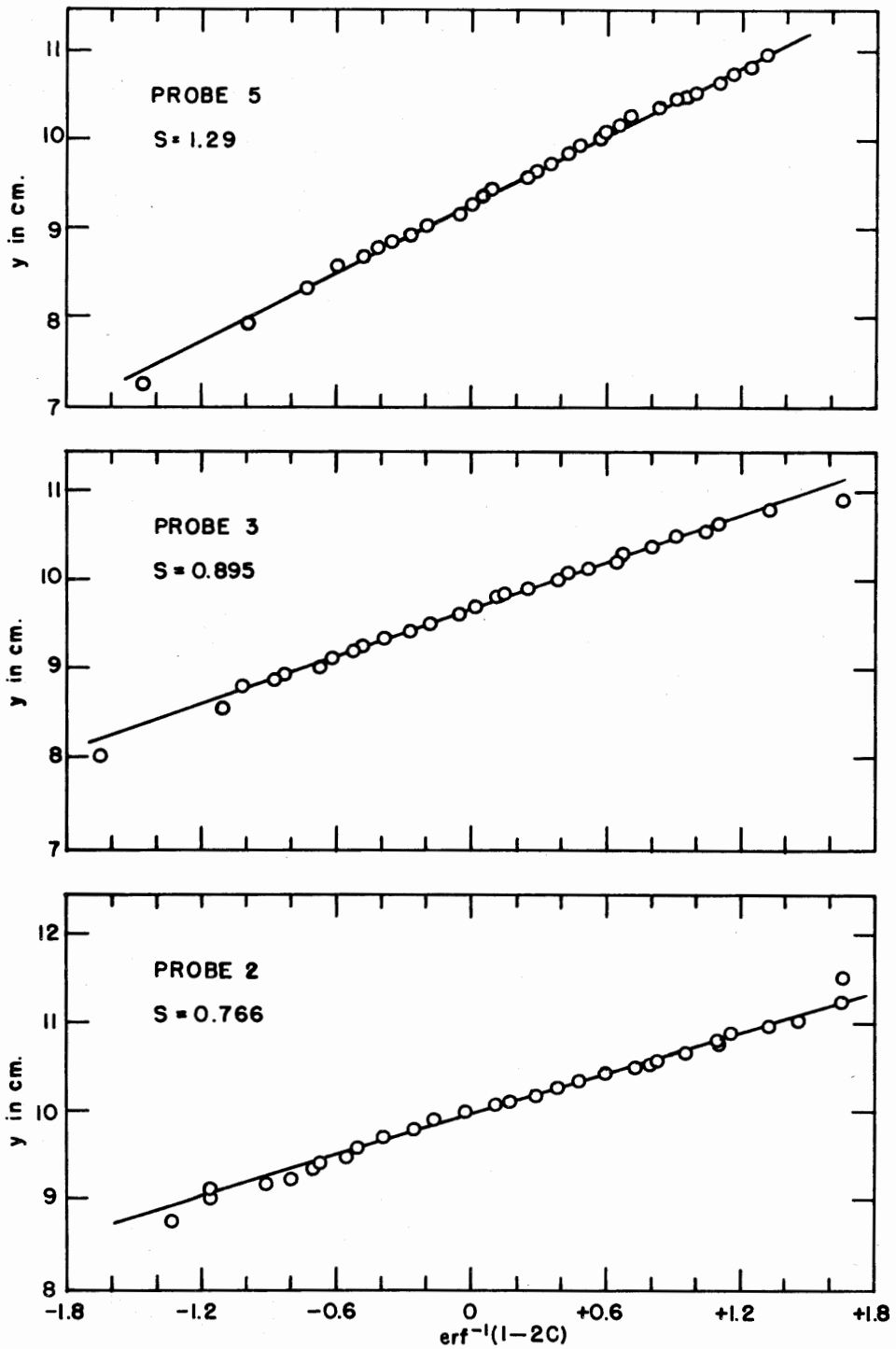

Figure 5.5 Concentration profiles at various stations for run C5.

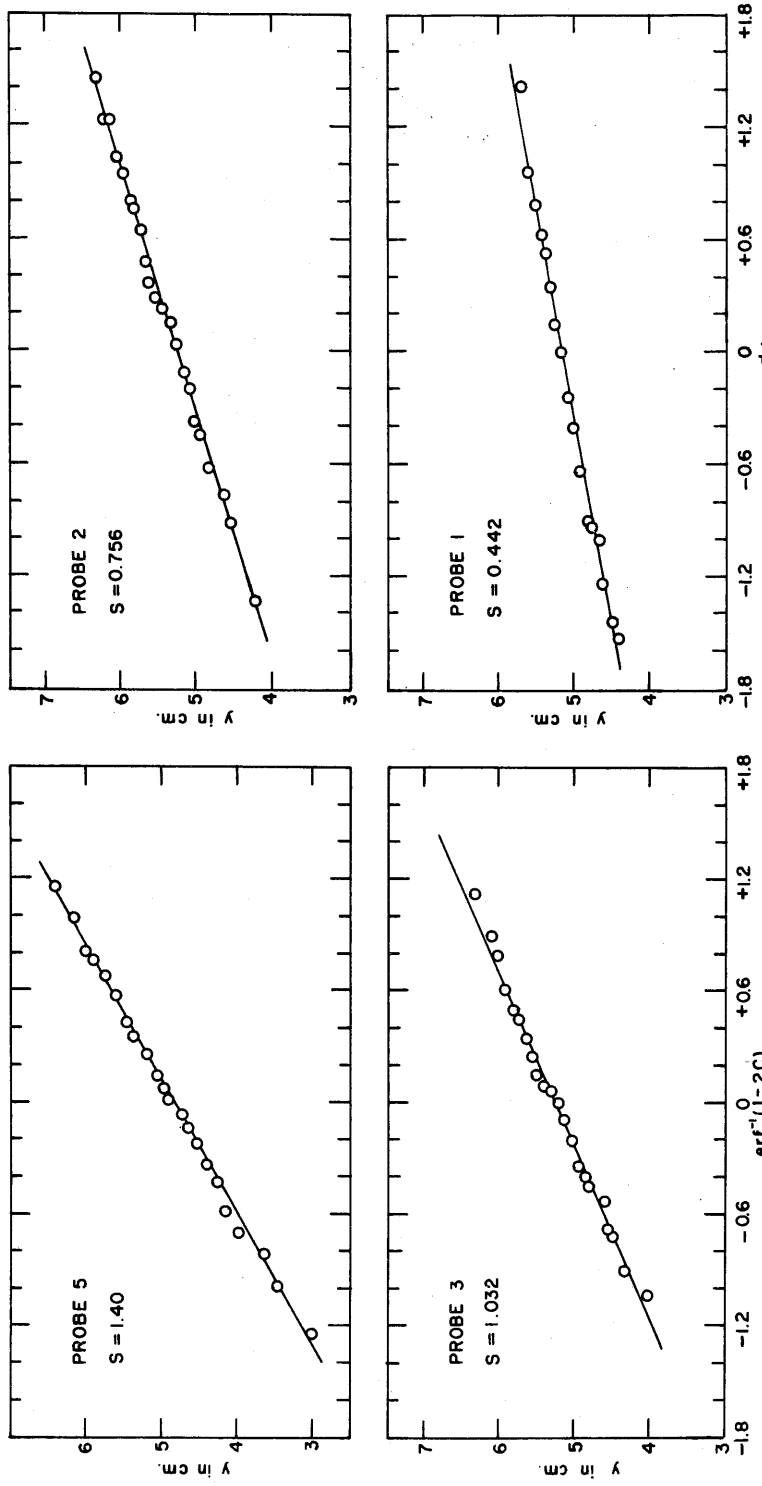

Figure 5.6 Concentration profiles at various stations for run D1.

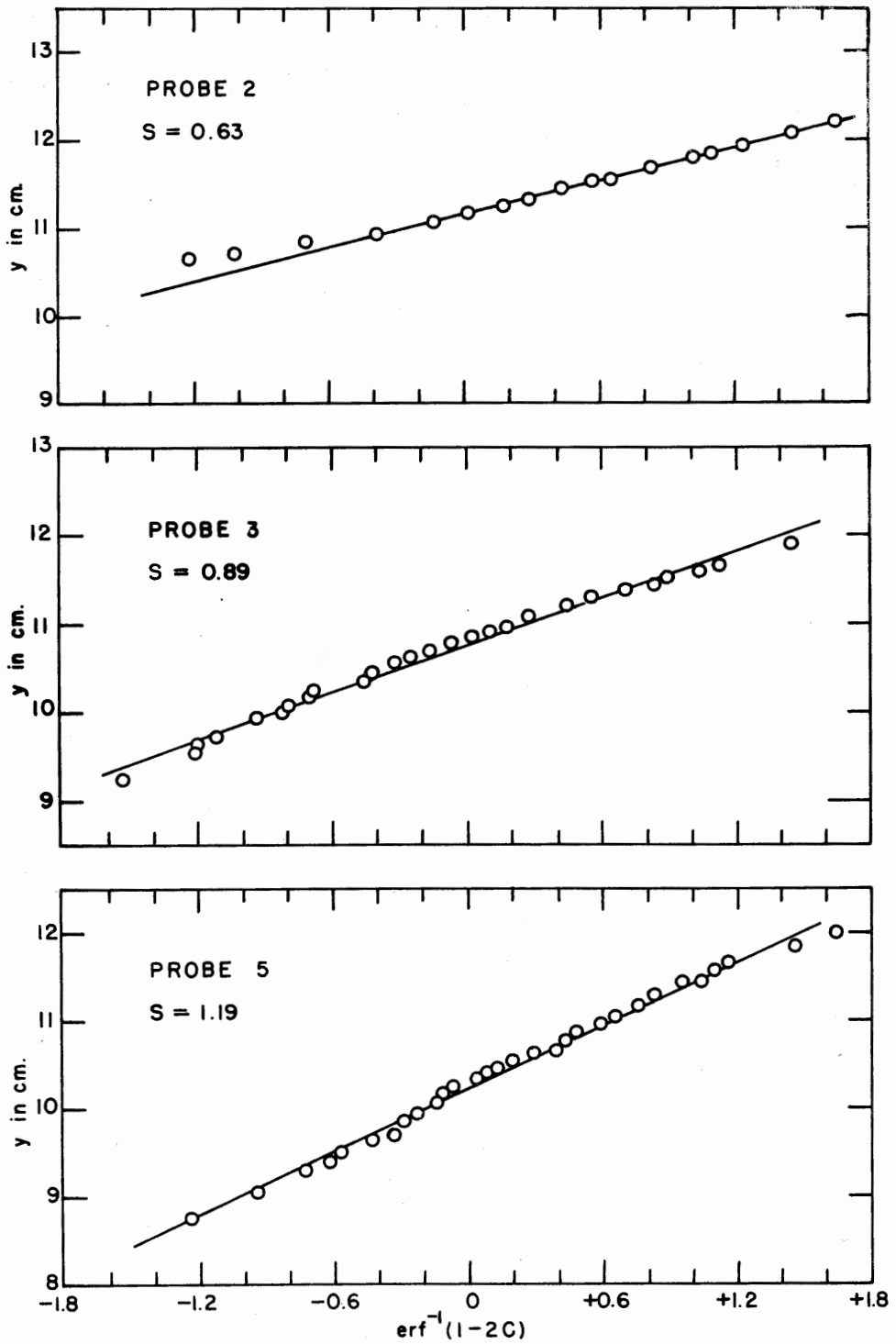

Figure 5.7 Concentration profiles at various stations for run D2.

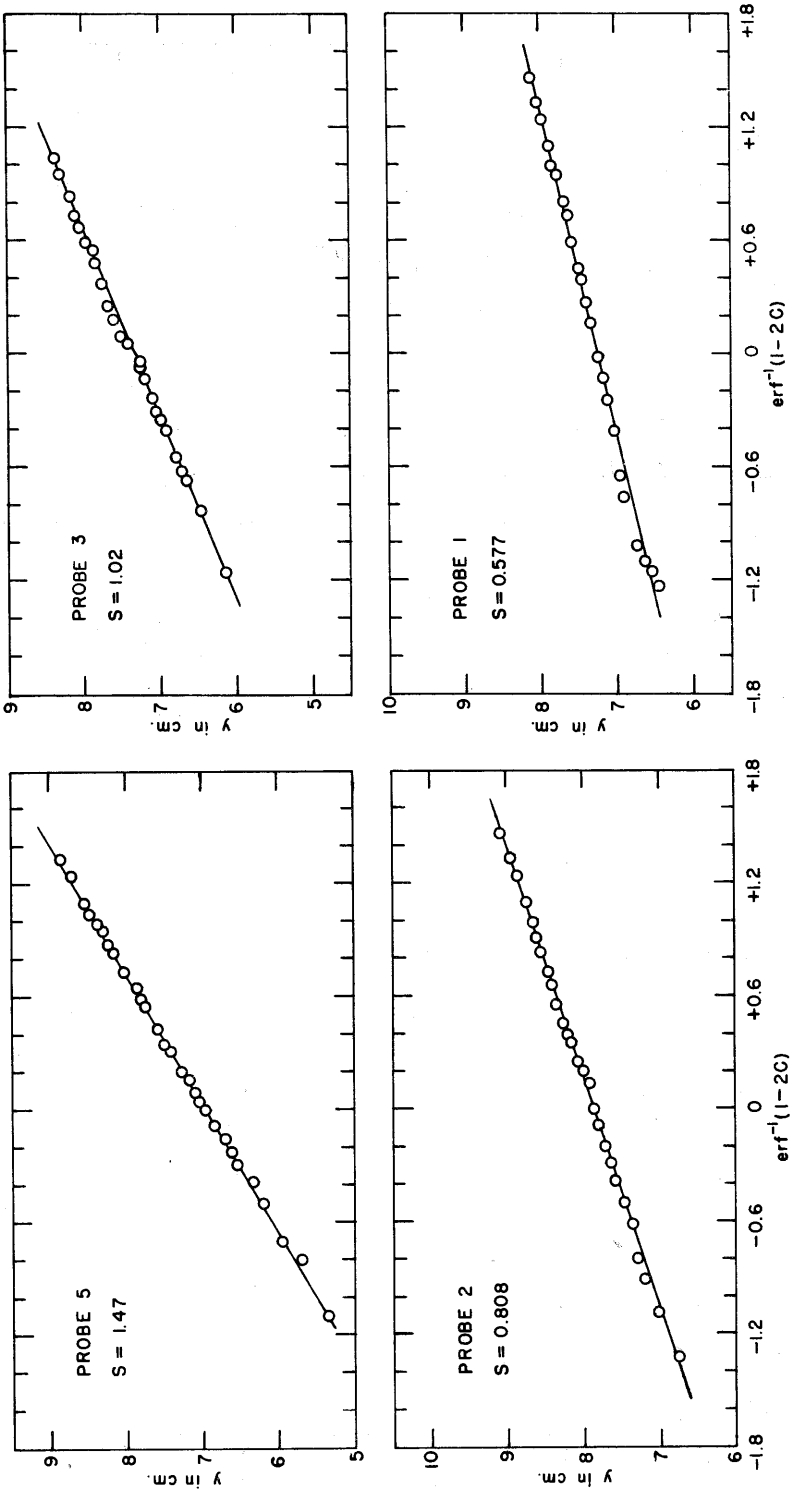

Figure 5.8 Concentration profiles at various stations for run D3.

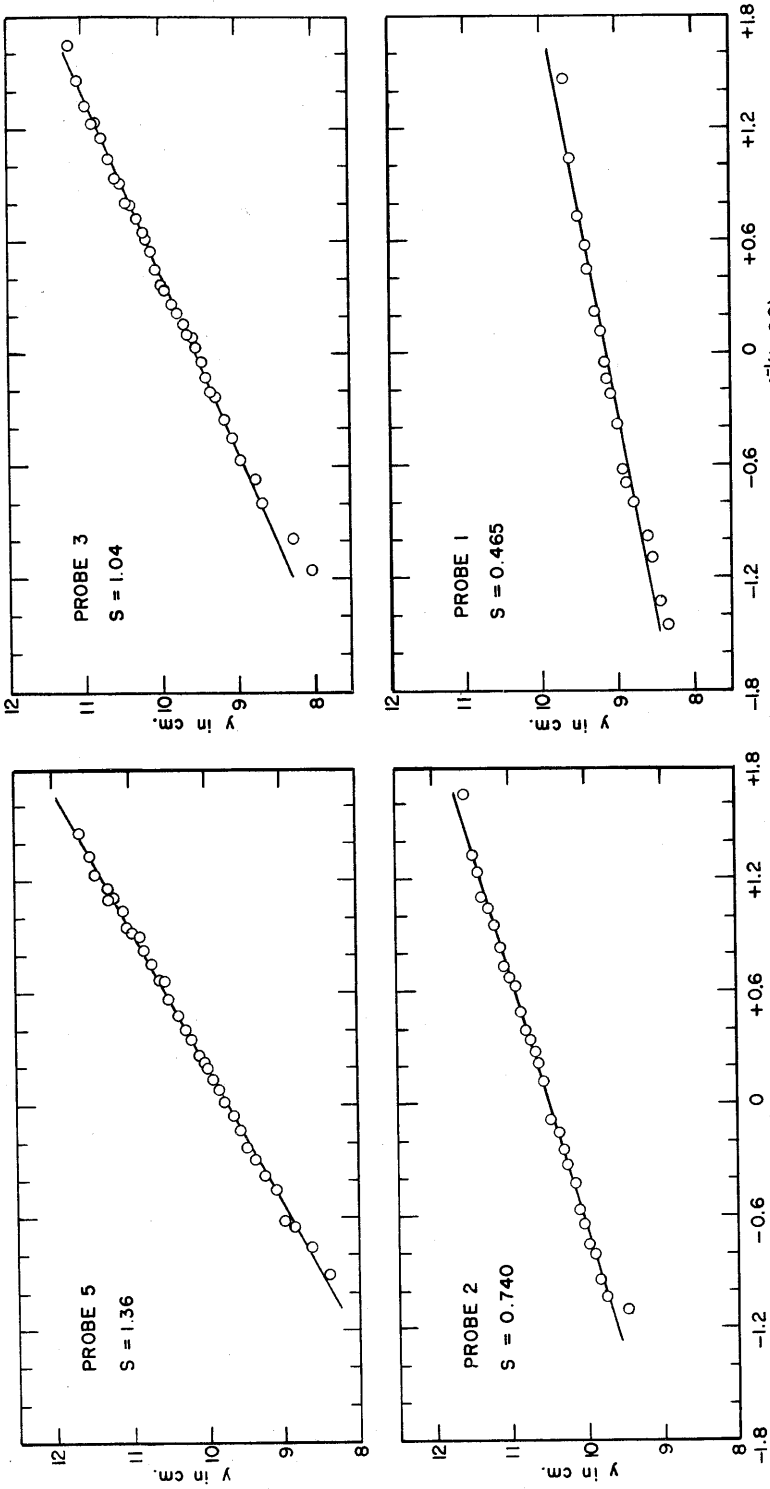

Figure 5.9 Concentration profiles at various stations for run D4.

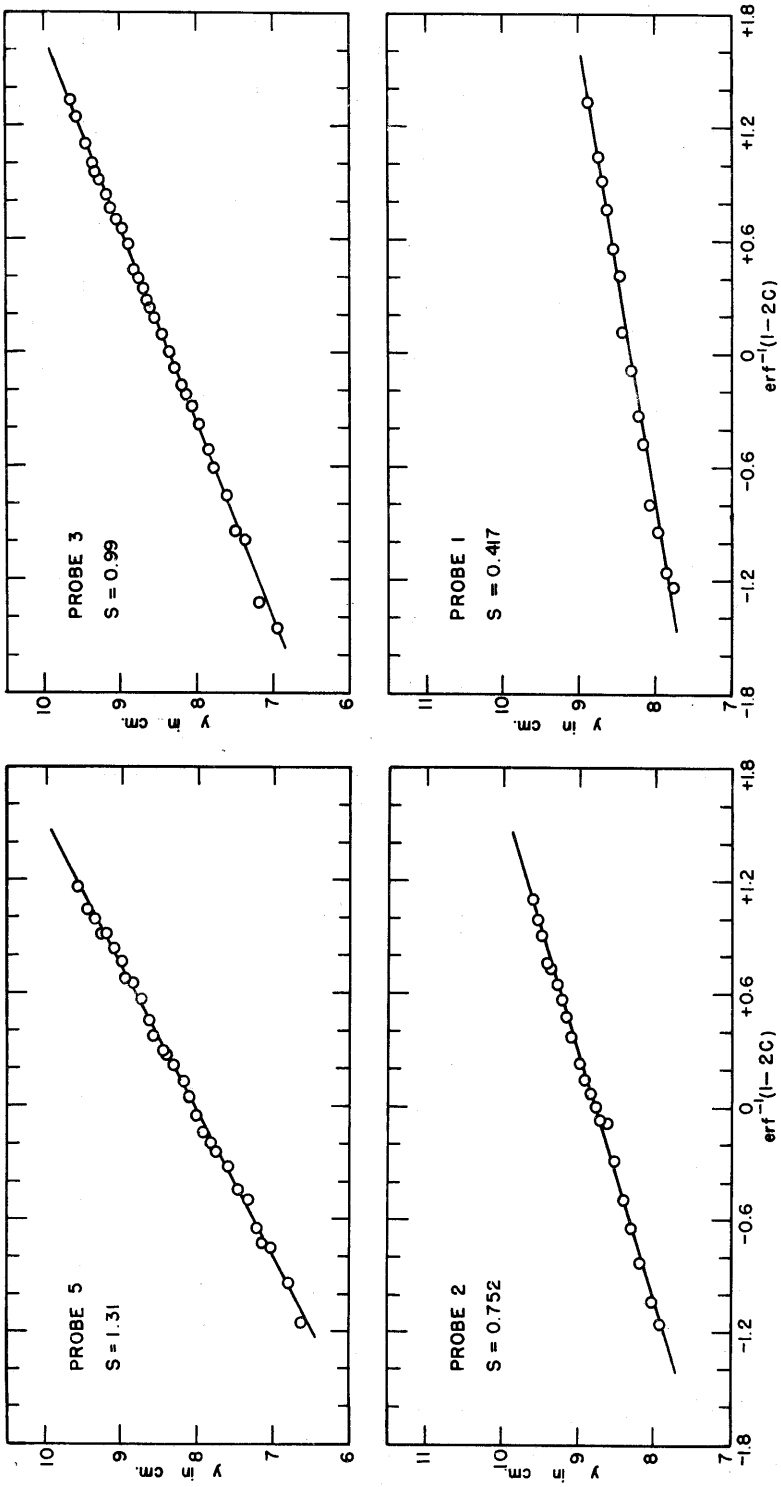

Figure 5.10 Concentration profiles at various stations for run D5.

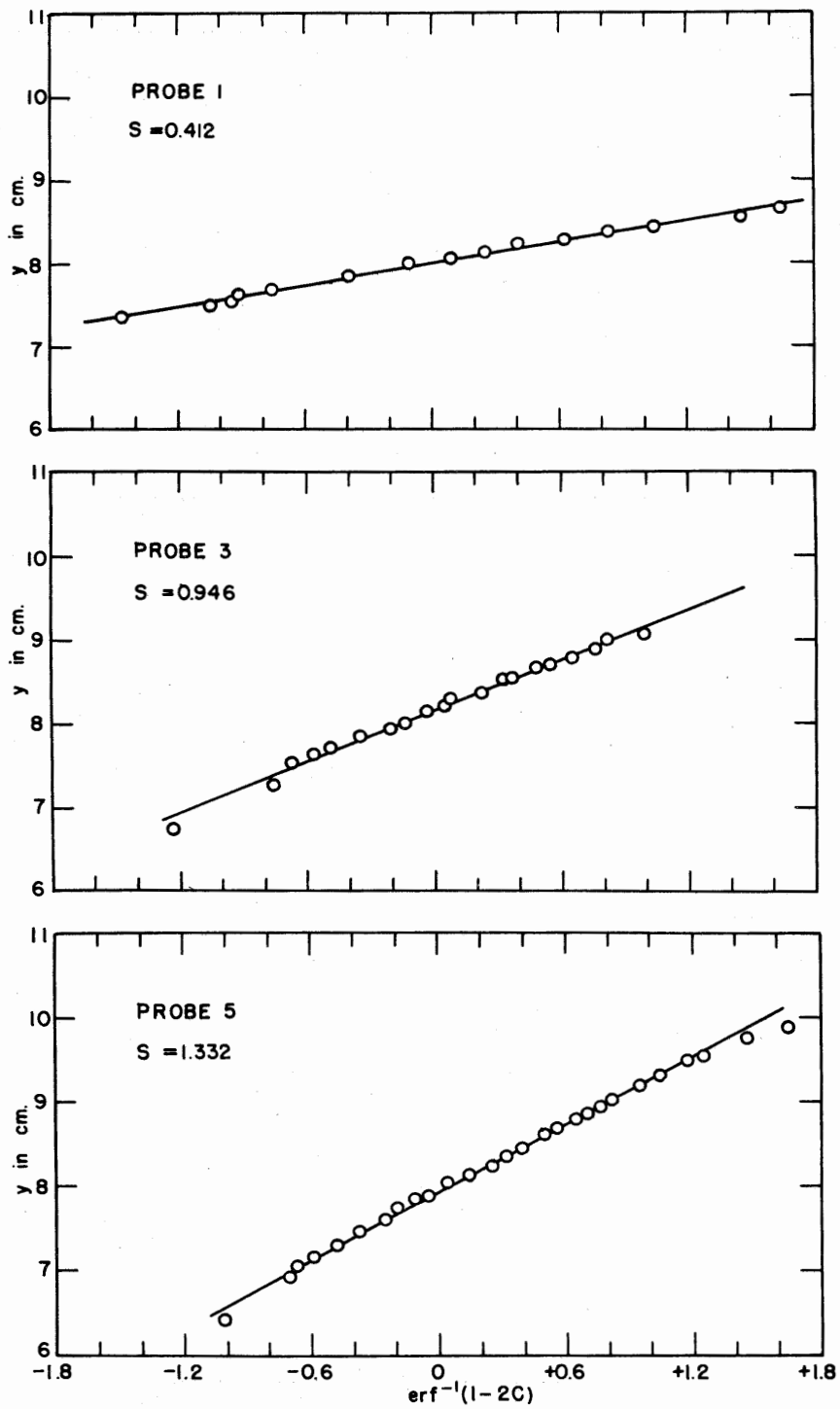

Figure 5.11 Concentration profiles at various stations for run E1.

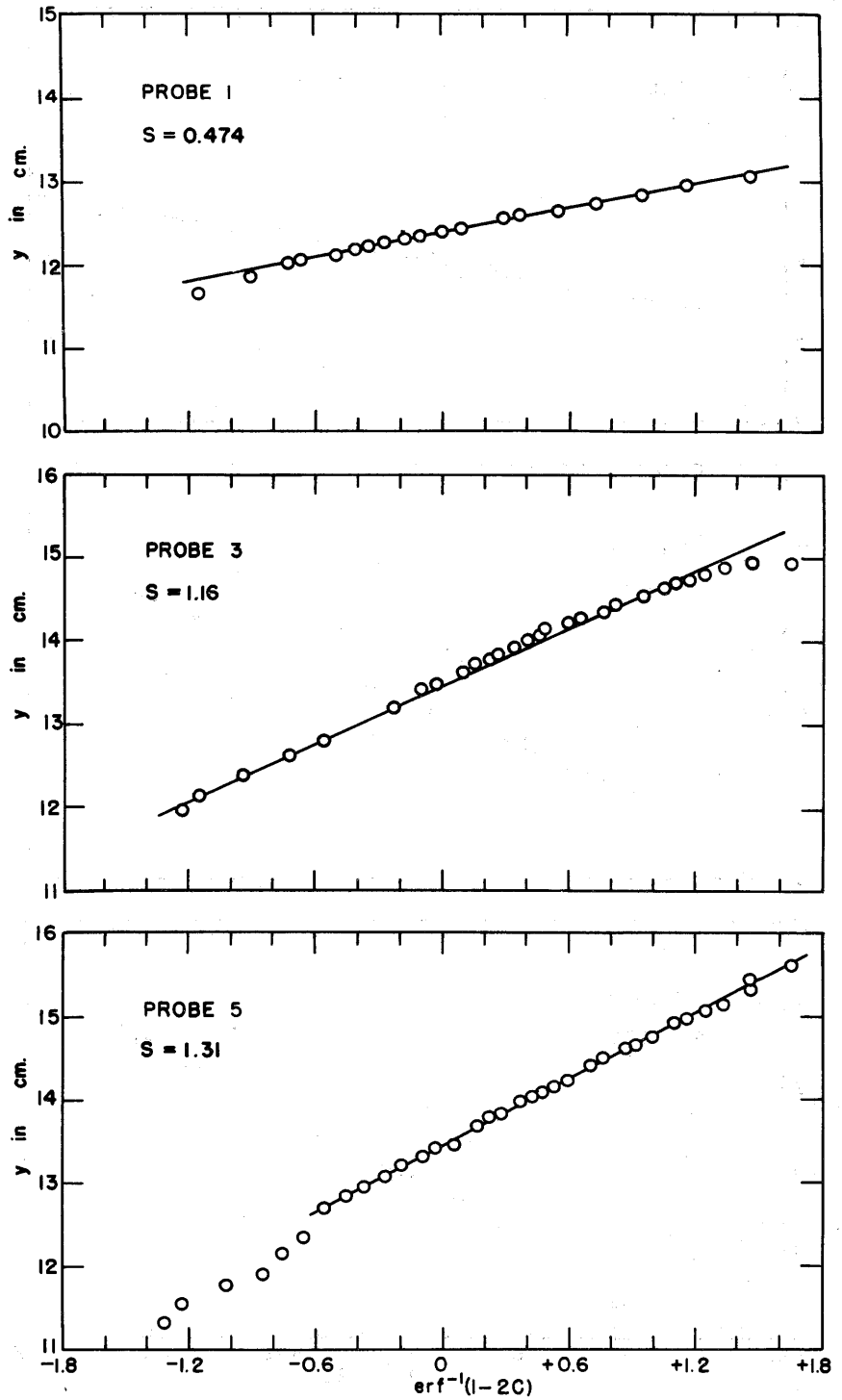

Figure 5.12 Concentration profiles at various stations for run E2.

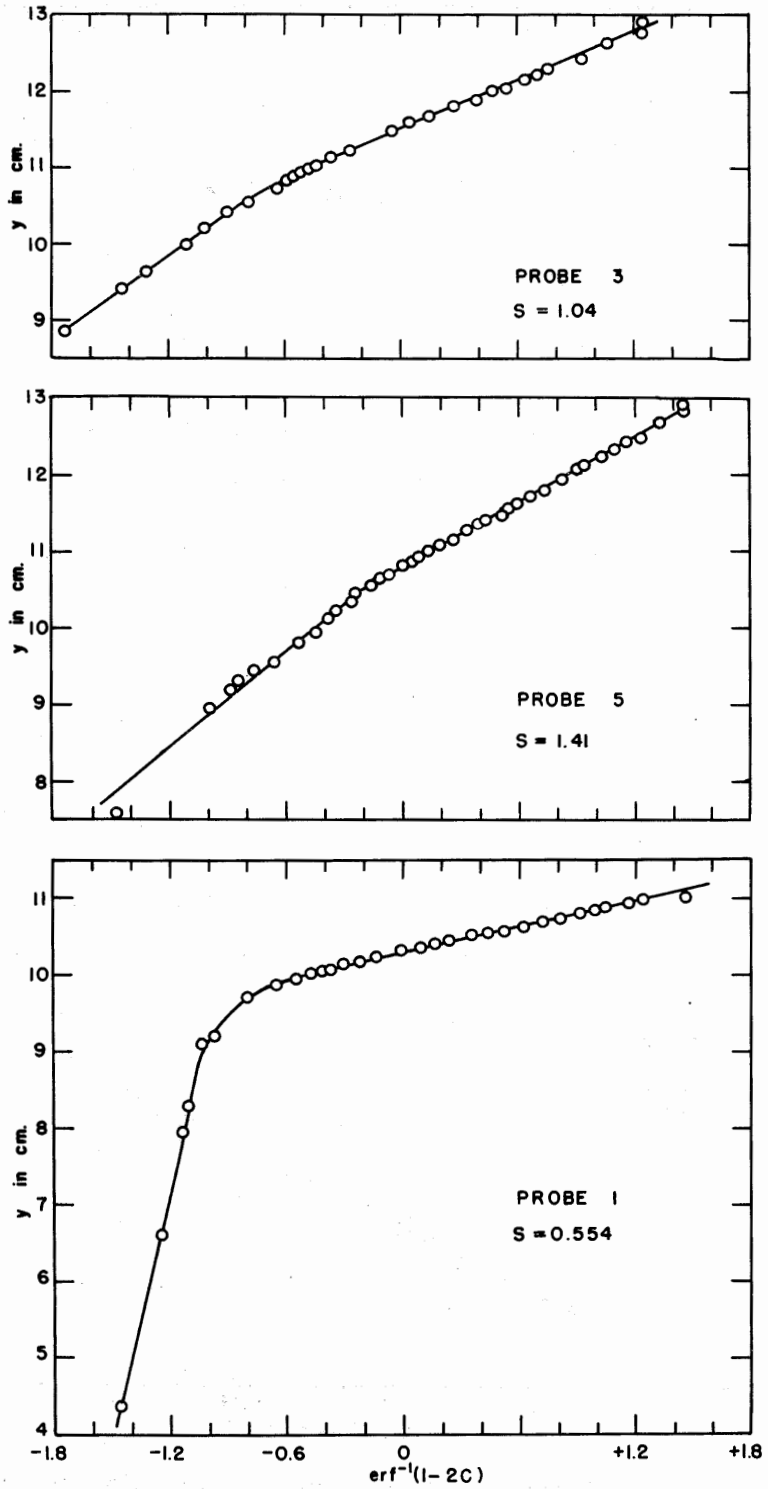

Figure 5.13 Concentration profiles at various stations for run E3.

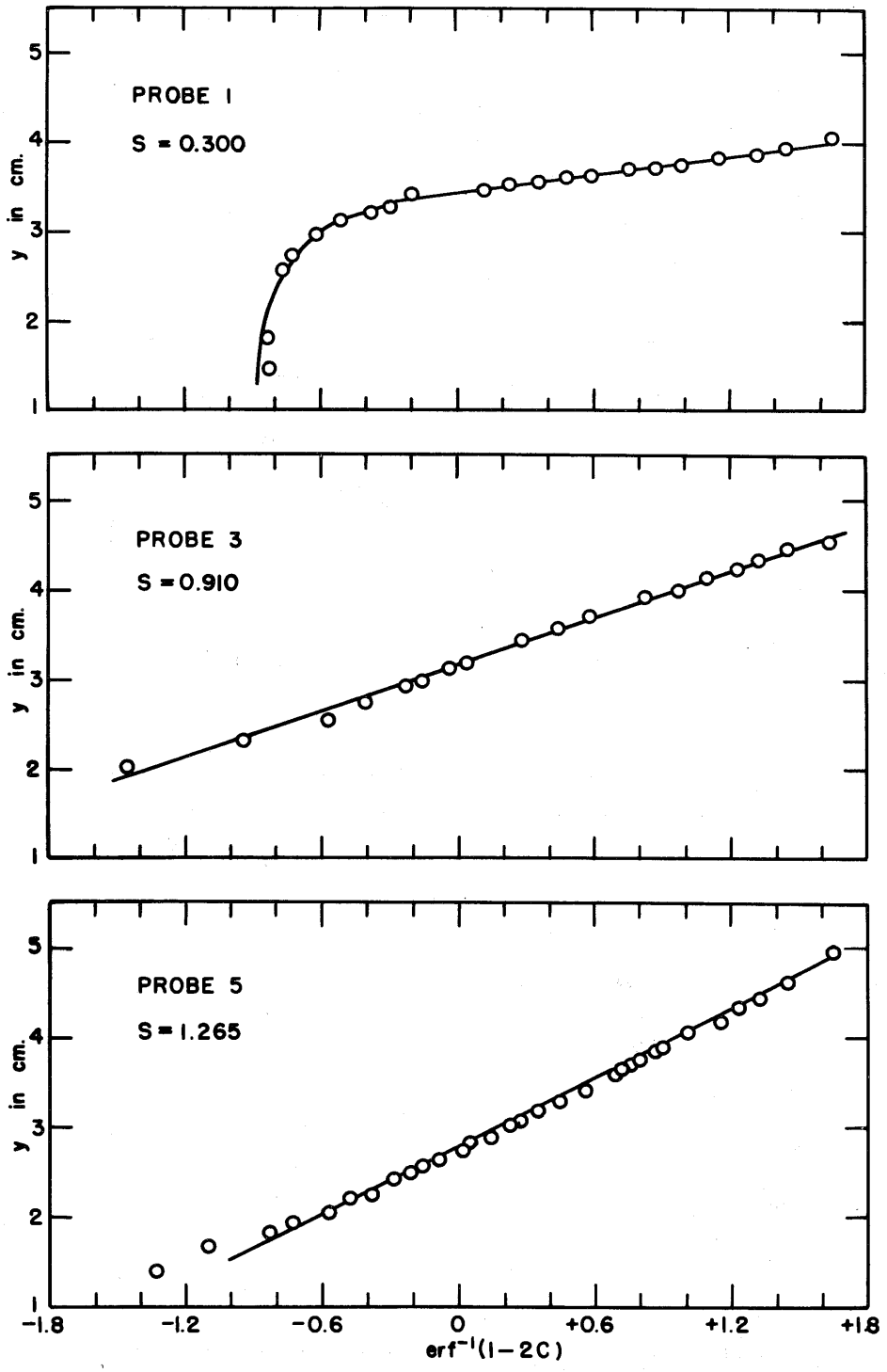

Figure 5.14 Concentration profiles at various stations for run E4.

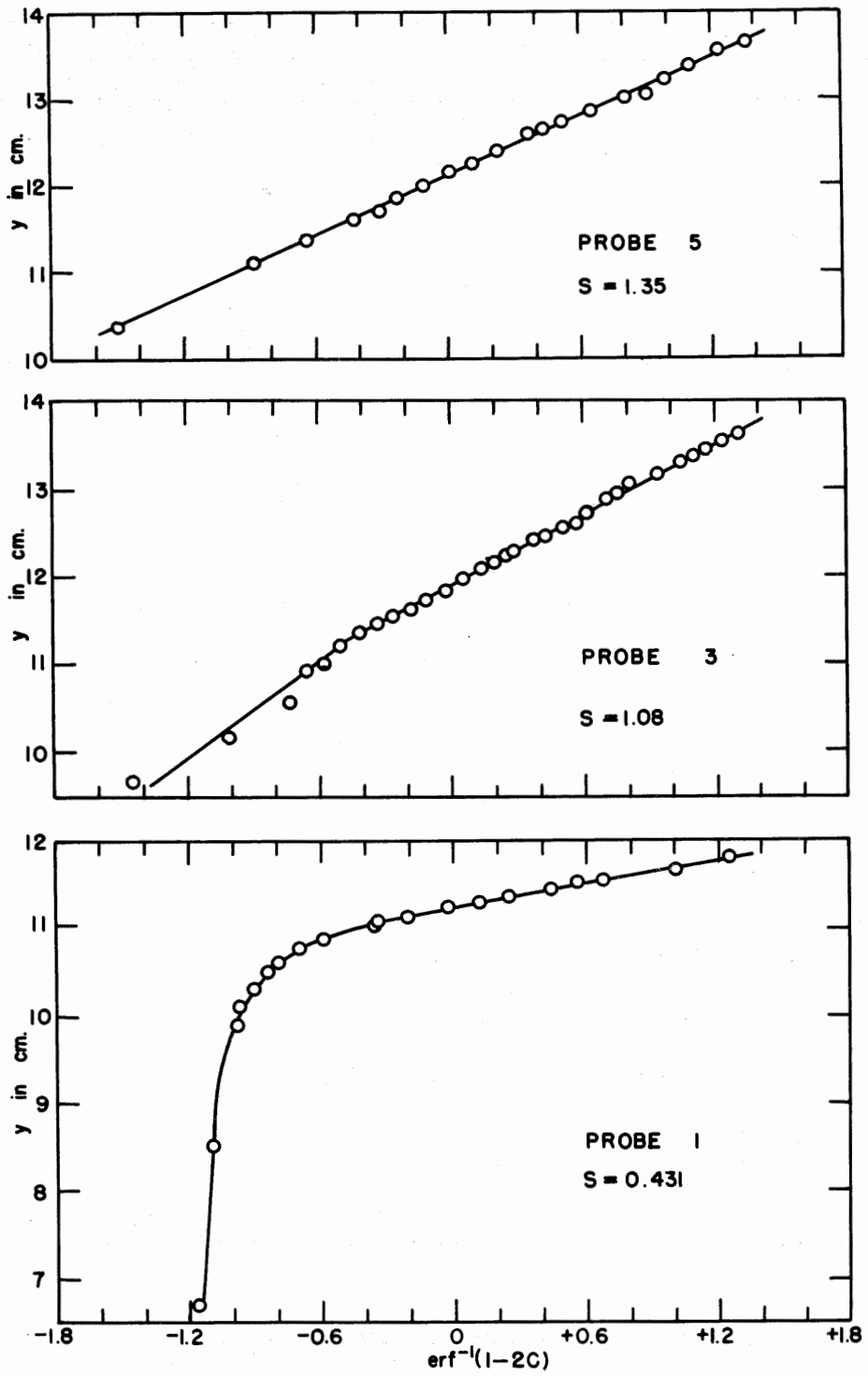

Figure 5.15 Concentration profiles at various stations for run E5.

Run No.	Probe I		Probe II		Probe III		Probe V	
	S	F(s)	S	F(s)	S	F(s)	S	F(s)
C1	-	-	0.600	1.210	0.925	1.610	1.20	2.200
C2	-	-	0.765	1.220	0.900	1.610	1.15	2.190
C3	-	-	0.765	1.235	0.951	1.610	1.31	2.165
C4	-	-	0.710	1.270	1.000	1.611	1.38	2.140
C5	-	-	0.766	1.245	0.895	1.610	1.29	2.162
D1	0.442	0.6395	0.756	1.220	1.032	1.609	1.40	2.185
D2	-	0.7375	0.630	1.250	0.890	1.610	1.19	2.160
D3	0.577	0.6771	0.808	1.234	1.020	1.609	1.47	2.175
D4	0.465	0.7320	0.740	1.247	1.040	1.610	1.36	2.160
D5	0.417	0.7048	0.752	1.240	0.990	1.609	1.31	2.165
E1	0.412	0.6962	-	-	0.946	1.609	1.332	2.170
E2	0.474	0.7980	-	-	-	1.611	1.310	2.140
E3	0.554	0.8275	-	-	1.040	1.610	1.410	2.125
E4	0.300	0.6044	-	-	0.910	1.610	1.265	2.200
E5	0.431	0.7731	-	-	1.080	1.610	1.351	2.147

Table 5.2 Experimentally determined slopes S and computed values of F(s).

Run		C1	C2	C3	C4	C5
U in cm/sec		0.0374	0.0351	0.0312	0.0190	0.0252
r	I	-	-	-	-	-
	II	0.0214	0.0335	0.0316	0.0217	0.0290
	III	0.0287	0.0267	0.0278	0.0270	0.0233
	V	0.0259	0.0235	0.0283	0.0295	0.0272

Run		D1	D2	D3	D4	D5
U in cm/sec		0.0253	0.0230	0.0134	0.0178	0.0227
r	I	0.0370	-	0.0464	0.0276	0.0260
	II	0.0298	0.0191	0.0273	0.0242	0.0274
	III	0.0319	0.0233	0.0255	0.0285	0.0280
	V	0.0316	0.0233	0.0292	0.0272	0.0272

Run		E1	E2	E3	E4	E5
U in cm/sec		0.0265	0.0158	0.00856	0.0304	0.0167
r	I	0.0273	0.0236	0.0248	0.0202	0.0210
	II	-	-	-	-	-
	III	0.0270	-	0.0232	0.0265	0.0302
	V	0.0294	0.0250	0.0243	0.0270	0.0267

Table 5.3 Values of r computed from Equation (5.17).

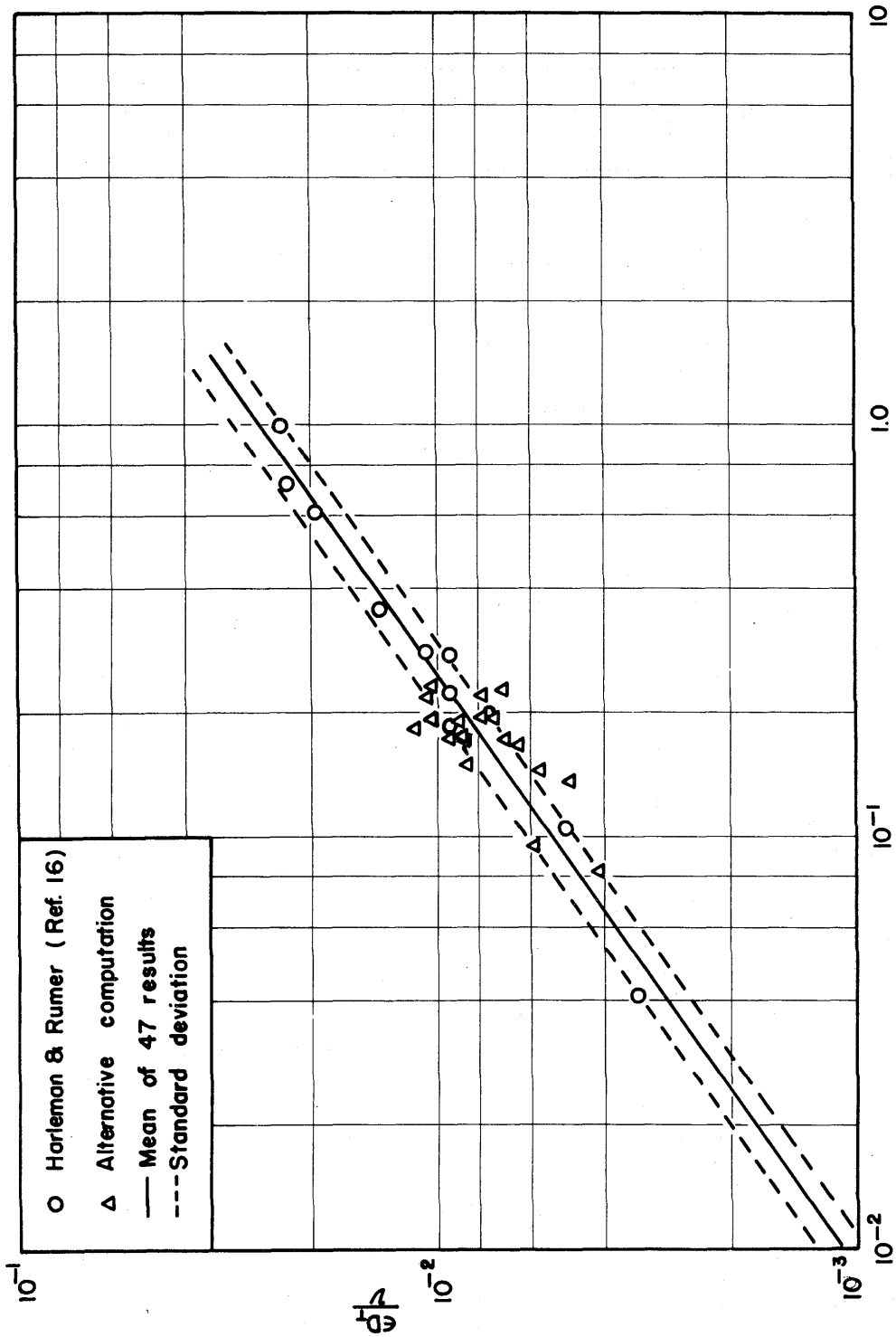

Figure 5.16 Dispersion coefficient versus particle Reynolds number for sodium chloride solutions.

It is seen that the value of r is indeed reasonably constant and

$$\begin{aligned} &\text{mean value of } r = 0.0267 \\ &\text{standard deviation} = \pm 0.0035 \end{aligned} \qquad (5.18)$$

The range of particle Reynolds numbers for which these results are valid is ostensibly from $O(10^{-2})$ to 2×10^{-1}, as the fluid is theoretically at rest at the stagnation point and reaches its maximum velocity downstream.

This implies that Harleman and Rumer's result i.e.

$$\frac{\epsilon D_T}{\nu} = 0.0265 \left(\frac{vd}{\nu}\right)^{0.7}$$

is reasonably valid. The result (5.18) is plotted on Figure 5.16 along with the experimental results from Harleman and Rumer's constant velocity, constant density experiments. The agreement is seen to be exceptionally good; the points marked by small triangles will be explained later.

In all these experiments stable half-bodies were observed, and no sign of any instability was present. The Rayleigh numbers for runs C1 through E5 are given in Table 5.4 and they are seen to be quite low; since the values of $\varkappa$, the ratio of the longitudinal dispersion coefficient to the lateral dispersion coefficient, are quite high also, it is not surprising the instability growth rates were low.

However, it is to be noted that the run E3 which has the highest Rayleigh number and lowest value of $\varkappa$ and therefore the highest growth rate is also the run previously mentioned as having a distinct break in the concentration profile (see Figure 5.13).

Some shapes of the half-bodies formed are shown in the photographs

Run Number	ℓ(cm)	$\Delta\rho$(gm/mℓ)	$Dx10^4$(cm^2/sec)	$\mu x10^2$ gm/cm.sec	Rayleigh Number	$\varkappa = D_L/D_T$
C1	1.07	0.00047	0.86	0.93	2.2	14.5
C2	1.02	0.00047	0.88	0.93	2.1	14.7
C3	1.16	0.00042	0.88	0.96	2.0	14.7
C4	1.22	0.00042	0.75	0.97	2.3	12.8
C5	1.14	0.00042	0.81	0.96	2.2	13.5
D1	1.24	0.0043	0.71	0.92	29	12.8
D2	1.06	0.0048	0.75	0.87	27	13.7
D3	1.30	0.0042	0.52	0.93	41	9.8
D4	1.21	0.0038	0.65	0.97	26	12.0
D5	1.16	0.0039	0.73	0.96	23	12.7
E1	1.18	0.010	0.81	0.96	53	13.5
E2	1.16	0.010	0.66	0.94	65	12.0
E3	1.25	0.010	0.57	0.96	80	8.9
E4	1.12	0.010	0.77	0.95	55	13.5
E5	1.20	0.010	0.82	0.95	54	11.6

Table 5.4 Rayleigh numbers at Probe V for experiments C1 through E5.

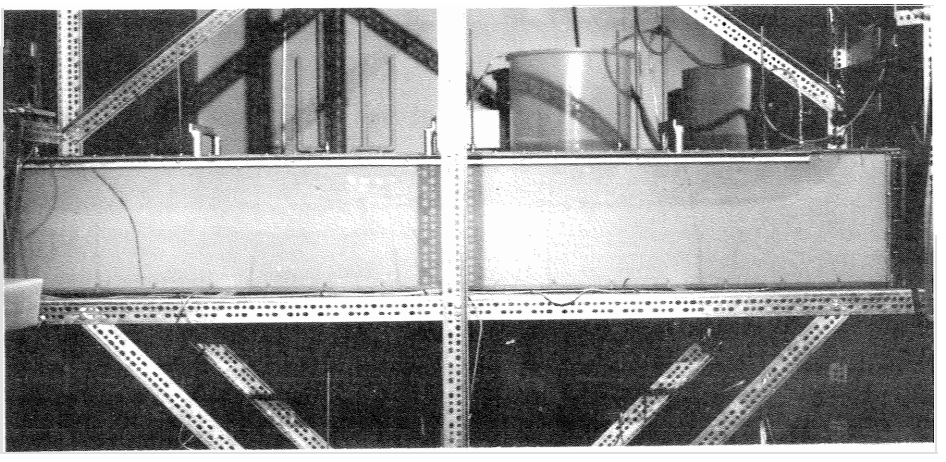

Figure 5.17a The half body shape for run E2 ($\Delta\rho = 0.01$, $Q_2/Q_1 = 0.687$). (Flow from left to right.)

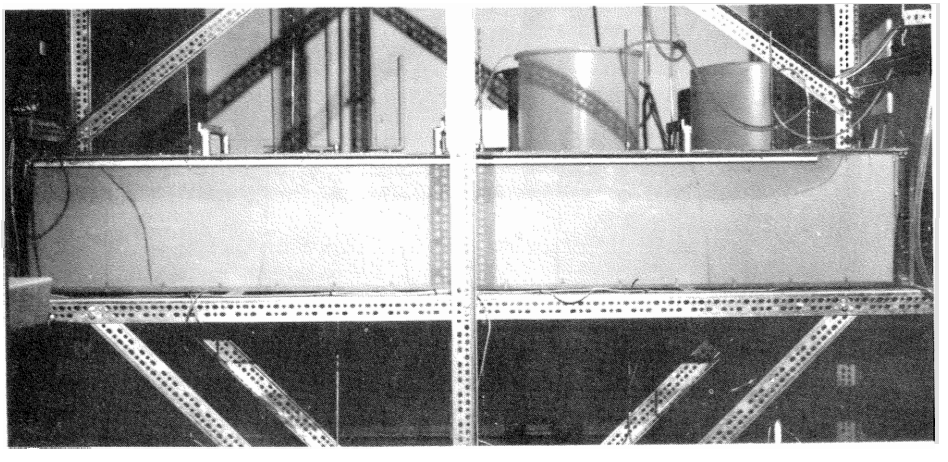

Figure 5.17b The half body shape for run E5 ($\Delta\rho = 0.01$, $Q_2/Q_1 = 0.584$).

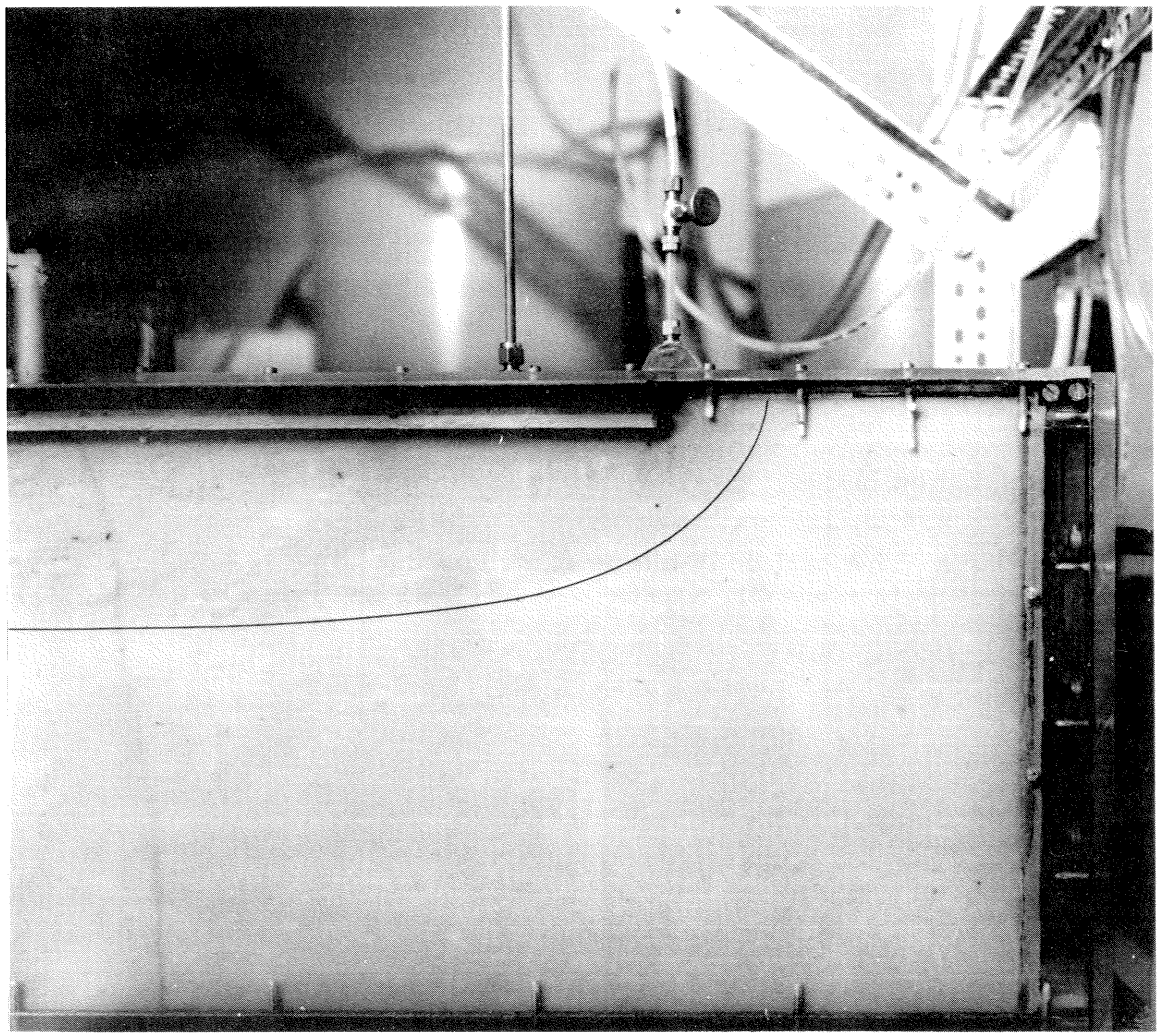

Figure 5.18 The theoretical half body superimposed on an experimental photograph of run E5.

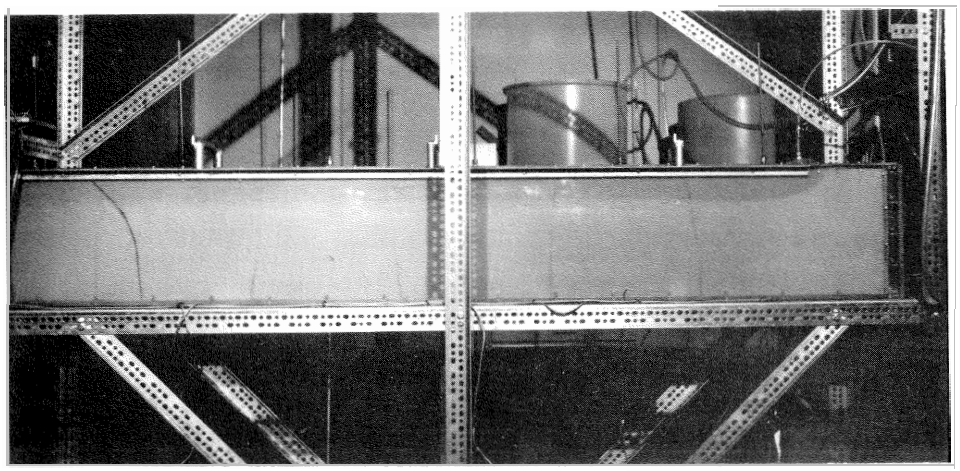

Figure 5.19a The half body shape for run D5 ($\Delta\rho = 0.004$, $Q_2/Q_1 = 0.355$).

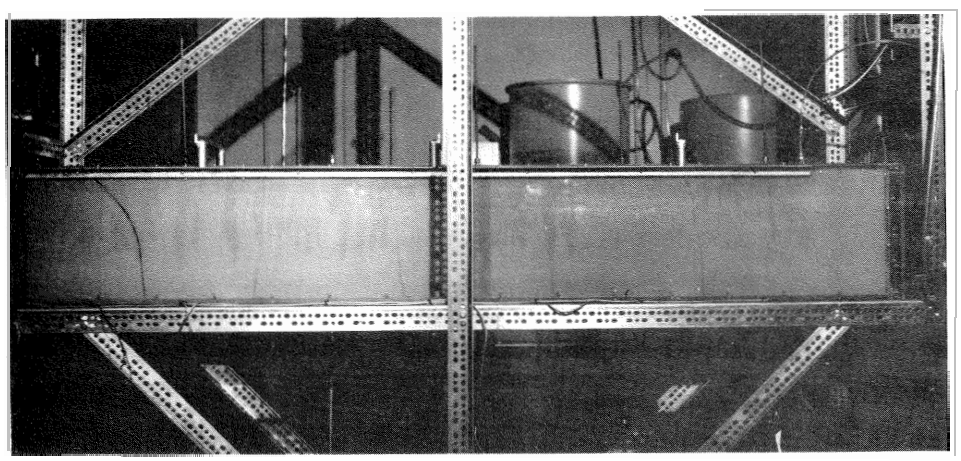

Figure 5.19b Run D5 after the flow had been stopped for 15 hours.

in Figure 5.17 - 5.19. The contrast in the photographs is not high since low dye concentrations were used to avoid complications with the conductivity probes. The approximate theoretical shape of the front of the half-body is superimposed on a photograph in Figure 5.18 and the agreement is seen to be quite good.

In Figure 5.19a is a photograph of the half-body for run D5 (Figure 5.19b) taken 15 hours after stopping the flow. The stationary two fluid system is seen to be quite unstable.

5.4 Alternative Computation

Under the assumptions that have been made in writing equation (5.1) for the mixing along a curved streamline it was possible to describe the mixing by an equation of the form

$$y - y_o = f(s) \cdot \text{erf}^{-1} (1 - 2C)$$

where $f(s)$ is purely a function of the shape of the streamline, the velocity along it and the dispersion coefficient.

Now between probes III and V the velocity along the interface is nearly constant since the interface is almost horizontal (see Figures 5.17 - 5.19). Thus it is possible to assume D_T is constant between III and V, in which case $f(s)$ can easily be deduced to be

$$f(s) = 2(D_T(s - s_o)/q)^{\frac{1}{2}}$$

where

s_o is some fictitious origin.

Hence it is possible to write

$$y - y_o = 2(D_T(s - s_o)/q)^{\frac{1}{2}} \operatorname{erf}^{-1}(1 - 2C)$$

and from section 5.1

$$(\frac{S}{2})^2 = \frac{D_T(s - s_o)}{q}$$

where S is the slope of the experimentally determined y versus $\operatorname{erf}^{-1}(1 - 2C)$ curve. Now since D_T/q is constant and the interface is almost horizontal

$$\frac{D_T}{q} = \frac{(S_V^2 - S_{III}^2)}{4(x_V - x_{III})}$$

and for these experiments

$$4(x_V - x_{III}) = 320 \text{ cm}.$$

It now becomes possible to determine D_T/q for the experimental runs A1 through B4 for which the ratio of flow of pure water to salt water is not available.

The experimental curves of y versus $\operatorname{erf}^{-1}(1 - 2C)$ are plotted in Figures 5.20 through 5.26 and the results tabulated in Table 5.5 along with similar results for experiments C1 through E5.

The results are plotted on Figure 5.16 as the small triangles, the small circles are Harleman and Rumer's (16) constant density experiments.

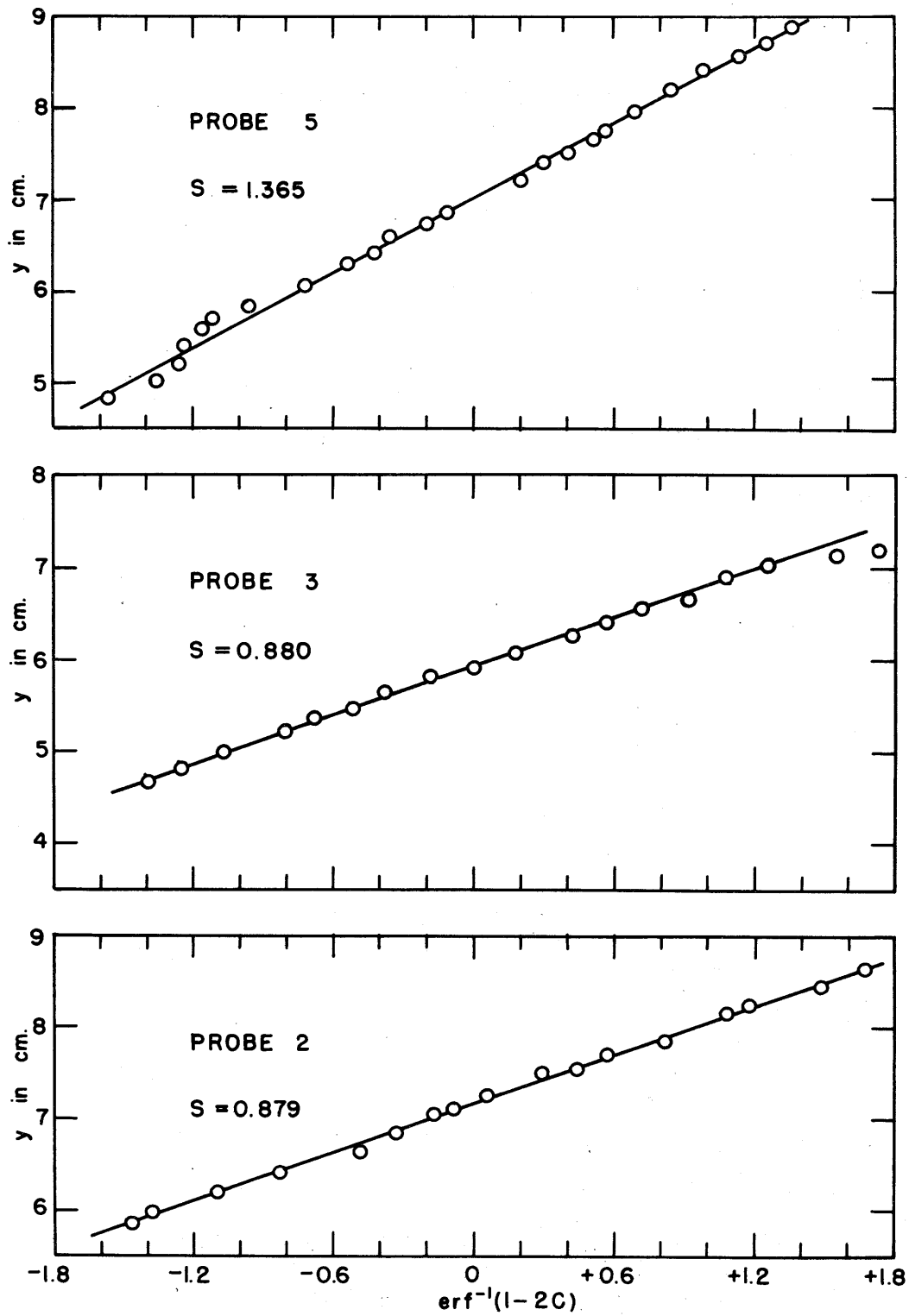

Figure 5.20 Concentration profiles at various stations for run A1.

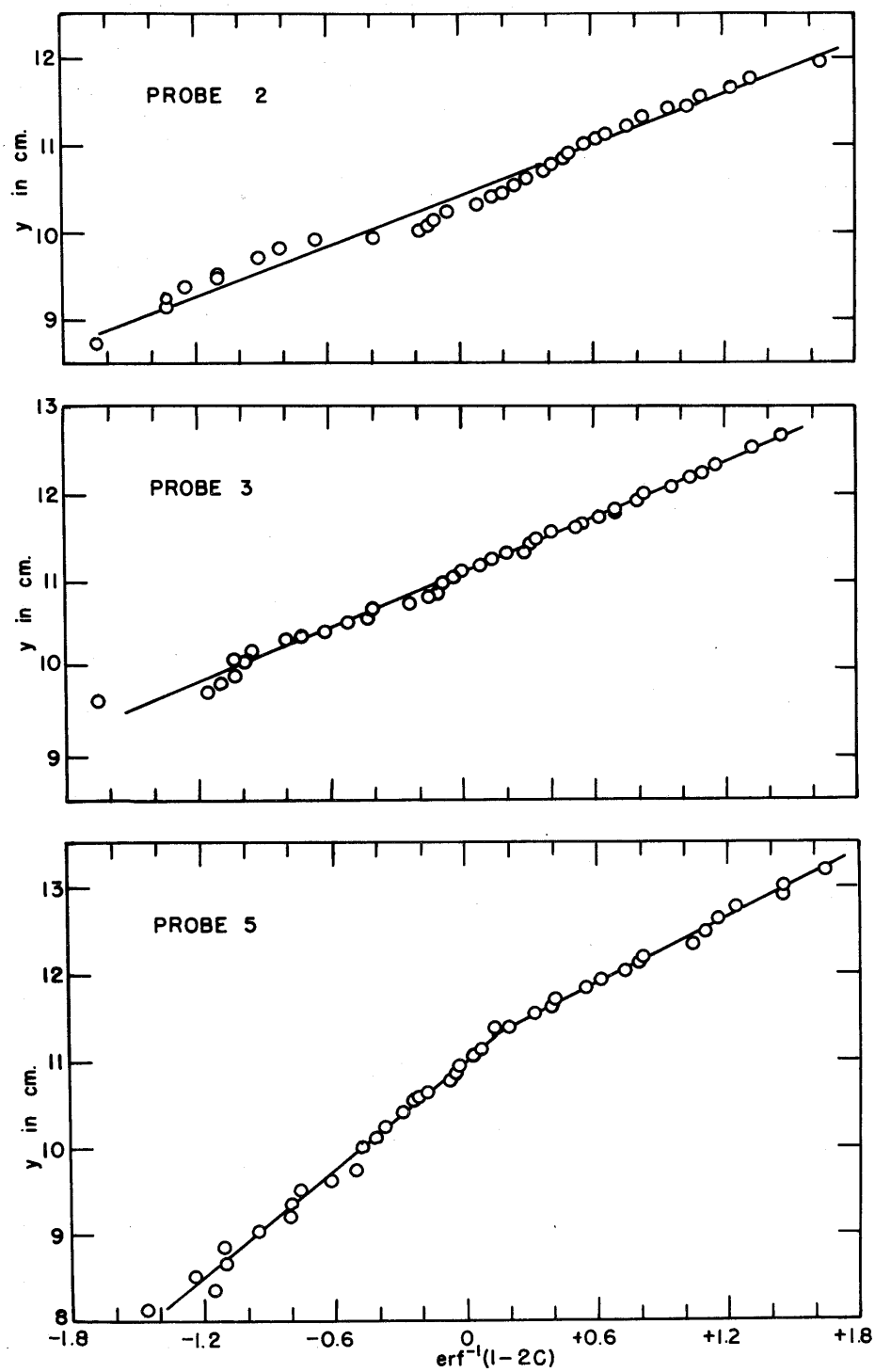

Figure 5.21 Concentration profiles at various stations for run A2.

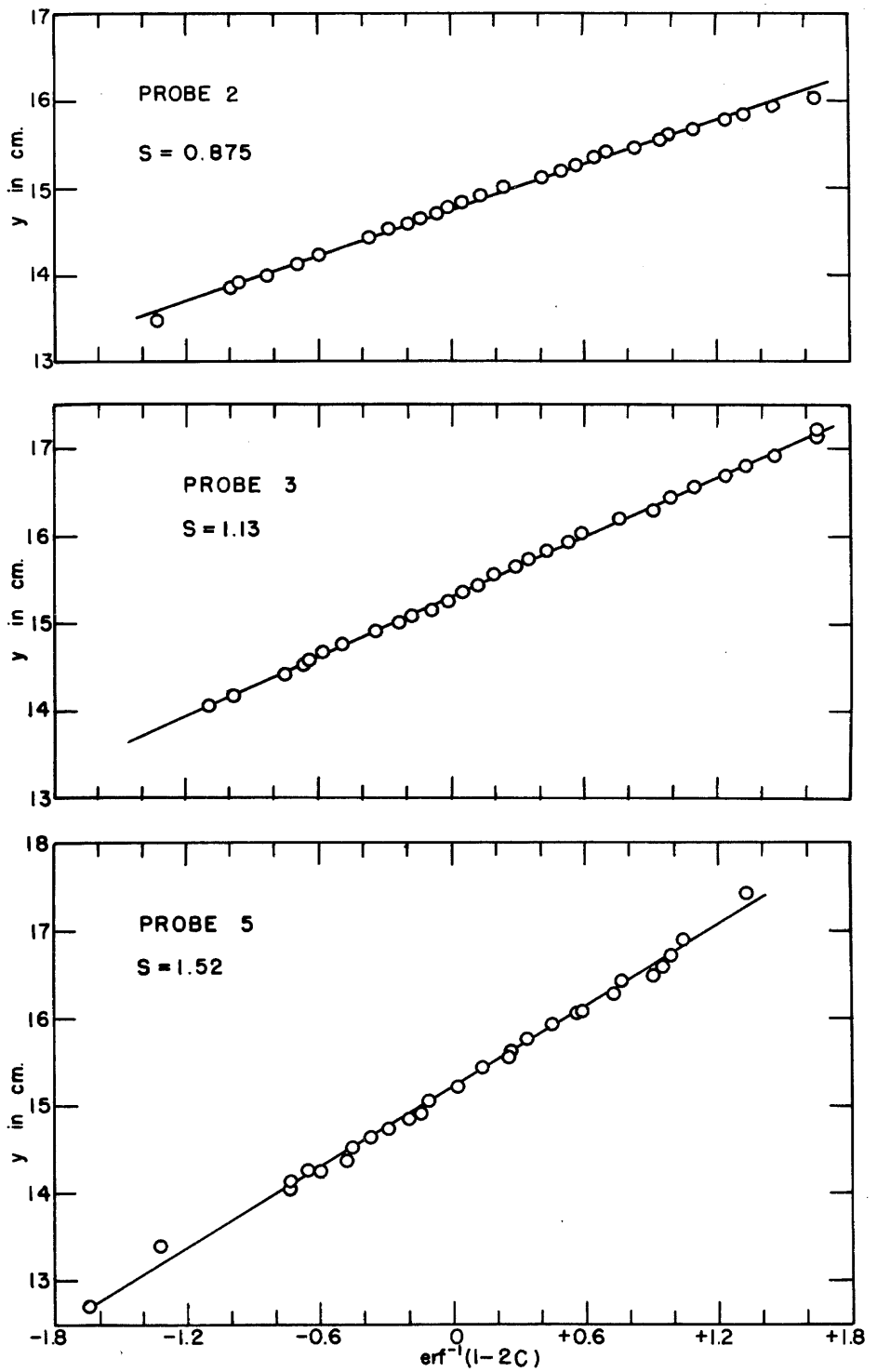

Figure 5.22 Concentration profiles at various stations for run A3.

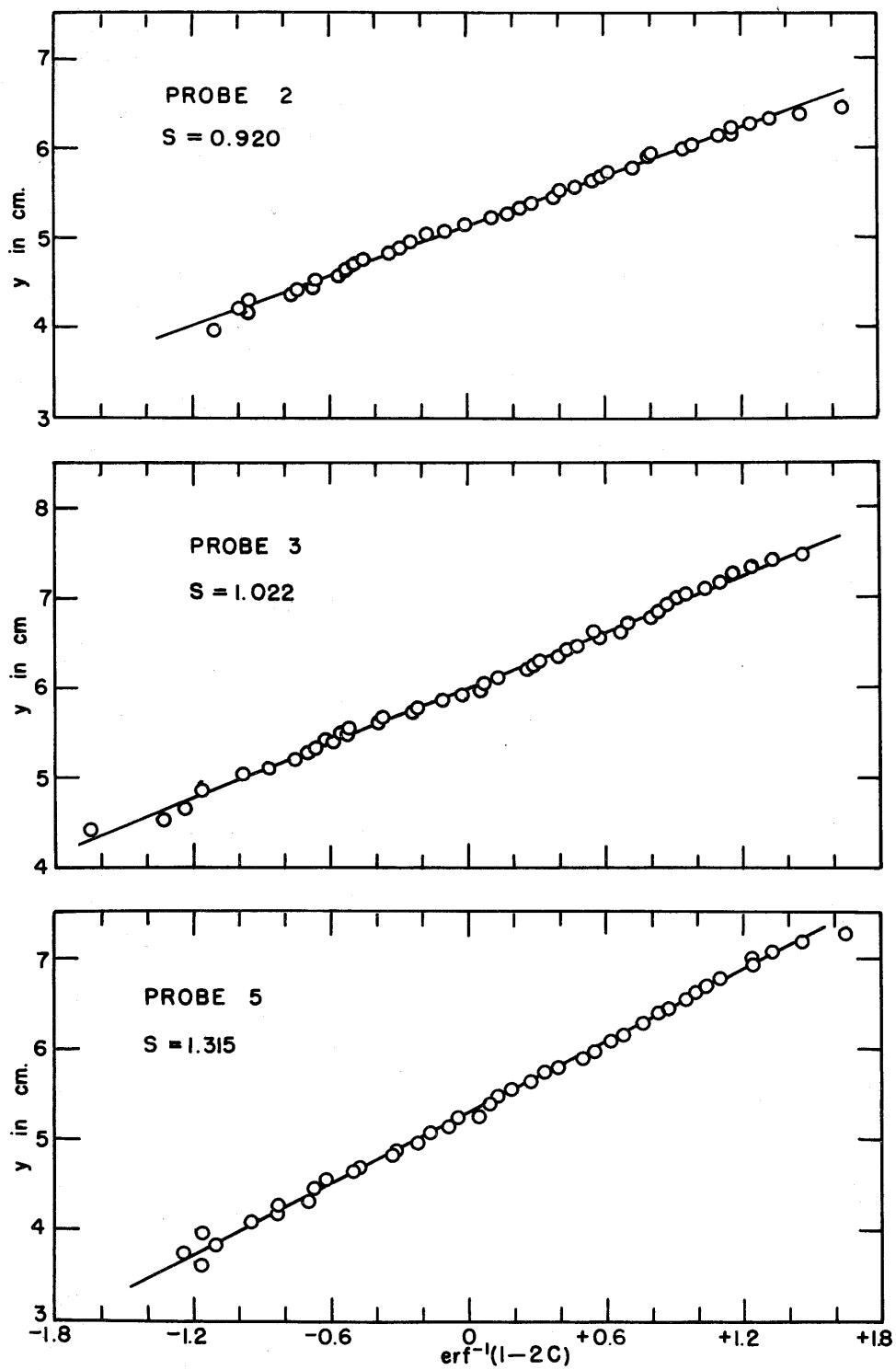

Figure 5.23 Concentration profiles at various stations for run B1.

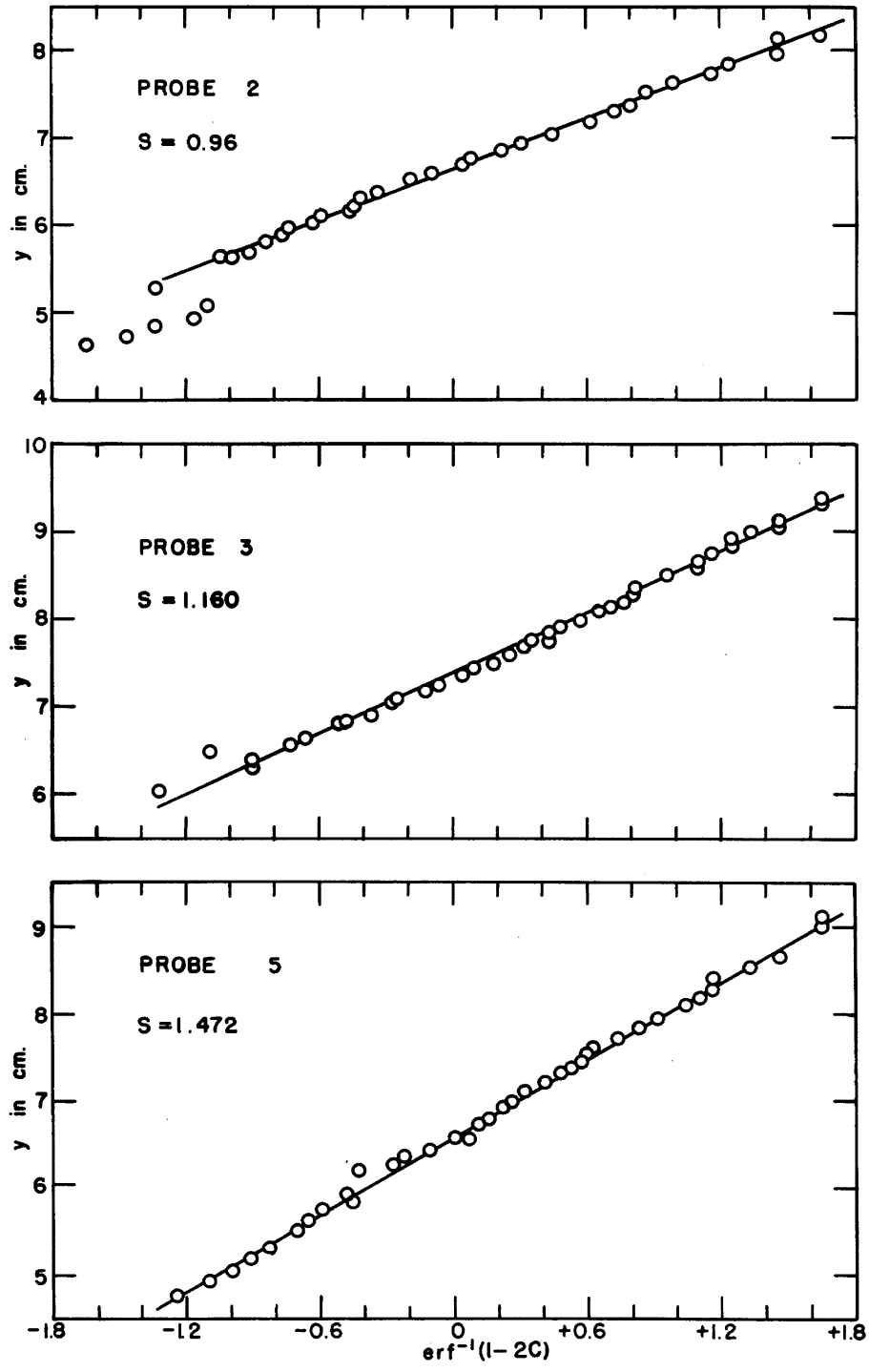

Figure 5.24 Concentration profiles at various stations for run B2.

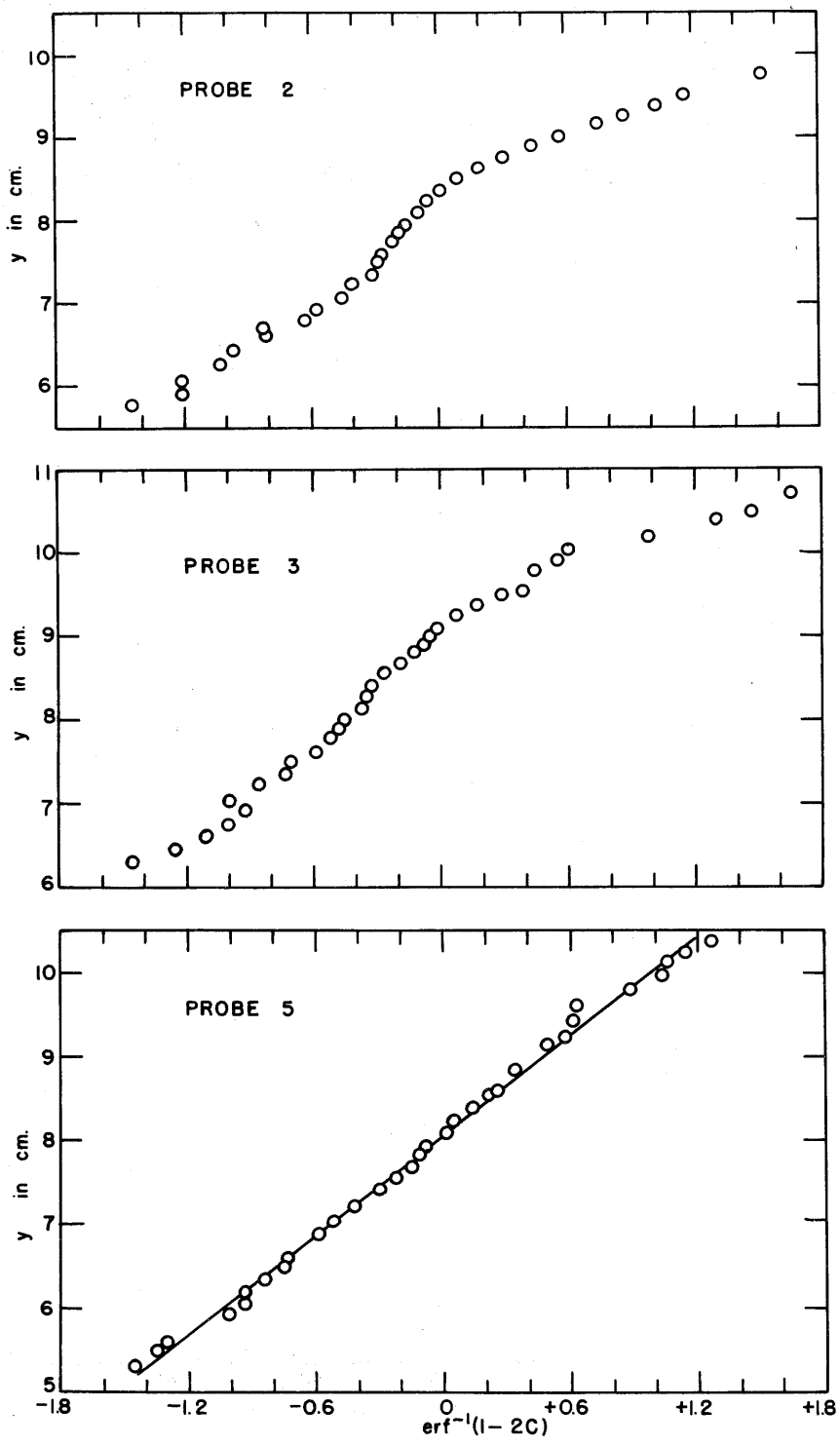

Figure 5.25 Concentration profiles at various stations for run B3.

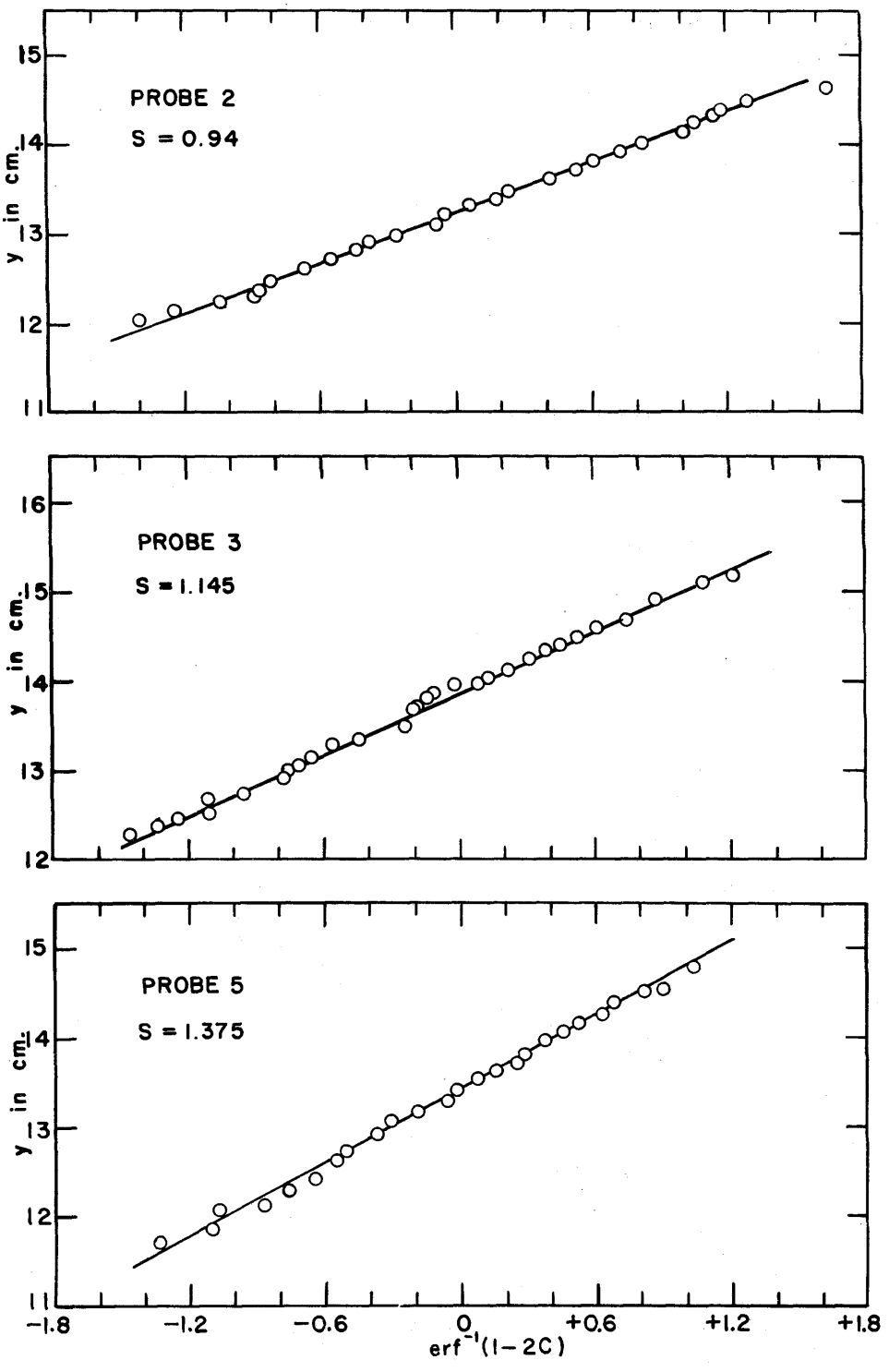

Figure 5.26 Concentration profiles at various stations for run B4.

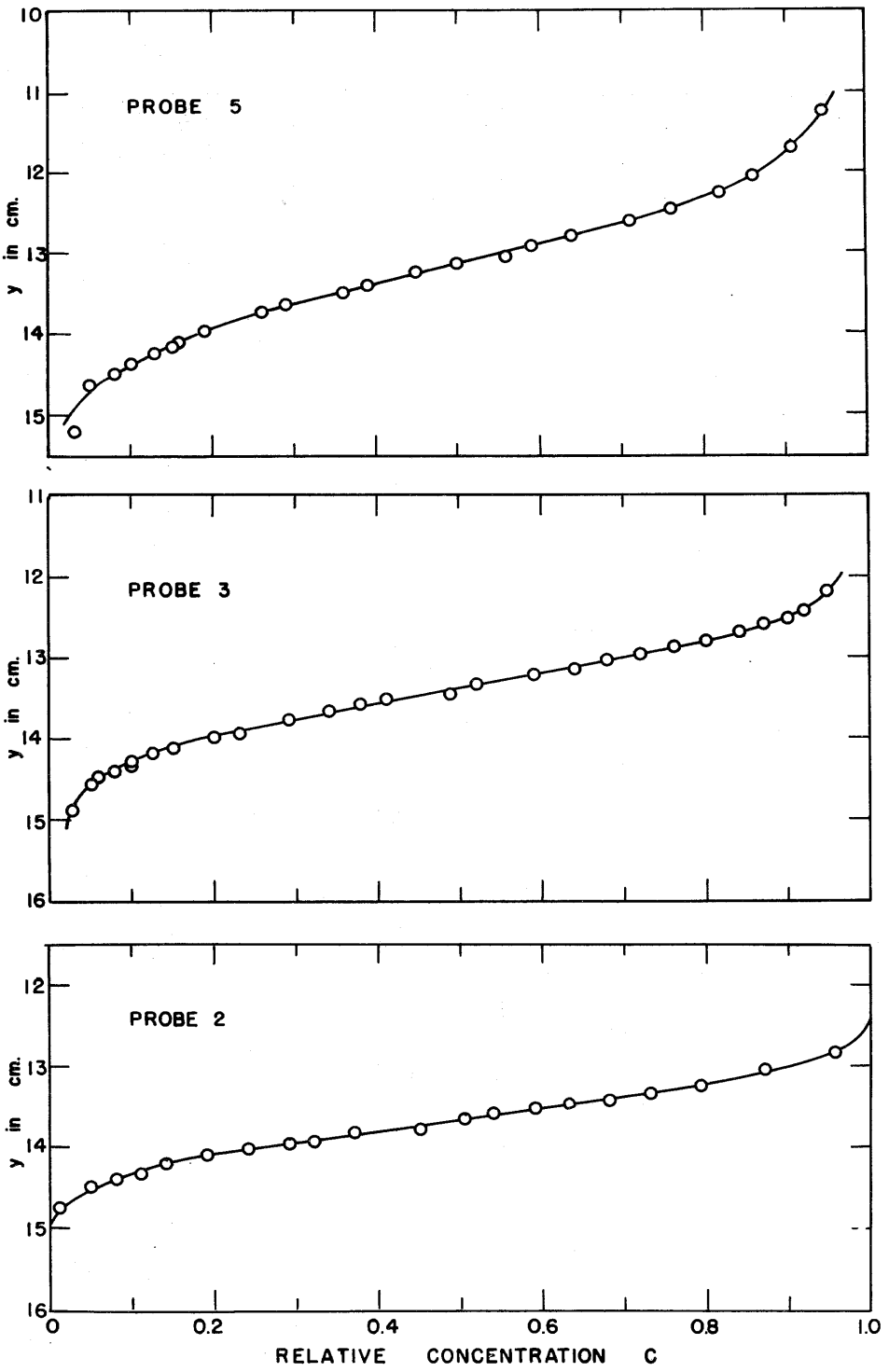

Figure 5.27 The actual shapes of a concentration profile for run C4 at probes II, III and V.

Run	Slope		D/q x 10^3	$\epsilon D/\nu$ x 10^2	Re
	III	V			
A1	0.879_{II}	1.365	3.41	1.02	0.232
A2	-	-	-	-	-
A3	1.130	1.520	3.22	1.12	0.181
B1	1.022	1.315	2.12	0.69	0.172
B2	1.160	1.472	2.58	0.87	0.176
B3	-	-	-	-	-
B4	1.145	1.375	1.84	0.48	0.136
C1	0.925	1.20	1.83	0.78	0.220
C2	0.900	1.15	1.59	0.70	0.227
C3	0.951	1.31	2.53	1.06	0.218
C4	1.000	1.38	2.82	0.93	0.171
C5	0.995	1.29	2.10	0.78	0.193
D1	1.032	1.40	2.79	0.86	0.171
D2	0.890	1.19	1.94	0.73	0.195
D3	1.020	1.47	3.50	0.59	0.095
D4	1.040	1.36	2.40	0.85	0.149
D5	0.990	1.31	2.30	0.64	0.167
E1	0.946	1.33	2.78	1.02	0.191
E2	-	-	-	-	-
E3	1.040	1.41	2.52	0.41	0.084
E4	0.91	1.27	2.42	0.89	0.190
E5	1.08	1.35	2.06	0.57	0.145

Table 5.5 Values of the dispersion coefficient and particle Reynolds number.

Some experiments are omitted, namely A2, B3 and E2 as it was impossible to draw a single straight line through the plotted points. This could be a result of amplifier failure in the recorder or a discontinuity in the fluid flow rates.

The accuracy of this method is not good since the error in D_T/q is twice the sum of the errors made in measuring the slopes of the two straight lines and this can be large. Consequently, there is a spread of results on Figure 5.16 but in general the agreement is fair.

5.5 Interface Instability

An experiment was undertaken to determine if an instability with a rapid growth rate could be generated in the experimental apparatus. The approximate linear theory of Chapter 4 predicted that the growth rates of instabilities would be bounded; however, it seems possible that if the Rayleigh number were large and the ratio of longitudinal to lateral dispersion coefficients small enough ($\varkappa$ small) then a visible instability could be developed.

It has already been shown that the Rayleigh number can be increased and $\varkappa$ decreased by reducing the flow velocity; thus an experiment at a low flow velocity was attempted.

The difficulty with such an experiment is that it is not possible to develop a half-body and then slow the flow down to find an instability because the Rayleigh number

$$\lambda = \frac{gk\ell(\rho_2 - \rho_1)}{\epsilon D_T \mu}$$

depends on the velocity and the time for which the flow has been moving at that velocity since

$$\ell = \left(\frac{\pi D_T x}{U}\right)^{\frac{1}{2}}$$

and D_T depends on the velocity. Consequently the number ℓ which is the characteristic length changes with the velocity. In other words the dispersion region occurring at any given point is smaller than that which would have occurred had the fluid been at the lower velocity all the time; the Rayleigh number at any point is therefore larger than that which occurred at the higher velocity, since D_T decreases with velocity. Consequently, the new flow will be more unstable immediately after the flow is slowed. In Figures 5.28 and 5.29 the flow has been slowed to an average downstream superficial velocity of $U_m = 0.0019$ cm/sec and an instability can be seen in Figure 5.28a. The subsequent photographs Figures 5.28b, 5.29a, 5.29b show the region of instability being swept away from the upstream side and being replaced by a stable flow since the amplification decreases as ℓ gradually increases (see page 143).

It is also obviously impossible to have one fluid upon the other and then start the flow, consequently it is necessary to set the main flow and introduce a saline flow through the slit and watch it progress downstream. This introduces a "front" to the flow which again distorts the overall flow pattern. It is difficult to observe just where the instability occurs, see Figures 5.30 a - f.

A 3% salt solution was made up which gave a density difference of 2.1% and injected into a uniform flow through the sand bed. The

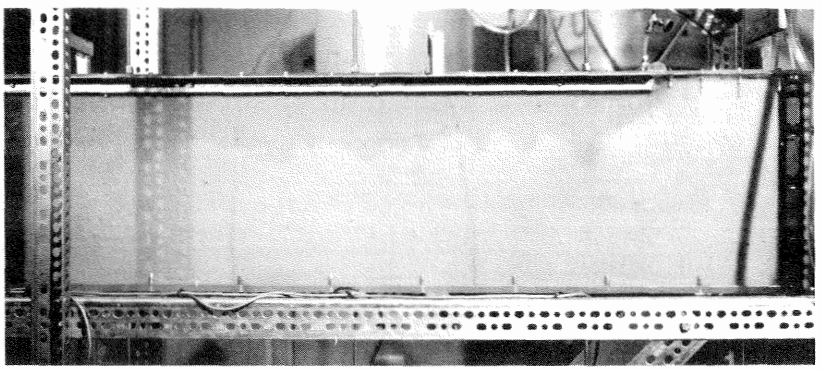

Figure 5.28a An interface shape approximately 15 minutes after slowing the flow to 0.004 cm/sec ($\Delta\rho$ = 0.02).

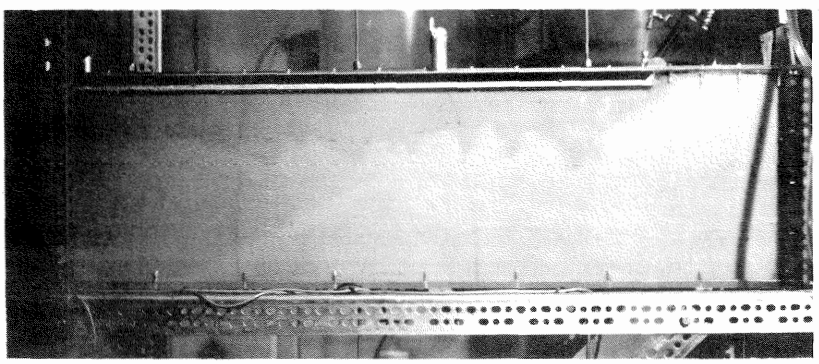

Figure 5.28b The same interface 6 minutes later.

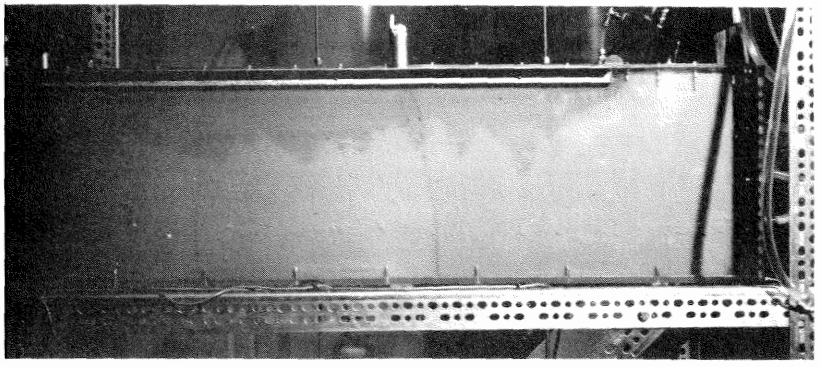

Figure 5.29a The interface shown in Figure 5.28b taken 5 minutes later.

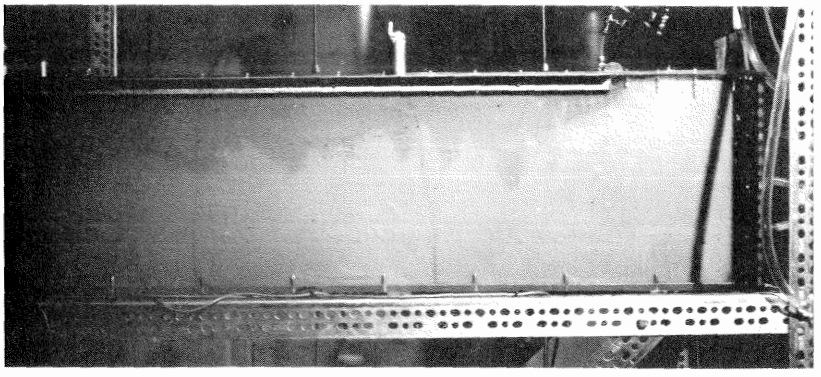

Figure 5.29b The same interface as above 5 minutes later.

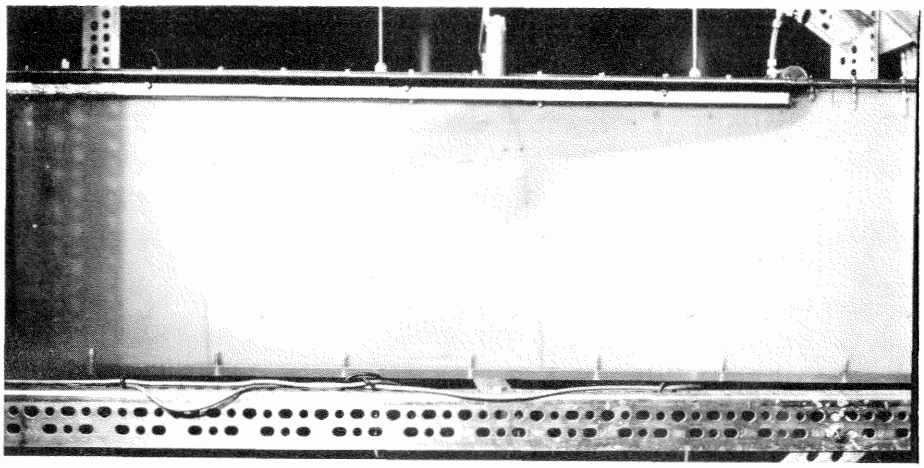

Figure 5.30a The growth of an instability is shown at 5 minute intervals ($\Delta\rho = 0.02$, $U_m = 0.004$ cm/sec).

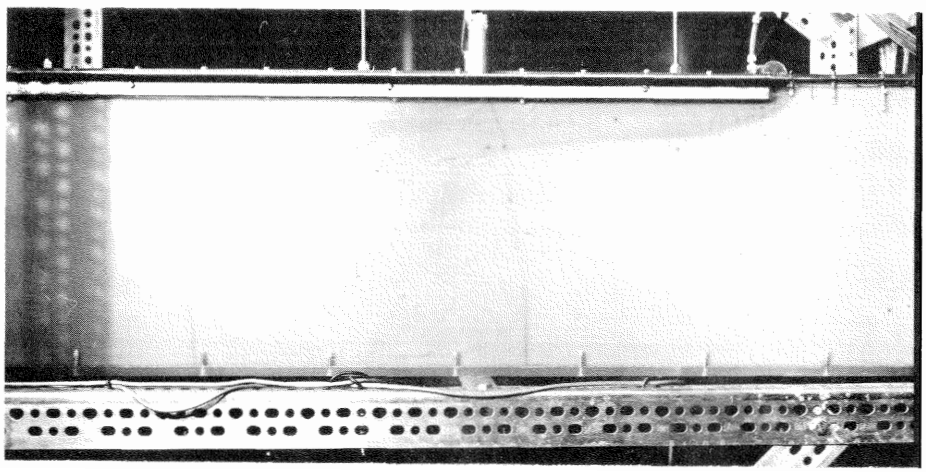

Figure 5.30b

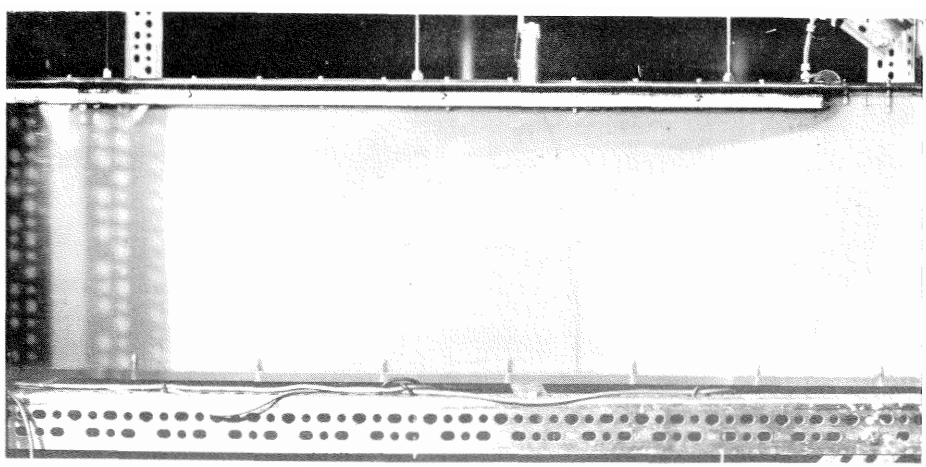

Figure 5.30c

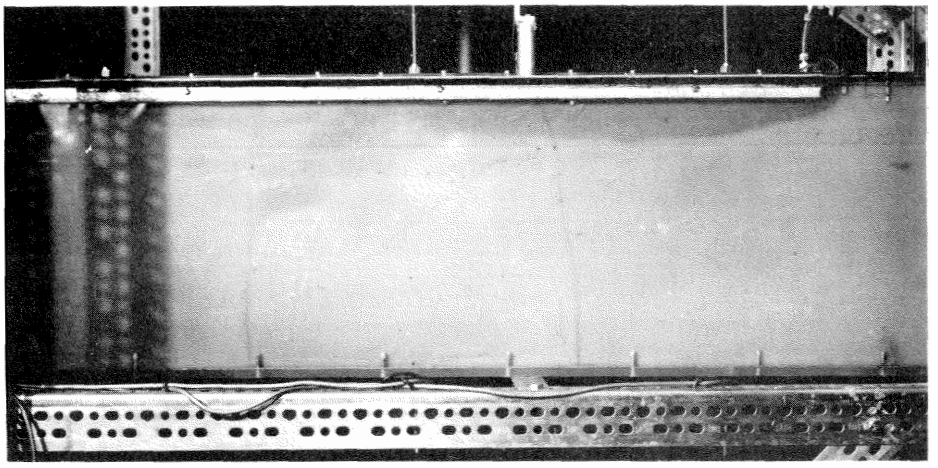

Figure 5.30d

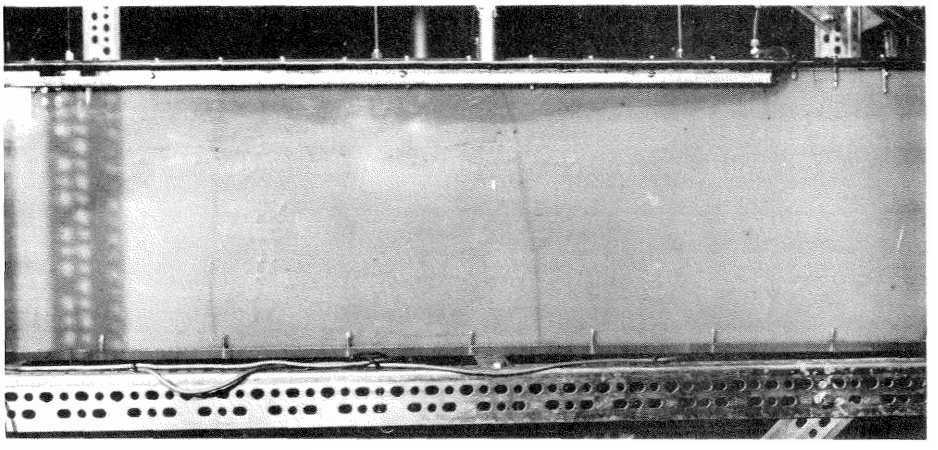

Figure 5.30e

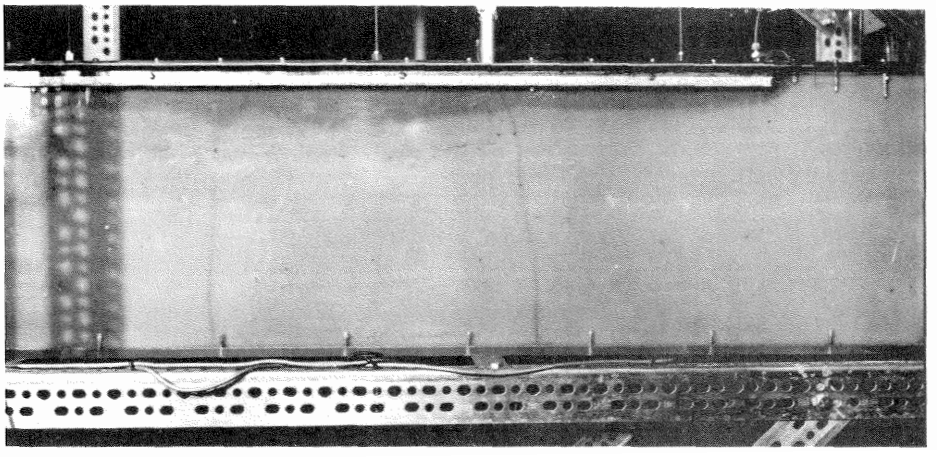

Figure 5.30f

following parameters were recorded

$\epsilon = 0.34$

$gk = 11.9 \times 10^{-4}$ cm^3/sec^2

$\mu = 0.0094$ gm/cm.sec

$U_m = 0.004$ cm/sec

$\rho_2 - \rho_1 = 0.021$ gm/cm^3

$D_T = 48 \times 10^{-6}$ cm^2/sec

$x \sim 40$ cm

$\ell = \left(\frac{\pi D x}{U_m}\right)^{\frac{1}{2}}$

$= 1.23$ cm

Thus

$\lambda = 200$

$\varkappa = 51.5 \left(\frac{U_m d}{\nu}\right)^{0.5}$, (Harleman and Rumer (16))

$= 4.5$

It is of interest to compute the amplification predicted by the linear theory for the time taken to travel 2ℓ or about 2.4 cm. From Chapter 3 with

$\lambda = 200$

$\varkappa = 5.0$

$(\alpha c_i)_{max} \simeq 0.3$

Thus the amplification

$\mathcal{A} = e^{(\alpha c_i)_{max} \cdot \frac{TU_o}{\ell}}$

where

$$T = \frac{2.4}{U_m} = 0.6 \times 10^3 \text{ seconds}$$

$$U_o = \frac{gk(\rho_2 - \rho_1)}{\epsilon\mu}$$

$$= 7.6 \times 10^{-3} \text{ cm/sec}$$

giving

$$\mathcal{A} = e^{1.1} = 3$$

This implies that the wave almost trebles in amplitude in moving about 2.5 cm which is quite a high amplification, and the unstable waves would soon become visible, which in fact they did (see Figure 5.30f). The fastest growing wave at this point has a wavelength given by

$$\alpha_m = \frac{2\pi\ell}{\lambda_m}$$

$$= 1.8$$

i.e. $\lambda_m \approx 4.0$ cm

and this looks reasonable from the photographs in Figure 5.30f.

This is in comparison with the runs C1 through E5 where the Rayleigh numbers and values of $\mathcal{R}$ are given in Table 5.4. Consider run E2 for example

$$\lambda = 65$$

$$\ell = 1.16$$

$$U_m = 0.0267$$

$$U_o = 3.7 \times 10^{-3}$$

$$\varkappa = 12$$

The time taken to travel 2ℓ is

$$T = 80 \text{ seconds}$$

hence the amplification

$$\mathcal{A} = e^{(\alpha c_i)_{max} \cdot \frac{TU_o}{\ell}}$$

$$\simeq e^{(\alpha c_i)_{max}/4}$$

Since the Rayleigh number is less the 200 and $\varkappa = 12$ the maximum growth rate will be much less than 0.3 (see Figure 3.10); consequently the amplification will be close to 1, in sharp contrast to the previous example.

CHAPTER SIX

DISCUSSION OF RESULTS AND CONCLUSIONS

6.0 Recapitulation

A study has been undertaken to investigate a two-fluid flow in a homogeneous isotropic saturated porous medium. In Chapter 2 an approximate theory was presented for the shape of the interface of two fluids of slightly different density in parallel motion in a confined porous medium. It was shown that the solution where the densities of the two fluids were equal could be taken as the zeroth order term in a regular perturbation expansion of the interface shape and the velocity potentials. The mixing of the two fluids along the interface was investigated and an approximate solution obtained for the dispersion equation along the interface.

In Chapter 3 the stability of a horizontal interface was investigated and the result obtained that the interface is always unstable and that the growth rates of unstable waves were bounded, leading to a quasi-stable flow.

Chapter 4 outlined the experimental apparatus and methods used to study the interfacial mixing experimentally; and the experimental results were presented in Chapter 5.

In this concluding chapter the results of the analysis and experiments will be discussed and a summary of conclusions given.

6.1 Stability Analysis

The stability analysis depends on the fact that it is possible

to write down equations of motion which govern the motions of the fluid particles averaged over several pore spaces, rather than the motions within the pores. Using these "average" equations it is possible to consider the stability of perturbations to the density profile produced by the lateral dispersion along the interface. If these perturbations to the density profile and velocity field are to have any meaning they must of course be of the scale of several pore sizes themselves and the linearized theory offered is therefore for perturbations which are not infinitesimal in the usual sense. Numerous interesting points come out of the analysis and these are enumerated below.

(i). The role of longitudinal dispersion is rather surprising in that although it plays a major role in the stability of the system it does not influence the basic density profile. This arises from the fact that to a zeroth order the concentration gradients in the longitudinal direction are small compared to the lateral gradients. However, to the perturbation order the concentration gradients are of equal order.

(ii). The analogy with viscous fluids pointed out by Wooding (3) again becomes evident when the stability equation is found to be very similar to the Orr-Sommerfeld equation of viscous fluids. The major simplification of this problem over the viscous flow problem is that the velocity field is uniform and as a result it is possible to prove that arbitrary disturbances must have a phase velocity equal to the fluid velocity; this reduces the equation to a purely real equation with real boundary conditions.

(iii). The fact that some unstable waves always exist is not surprising as the same result appears in the viscous shear layer problem (see Tatsumi and Gotoh (27)).

(iv). Local growth rates of instabilities are bounded according to this linear theory. This means that there will be no sudden growth of unstable waves such as Benjamin (29) found for a thin layer of viscous liquid running down a vertical flat surface. In that case it has been shown by Benjamin that although unstable waves always exist their growth rates do not become unbounded until a Reynolds number of about 4, whereupon there is a rapid growth of the most unstable wave.

No such behavior occurs here according to the local linear theory presented. Consequently there should be a gradual transition involving slow wave growth giving in effect a quasi-stable flow. However, the problem is somewhat complicated by the growth of the dispersion zone, as discussed below.

(v). The study presented in this work considers only local stability by assuming that the width of the dispersion zone does not increase rapidly with position X. The Rayleigh number

$$\lambda = \frac{gk\ell(\rho_2 - \rho_1)}{\epsilon D_T \mu}$$

assumed constant locally, actually increases with X for

$$\ell = \left(\frac{\pi D_T X}{U}\right)^{\frac{1}{2}} .$$

Consequently the analysis given here can only be regarded as valid for waves whose length is such that they do not extend over a length within which the Rayleigh number changes significantly. This is equivalent to saying that the waves do not extend over a length for which the dispersion zone widens significantly. Obviously, the admissable wavelengths under this criterion are going to depend on the location since the Rayleigh number changes less rapidly as X increases.

From above it is easily shown that the changes in Rayleigh number with X is given by

$$\frac{\Delta\lambda}{\lambda} = \frac{\Delta X}{2X}$$

Now suppose that a $2\frac{1}{2}\%$ change in the Rayleigh number over one wavelength would be a tolerable approximation, then the allowable wavelength L in terms of n-multiples of ℓ would be $(\Delta X = n\ell)$

$$\frac{n\ell}{2X} = 0.025$$

$$\text{i.e.} \quad n = 0.05 \left(\frac{UX}{\pi D_T}\right)^{\frac{1}{2}}$$

A lower bound on the valid wave numbers can then be given in terms of X for

$$\alpha = \frac{2\pi\ell}{L}$$

and

$$L = n\ell$$

Thus the results will tend to become invalid for wave numbers less

than

$$40\ \pi \left(\frac{\pi D_T}{UX}\right)^{\frac{1}{2}}$$

The problem of computing the rate of growth of any particular wave as it is swept downstream is not simple and will be the subject of a later study.

(vi). As the longitudinal velocity U increases the growth rates of unstable waves decreases. This is an expected result, for increasing the velocity increases the rate of both the longitudinal and lateral dispersion which will tend to overcome any excursions made by the lighter fluid into the heavier or vice versa.

(vii). The exact solution for the linearized density profile and the variational method of Chandrasekhar for the error function density profile give quite compatible results for the neutral stability curves, Figure 3.2. While both methods are not exact they without doubt give all the essential characteristics of the solution.

(viii). The Rayleigh number

$$\lambda = \frac{gk\ \ell\ (\rho_2 - \rho_1)}{\epsilon\ D_T \mu}$$

can be interpreted as the ratio of two velocities:

$$U_o = \frac{gk(\rho_2 - \rho_1)}{\mu} \quad ,$$

which is the vertical velocity with which a column of fluid of density ρ_2 would descend into a porous medium saturated with a fluid of density ρ_1 ; and

$$\frac{\epsilon D_T}{\ell} \quad ;$$

which can be regarded as the "velocity of dispersion". For when D_T is constant it can easily be shown that

$$2D_T t = \sigma_y^2$$

where

$$\sigma_y^2 = \int_{-\infty}^{\infty} y^2 C(y)\, dy$$

and since

$$\ell = \left(\frac{\pi D_T X}{U}\right)^{\frac{1}{2}}$$

$$= (\pi D_T t)^{\frac{1}{2}}$$

$$= \sqrt{\frac{\pi}{2}} \cdot \sigma_y$$

then

$$\frac{\epsilon D_T}{\ell} = \frac{\epsilon}{2\pi} \cdot \frac{\sigma_y}{t}$$

which is equivalent to the rate of increase of the standard deviation of the density profile or a "dispersion velocity".

A high Rayleigh number implies that the velocity of descent of

the dense fluid is larger than the "dispersion velocity" and hence instability growth rates should be high, conversely a low Rayleigh number implies that the dispersion velocity is high and the flow will be more stable.

(ix). The instability theory presented has been only for two-dimensional disturbances. Since it has been shown that there always exist two-dimensional disturbances which are unstable an analogy with Squire's theorem (Squire, (30)) need not be sought. It can easily be shown (see Appendix A) that the neutral stability curves for three-dimensional disturbances have exactly the same form as for two-dimensional disturbances. A rigorous study of the relative maximum growth rates of unstable two-dimensional and three-dimensional disturbances at a given Rayleigh number such as Watson (31) has done for parallel viscous flows has not been attempted, and this may be of interest for further study.

6.2 Dispersion and Interfacial Mixing

A basic approximation in the study of the mixing along the curved interface is that the shape of the density interface, a free surface, can be described by the solution of the equal density problem with both layers traveling at the same speed. Although it is not at all evident a priori that the behavior of the solution for unequal densities will be similar to that for equal densities it has been demonstrated in Chapter 2 that it is possible to simplify the problem in this way. If this simplification were not possible it would be

necessary to solve the extremely difficult exact problem.

It is interesting to consider what would happen if instead of a two-dimensional slit being used to introduce the saline flow a point source had been used. It is felt that in this case the quasi-stable flow would not develop since it would be possible for the main flow to travel around the source and thus form a convective plume of sinking fluid.

The results of the mixing theory depend on the assumption that the lateral dispersion coefficient D_T depends on the velocity in the following way *

$$\frac{\epsilon D_T}{\nu} = r\left(\frac{vd}{\nu}\right)^{\omega}$$

where r and ω are constants

d is the mean particle size

v is the superficial velocity

ν is the kinematic viscosity

ϵ is the porosity .

This semi-empirical result is confirmed in the present set of experiments, and the value of r (0.0267) obtained when $\omega = 0.7$ compares very favorably with the value 0.0265 obtained by Harleman and Rumer (16) for constant-velocity constant-density experiments over a similar range of particle Reynolds numbers. This empirical 7/10 power law should be regarded in much the same way as the 1/7 power law for turbulent flow in pipes. While there is a sound similitude reasoning* for choosing the

*See footnote added in proof page 156.

groups of variables as above there is no apparent reason for the 7/10 index apart from the fact that it fits the experimental results.

These experiments were carried out with the heavier fluid on top. If the density difference of the two fluids were to effect the dispersion phenomenon at all it seems logical that the influence would be greatest under these conditions. However, the experimental results seem to indicate that for the density differences used (up to 1%) there is no observable influence on the dispersion. It seems likely that if there is no influence with the denser fluid on top, then there would be no influence with the denser fluid below.

An extensive study of lateral dispersion, such as Pfannkuch (10) has carried out for longitudinal dispersion, should be undertaken for a wide range of Schmidt and Reynolds numbers. The results of such a study would be an extremely valuable contribution to the knowledge of lateral dispersion.

6.3 Conclusions

The principal conclusions of this investigation are enumerated below.

1. Instability of Flow

   (i) It has been theoretically proven that horizontal two-dimensional flows in a saturated porous medium with a denser fluid on top are always unstable.

   (ii) The wavelengths of the class of unstable waves are bounded below by the wavelength of the neutrally stable wave.

(iii) The growth rates of two-dimensional unstable waves are low and bounded above, and the breakup of a stable flow is never sudden.

(iv) An increase in the velocity of such a flow system decreases the growth rate of unstable disturbances.

(v) The two parameters controlling the growth rate of instabilities are the Rayleigh number

$$\lambda = \frac{gk\,\ell\,(\rho_2 - \rho_1)}{\epsilon\, D_T \mu}$$

where

$$\ell = \left(\frac{\pi\, D_T\, X}{U}\right)^{\frac{1}{2}}$$

and the ratio of longitudinal and lateral dispersion coefficients

$$\varkappa = \frac{D_L}{D_T}$$

The flow is stabilized by decreasing the Rayleigh number or increasing $\varkappa$.

(vi) Experimental observations show that it is possible for such a quasi-stable flow to exist.

2. Mixing Layers

(i) The lateral dispersion coefficient of sodium chloride solutions in horizontal motion above pure water does not appear to be influenced by the density difference of the

solutions for density differences up to 1%. It is the opinion of this investigator that there will be no influence when the heavier fluid is below.

(ii) The sole influence of the density difference is in determining the spectrum of admissable unstable waves at the density interface and governing their growth rate.

(iii) It has been proved possible to represent the mixing along an interface developed by a two-dimensional half body as if the flow had always been in rectilinear motion and mixing had begun at some virtual point.

*See page 153.

More recent work has disclosed that this result is true only for constant Schmidt number ν/D_m (D_m molecular diffusivity) and in fact when the flow is completely laminar the dispersion is quite independent of the viscosity and hence the Reynolds number.

APPENDIX A

The three-dimensional equations of motion of perturbation order are

$$\frac{\partial u}{\partial x} + \frac{\partial v}{\partial y} + \frac{\partial w}{\partial z} = 0$$

$$\frac{\partial p}{\partial x} + u = 0$$

$$\frac{\partial p}{\partial y} + \theta + v = 0$$

$$\frac{\partial p}{\partial z} + w = 0$$

$$\frac{\partial \theta}{\partial t} + \mathcal{U} \frac{\partial \theta}{\partial x} + v\, \Theta'(y) = \frac{1}{\lambda_L} \frac{\partial^2 \theta}{\partial x^2} + \frac{1}{\lambda_T} \left(\frac{\partial^2 \theta}{\partial y^2} + \frac{\partial^2 \theta}{\partial z^2} \right)$$

If arbitrary sinusoidal disturbances of the form

$$\left\{u,v,w,\theta,p\right\} = \left\{u(y),v(y),w(y),\theta(y),p(y)\right\} e^{i(\alpha x + \beta z - \alpha c t)}$$

(where α and β are the horizontal wave numbers in the x and z directions respectively) are substituted into the equations above and $u(y),w(y),\theta(y)$, and $p(y)$ eliminated the following equation for $v(y)$ results

$$[D^2 - \beta^2 - \kappa\alpha^2][D^2 - (\alpha^2 + \beta^2)]\, v(y)$$

$$= \lambda_T(\alpha^2 + \beta^2)\, \Theta'(y)v(y) + i\lambda_T\alpha\, (\mathcal{U} - c)[D^2 - (\alpha^2 + \beta^2)]\, v(y) \quad ,$$

and as before for neutrally stable disturbances $\mathcal{U} - c = 0$. The equation for neutral stability is

$$[D^2 - (\beta^2 + \varkappa\alpha^2)][D^2 - (\alpha^2 + \beta^2)]\, v(y)$$

$$= \lambda_T (\alpha^2 + \beta^2)\, \Theta'(y)\, v(y) \quad .$$

When $\varkappa = 1$ then it is obvious that neutrally stable three-dimensional disturbances with an equivalent wave number $\gamma^2 = \alpha^2 + \beta^2$ have the same Rayleigh number as neutrally stable two-dimensional disturbances, i.e., when $\beta = 0$, since the equation has the same form for both. However, when $\varkappa = 1$ the equivalent three-dimensional disturbance will have a somewhat different Rayleigh number at neutral stability since the $\varkappa$ term multiplies only the α^2 term in the first bracket above. It is difficult to surmise from the equation what the respective growth rates of equivalent two and three-dimensional disturbances will be and it has not been rigorously investigated. An investigation of the respective growth rates may be a worthwhile study later.

APPENDIX B

Case I : $\lambda < \dfrac{2\alpha^2 \kappa}{1 - 2\alpha c_i}$

The determinant on page 52 can be simplified by carrying out the following sequence of operations.

(i) Multiply R1 by α and add to R3, divide R1 by α.

(ii) Multiply R1 by α^2 and subtract from R5, divide R1 by α^2.

(iii) Multiply R1 by α^3 and add to R7, divide R1 by α^3.

(iv) Carry out a similar operation with respect to R2 and R4, R6, R8.

(v) The determinant now has all zeros in C1 except for the first term and all zeros in C3 except for the second term and is consequently reduced to a 6 x 6 determinant.

(vi) Multiply R1 by $\alpha + \beta$ and add to R3, divide R1 by $\alpha + \beta$.

(vii) Multiply R1 by $\alpha^2 + \alpha\beta + \beta^2$ and add to R5, divide R1 by $\alpha^2 + \alpha\beta + \beta^2$.

(viii) Carry out a similar operation with respect to R2 and R4 and R6.

(ix) The determinant then has a factor $\alpha - \beta$ in C1 and $\beta - \alpha$ in C2 and when these are factored out becomes a 4 x 4 determinant.

(x) Multiply R1 by $\gamma - (\alpha + \beta)$ and subtract R3 from R1.

(xi) Multiply R2 by $\gamma + \alpha + \beta$ and subtract R4 from it.

(xii) Interchange rows and columns.

(xiii) Add C1 to C3 and C2 to C4.

(xiv) Divide C3 by $\gamma - (\alpha + \beta)$ and C4 by $\gamma + \alpha + \beta$.

(xv) Multiply C3 by $\gamma - \delta$ and C4 by $\gamma - \delta$ and divide R1 and R2 by $(\gamma - \delta)$.

(xvi) The determinant now has enough zeros to make expanding by cofactors very simple.

Case II : $\lambda = \frac{2\alpha^2 \kappa}{1 - 2\alpha c_i}$

The determinant on page 53 is simplified in the following manner.

(i) Repeat the same operations as in Case I down to (ix).

(ii) Add R1 to R2 and subtract R4 from R3.

(iii) Multiply R1 and R4 by 2.

(iv) Subtract R2 from R1 and add R3 to R4.

(v) Multiply out by cofactors.

Case III : $\lambda > \frac{2\alpha^2 \kappa}{1 - 2\alpha c_i}$

The determinant on page 55 is simplified in the following manner.

(i) Divide C5 and C7 by $\cos\gamma$.

(ii) Divide C6 and C8 by $\cosh\delta$.

(iii) Add C1 to C5 and C2 to C6.

(iv) Add C3 to C7 and C4 to C8.

(v) Repeat instructions (i) through (ix) as for Case I to reduce to a 4 x 4 determinant.

(vi) Add R1 to R2 and R4 to R3.

(vii) Multiply R1 by 2 and add R2 to R1.

(viii) Multiply R4 by 2 and add R3 to R4.

(ix) Multiply through by $\cos\gamma$ and $\cosh\delta$.

(x) Expand by cofactors to give equations (3.53) and (3.54).

REFERENCES

1. Wentworth, C. K., Factors in the behavior of ground water in a Ghyben-Herzberg system, Pacific Science, 1, 172, 1947.

2. Carrier, G. F., The mixing of ground water and sea water in permeable subsoils, J. Fluid Mech., 4, 479, 1958.

3. Wooding, R. A., Mixing layer flows in a saturated porous medium, J. Fluid Mech., 19 (1), 103-112, May, 1964.

4. Wooding, R. A., Steady state free thermal convection of a liquid in a saturated permeable continuum, J. Fluid Mech., 2 (3), 273-285, May, 1957.

5. Harleman, D. R. F., and R. R. Rumer Jr., The dynamics of salt water intrusion in porous media, M. I. T. Hydrodynamics Laboratory Report No. 55, 125 p., August, 1962.

6. Bear J., and G. Dagan, The transition zone between fresh and salt waters in coastal aquifers, Prog. Rept. No. 2, Tech. Rept. No. 4, Technion Res. and Dev. Foundation, Technion, Haifa Israel, 46 p., July, 1963.

7. Scheidegger, A., The random walk model with auto-correlation of flow through porous media, Canadian J. of Physics, 36, 649-658, 1958.

8. Saffman, P. G., Dispersion due to molecular diffusion and macroscopic mixing in flow through a network of capillaries, J. Fluid Mech., 7 (2), 194-208, February, 1960.

9. Taylor, G. I., Dispersion of soluble matter in solvent flowing slowly through a tube, Proc. Roy. Soc., A219, 196-203, 1953.

10. Pfannkuch, H. O., Contribution a l'etude des deplacements de fluides miscibles dans un mileau poreux, Revue de l'Institut Francais due Petrole, XVII (2), 215-270, February, 1963.

11. Bischoff, K. B. and O. Levenspiel, Fluid dispersion - Generalization and comparison of mathematical models, I - Generalization of models, Chem. Eng. Sci., 17, 245-255, 1962.

12. Bischoff, K. B. and O. Levenspiel, Fluid dispersion - Generalization and comparison of mathematical models, II - Comparison of models, Chem. Eng. Sci., 17, 257-264, 1962.

13. Scheidegger, A. E., General theory of dispersion in porous media, J. Geophys. Res., 66 (10), 3273-3278, 1961.

14. De Josselin de Jong, G., and M. J. Bossen, Discussion of paper by Jacob Bear, 'On tensor form of dispersion in porous media', J. Geophys. Res., 66 (10), 3623-3624, 1961.

15. Bear, Jacob, On the tensor form of dispersion in porous media, J. Geophys. Res., 66 (4), 1185-1197, 1961.

16. Harleman, D. R. F., and R. R. Rumer, Longitudinal and lateral dispersion in an isotropic porous medium, J. Fluid Mech., 16 (3), 385-394, 1963.

17. Wooding, R. A., Convection in a saturated porous medium at large Rayleigh number or Peclet number, J. Fluid Mech., 15, 527-544, 1963.

18. Saffman, P. G., and Taylor, G. I., The penetration of a fluid into a porous medium or Hele-Shaw cell containing a more viscous liquid, Proc. Roy. Soc., A245, 312-329, 1958.

19. Wooding, R. A., The stability of an interface between miscible fluids in a porous medium, ZAMP, XIII, 255-265, 1962.

20. Wooding, R. A., The stability of a viscous liquid in a vertical tube containing porous material, Proc. Roy. Soc., A252, 120-134, 1959.

21. Wooding, R. A., Instability of a viscous liquid of variable density in a vertical Hele-Shaw cell, J. Fluid Mech., 7 (4), 501-515, April, 1960.

22. Wooding, R. A., Free convection of fluid in a vertical tube filled with porous material, J. Fluid Mech., 13 (1), 129-144, May, 1962.

23. Polubarinova-Kochina, P. Ya. Theory of ground water movement, 613 p., Princeton University Press, 1962.

24. Li, Wen-Hsiung, Band diffusion with variable parameters along the flow, J. Eng. Mech. Div., Proc. A.S.C.E., 90 (EMS), 343-361, October, 1964.

25. Chandrasekhar, S., The stability of a viscous flow between rotating cylinders, Mathematika, 1, 5-13, 1954.

26. Morse, P. M., and H. Feshbach, Methods of Theoretical Physics, Vol. I, 997 p., McGraw-Hill, 1961.

27. Tatsumi, T., and K. Gotoh, The stability of free boundary layers between uniform flows, J. Fluid Mech., 7, 433-441, 1960.

28. Esch, R. E., The instability of a shear layer between two parallel streams, J. Fluid Mech., 3, 289-303, 1957.

29. Benjamin, T. B., Wave formation in laminar flow down an inclined plane, J. Fluid Mech., 2, 554-574, 1957. (Corrections in J. Fluid Mech., 3, 657, 1958.)

30. Squire, H. B., On the stability of three dimensional disturbances of viscous fluid flow between parallel walls, Proc. Roy. Soc., A142, 621-628, 1933.

31. Watson, J., Three dimensional disturbances in flow between parallel planes, Proc. Roy. Soc., A254, 562-569, 1960.